EPR SPECTROSCOPIC STUDIES OF THE ACTIVE SITES OF SOME HEME- AND COPPER-CONTAINING, OXYGEN-BINDING PROTEINS

Thesis by

Randall Heywood Morse

In Partial Fulfillment of the Requirements

for the Degree of

Doctor of Philosophy

California Institute of Technology

Pasadena, California

1981

(Submitted May 26, 1981)

Acknowledgments

I would like first to thank Sunney Chan for his patience and his dogged insistence on doing science rightly and thoroughly. I would also like to acknowledge Bill Goddard for many helpful discussions through the years, and for being so generous with his time; and J. D. Roberts, for his guidance and help in the early stages of my graduate career.

The Chan group has been great, and I thank them for sharing both in work and play; most especially, thanks to Gary Brudvig, Tom Stevens, Dave Bocian, Craig Martin and Dave Blair for their sundry contributions towards the work in this thesis. Craig is due a special word of appreciation for his part in the work on the laccases, which was equal to my own; Gary, for helping me get started on the calculations described in Chapter IV; Tom, for mentioning that Charles Cantor really might be the right man for me to postdoc with; and Sunney, for bringing us all together and providing us with an excellent environment to work in. I am also grateful to Bo Malmström for coming to Caltech and making our work on the laccases possible; to Harry Gray and Bob Kanne, for their contributions to that work; to Miss Ann-Catherine Carlsson in Göteberg for the preparation of fungal and tree laccase, as well as of type 2 copper-depleted tree laccase; to Ann English and Vanessa Lum for letting us have some of their tree laccase without material reward; and to Utpal Banerjee, for helping with the NMR work on the laccases. And of course, without the help of people like Emily, our secretary, Sig, Gabor, and Eric in the glass shop, Tom in the electronics shop, Charlie in the stockroom, Jan Mitchell in the analytical lab (soon to be a museum display), and all the other people who make Caltech run, nothing would get done, and Caltech would be like a

government institution. So they are due a 'thank you', as is Kathy Lewis for typing this thesis.

Perhaps more importantly than the above, I have been privileged to meet some fine people here who have made the good times great and the bad times tolerable. For that, I thank Bob, Jim and Patty, Tom, Gary, Colleen, Helen, Ken, Craig, Joe, Les, Mark, Jan, Sridhar, Rose, Sally, Barb, Dorothy and Lloyd, Sunney, Tan, and anybody else I may have forgotten.

Finally, a big 'thank you' and lots of love to Mom, Dad and Stu.

Abstract

All oxygen-utilizing proteins contain copper, iron, or both, at the oxygen-bonding sites. The ligand environment and geometry about the metal centers in these proteins must be crucial in determining their individual functions. This thesis reports studies in which the ligand nitric oxide is used as a spin probe to investigate the structure of the oxygen-binding sites of myoglobin and some inorganic heme analogues, and of tree and fungal laccase and cytochrome c oxidase.

Nitric oxide reacts with heme iron in ferrous hemeproteins, such as hemoglobin and myoglobin, to form six-coordinate paramagnetic complexes. Chapter II reports investigations on the EPR spectra of the nitric oxide complexes of ferrous myoglobin, cytochrome c, and Fe(II) protoporphyrin IX-imidazole, which change with temperature over the range 30 - 180 K. This temperature dependence could be due to motional/relaxation effects or to a chemical equilibrium. To resolve this matter, the technique of factor analysis was used to deconvolute the temperature-dependent EPR spectra. By this method it has been found that all of the spectra for any given complex can be reproduced by adding together varied amounts of two signals, demonstrating that the variation of the EPR spectra with temperature is due to an equilibrium between two species. The two species differ in enthalpy by no more than about 2 kcal/mol. The observed signals are interpreted as arising from two six-coordinate conformers of the nitrosylheme·nitrogen base complexes, differing primarily in the position of the iron with respect to the ligands and to the heme plane. The anomalous behavior of the terminal respiratory enzyme cytochrome c

oxidase, which exhibits only one EPR signal independent of temperature, suggests that the NO-oxygen may interact with the cuprous ion at the cytochrome $\underline{a}_3$-Cu_{a_3} site of the enzyme. These results have implications for studies in general on oxygen-carrying proteins.

In addition to being a strong-field ligand, NO is also a reactive molecule which can be oxidized to NO_2^- and NO_3^-, and reduced to N_2O, N_2 and NH_3. Chapter III details investigations of the reactions of NO with the copper-containing oxidases tree and fungal laccase, as well as with tree laccase depleted in type 2 copper. The oxidation states of the enzymes were monitored by EPR and optical spectroscopy, and the reaction products of NO were determined by NMR and mass spectroscopy. These studies show that NO reduces all three copper sites of fungal laccase. In addition, NO forms a specific complex with the reduced type 2 copper. NO similarly reduces all of the copper sites in tree laccase, but it also oxidizes the reduced sites produced by ascorbate or NO reduction. A catalytic cycle is set up in which N_2O, NO_2^- and various forms of the enzyme are produced. On freezing of fully reduced tree laccase in the presence of NO, the type 1 copper becomes reoxidized. This reaction does not occur with the enzyme depleted in type 1 copper, suggesting that it involves intramolecular electron transfer from the type 1 copper to NO bound to the type 2 copper. When the half-oxidized tree laccase is formed in the presence of NO, a population of molecules exists which exhibits a type 3 EPR signal. A triplet EPR signal is also seen in the same preparation, and is attributed to a population of the enzyme molecules in which NO is bound to the reduced copper of a half-oxidized

type 3 copper site. The implications of these results towards the structures of tree and fungal laccase are discussed.

Nitric oxide has also been used to probe the structure of the metal centers of cytochrome c oxidase, resulting in the discovery of three stable conformations of the oxidized enzyme [G. W. Brudvig, T. H. Stevens, R. H.Morse and S. I. Chan (1981) Biochemistry 20, in press]. These conformations differ in the structure of the cytochrome a_3-Cu_{a_3} site, which is the site of oxygen reduction, and are distinguishable by EPR spectroscopy. Two of the diagnostic EPR signals are unusual in that they cannot be interpreted simply in terms of normal Cu(II) or Fe(III) EPR signals. The "g5" conformation identified as a transient species occurring upon reoxidation of the reduced enzyme by O_2 [R. W. Shaw, R. E. Hansen and H. Beinert (1978) J. Biol. Chem. 253, 6637-6640] similarly exhibits an EPR signal not subject to simple interpretation. In view of the complexity of these three EPR signals, they are most likely due to the coupled cytochrome a_3^{+3}-$Cu_{a_3}^{+2}$ site of the oxidized enzyme. Chapter IV describes calculations of the energy levels of, and allowed EPR transitions from, the cytochrome a_3-Cu_{a_3} site under various conditions of exchange coupling and dipolar coupling, as a function of other parameters such as the magnitude of the rhombic zero-field splitting of the heme iron and distance between the two metal ions. On the basis of these calculations, one of the three unusual EPR signals from oxidized cytochrome c oxidase is deduced to arise from a strongly exchange-coupled ($|J| > 200\ cm^{-1}$) cytochrome a_3^{+3}-$Cu_{a_3}^{+2}$ site, one from a

weakly exchange-coupled ($|J| > 0.25\ cm^{-1}$) cytochrome $\underline{a}_3^{+3}$-$Cu_{a_3}^{+2}$ site, and one from an admixture of S = 5/2 and S = 3/2 states of the cytochrome $\underline{a}_3^{+3}$ site.

Table of Contents

Table of Contents (continued)

Abbreviations

Abbreviations used in this thesis: ADP, adenosine diphosphate; ATP, adenosine triphosphate; EPR, electron paramagnetic resonance; NADH, reduced nicotinamide adenine dinucleotide; MCD, magnetic circular dichroism; CD, circular dichroism; PPDME, protoporphyrin IX dimethyl ester; DMF, dimethylformamide; Me_2SO, dimethylsulfoxide; Mb, myoglobin; Hb, hemoglobin; Im-Heme-NO, nitrosylprotoporphyrin IX (imidazole) iron(II); NMeIm, N-methylimidazole; TPP, tetraphenylporphyrin; TpivPP, meso-tetra($\alpha,\alpha,\alpha,\alpha$,-O-pivalamidophenyl)porphyrin; BSA, bovine serum albumin; EDTA, ethylene diamine tetraacetic acid; Hepes, N-2-hydroxyethyl-piperazine-N'-2-ethanesulfonic acid; NMR, nuclear magnetic resonance; PPD, p-phenylene diamine; $t_{\frac{1}{2}}$, half time.

Chapter I. Introduction

Oxygen is one of the most widely utilized molecules in biology. Its great oxidizing potential, combined with its kinetic inertness, makes it ideally suitable as an electron acceptor for a host of biological oxidations. Nature, in its patient wisdom, has created a variety of proteins for catalyzing biologically useful reactions with oxygen in controlled fashion. These proteins may be classified according to the kinds of reactions they catalyze. Dioxygenases incorporate oxygen directly into substrate molecules; examples are tryptophan dioxygenase and metapyrocatechase. Mono-oxygenases, such as tryosinase and the microsomal mono-oxygenases, catalyze the general reaction

$$O_2 + RH + AH_2 \rightarrow ROH + H_2O + A \ . \qquad (1)$$

Oxidases are enzymes which catalyze reactions in which oxygen serves as a terminal electron acceptor, being reduced to peroxide or water; cytochrome c oxidase, laccase, and ascorbate oxidase are examples. Additionally, many organisms require proteins which serve to store or transport oxygen, such as hemoglobin and hemocyanin.

Proteins which store or transport oxygen, as well as those catalyzing reactions involving O_2, have in common that they contain one or more coordinated metal ions. At least one of the metal ions, which are always either copper or iron, or both, will have a free coordination site available for binding O_2. The need for coordinating oxygen is obvious for proteins involved in storage or transport. Those enzymes catalyzing

reactions using oxygen must coordinate the molecule not only to hold it in the proper spatial orientation, but more importantly to lower the activation energy to its reduction. The structural differences reflecting the functional differences in these two kinds of proteins are generally subtle. For example, the difference between tyrosinase, a mono-oxygenase, and hemocyanin, an oxygen carrier, both of which contain only a binuclear copper site for binding oxygen, appears not to lie in any differential in oxygen activation, but in slight geometrical differences in the active site which result in increased rates of ligand substitution and consequent enhanced reactivity with tyrosinase over hemocyanin (1).

The oxygen-carrying proteins are hemoglobin, myoglobin, hemocyanin, and hemerythrin. Structural investigations on the latter two proteins are still underway, but it is known that oxygen binds at a binuclear copper site in hemocyanin and at a binuclear, non-heme iron site in hemerythrin. In both cases, it is likely that oxygen forms a bridge between the two metal ions when it is bound to the protein (1). Hemoglobin and myoglobin have been structurally well characterized. Oxygen binds to a ferrous heme iron in both proteins; there is one such oxygen-binding site in myoglobin, and four in hemoglobin. The four oxygen-binding sites in hemoglobin bind oxygen in a cooperative fashion, and the cooperative mechanism has been one of the most thoroughly studied topics in protein chemistry. The other major subject of investigation on these two hemeproteins has been the detailed electronic and geometrical structure of the oxyheme unit. We will return to this subject.

A huge number of reactions is found in nature in which oxygen is incorporated into substrate molecules, in whole or in part, and a corresponding variety of oxygenases exists which catalyze these reactions. Both heme and copper oxygenases occur naturally, and many of these have been studied from both structural and mechanistic viewpoints. As my work at Caltech has focused on the structural properties of the oxidases and oxygen-carrying proteins, I will not attempt to review structure and mechanism in the oxygenases here.

The reduction of oxygen to two molecules of water is catalyzed by ascorbate oxidase, ceruloplasmin, laccase, and cytochrome c oxidase. All of these enzymes contain a pair of metal ions in close proximity where oxygen can bind, and all have at least four metal centers per enzyme molecule. Among these enzymes, only cytochrome c oxidase, which has two iron atoms in the form of heme a, contains coordinated metal ions other than copper.

The physical and chemical properties of the copper centers found in the oxidases vary considerably, and a system of classification has been devised in which most of these copper centers, as well as those found in enzymes involved in other reactions with oxygen or in electron transport, can be categorized (2). The accepted definitions are:

1. Type 1 Cu^{+2} is characterized by a strong blue color (extinction coefficient greater than 10^3 M^{-1} cm^{-1}), and an EPR spectrum with a narrow hyperfine splitting in the $g_{||}$ region ($|A_z| < 0.010$ cm^{-1}).

2. Type 2 Cu^{+2} has EPR parameters similar to those of simple inorganic cupric complexes, such as square planar $Cu(histidine)_2$, with $g_{||}$ near 2.24 and $|A_{||}| > .014$ cm^{-1}, and is capable of binding some anions, such as F^-.
3. Type 3 copper centers consist of a pair of copper ions which are EPR nondetectable even in the oxidized state, due to exchange coupling. These centers have a strong absorption band in the near-ultraviolet spectral region which disappears upon reduction of the copper ions.

Ceruloplasmin, ascorbate oxidase, and laccase contain all three types of copper. Since the work in this thesis focuses on cytochrome c oxidase and laccase among the oxidases, these enzymes will now be discussed in some detail.

Cytochrome c oxidase and laccase, although similar in catalyzing the reduction of oxygen to water, differ greatly in their biological functions. The laccases are extracellular enzymes which serve as biological oxidants by coupling the reduction of oxygen to the oxidation of organic substrates. Cytochrome c oxidase, on the other hand, uses the potential difference between cytochrome c, which it oxidizes, and oxygen, to create a proton gradient which in turn is used (via the action of F1-ATPase) to drive the phosphorylation of ADP to ATP. In this way, energy derived from the activity of the electron transfer chain can be stored within the cell in a readily utilizable form. From a functional standpoint, then, one might say that laccase transfers oxidizing

equivalents from oxygen to a variety of organic substrates, whereas cytochrome c oxidase transfers reducing equivalents (electrons, in fact!) from cytochrome c to oxygen, conserving part of the energy in the process.

Structurally, the enzymes are similar in that they each possess four metal centers, two of which are in close proximity and which are believed to be the oxygen-binding sites. In both enzymes these two metal centers cooperatively accept two electrons from the other two metal sites, which are magnetically isolated and which serve as the primary acceptors. On the other hand, whereas laccase has four copper atoms per enzyme molecule, one each of the type 1, 2, and 3 copper centers, cytochrome c oxidase has two iron atoms, in the form of heme a, and two copper atoms, which are not categorizable as type 1, 2, or 3 copper sites, per functional unit. One of the objectives of this thesis is to understand the way in which the differences in the structures of the metal centers of laccase and cytochrome c oxidase determine their different functional roles in nature, with particular attention on the differences in the oxygen-binding sites. Before discussing the approaches used to attain this and other objectives of this thesis, though, I will first elaborate on the function and structures of cytochrome c oxidase and the laccases.

Two types of laccase, tree laccase (from *Rhus vernicifera*) and fungal laccase (from *Polyporus versicolor*) were used in the studies reported herein. Tree laccase is dissolved in the latex of the lacquer tree, along with some phenols. When the tree is damaged, the latex

seeps out, and upon contact with air the phenols are oxidized by the laccase to free radicals which polymerize to form a natural polyphenolic plastic, which can then heal the wound. Fungal laccase is believed to be involved in the degradation of lignin, which is a component of the wood on which the fungus lives (3).

Structural and kinetic studies on the laccasses have paralleled each other. The principal aims of these studies have been to elucidate the ligand structures and geometries of the copper centers, and to understand the order and mechanism of electron transfer to oxygen. A variety of approaches, including EPR, optical, and resonance Raman spectroscopies, MCD, CD, magnetic susceptibility, spectrophotometric titrations, stopped-flow studies, and inhibitor studies, has been brought to bear on these enzymes, and a good deal is now understood regarding their structure and mechanism. Many important details, however, remain to be worked out.

Both tree and fungal laccase are water-soluble enzymes, giving deep blue solutions at less than millimolar concentrations when oxidized. The enzymes may be reduced by anaerobic addition of reductant such as ascorbate or NADH, yielding colorless solutions. The molecular weights are about 60,000 and 120,000 for the fungal and tree enzyme, respectively. The optical and EPR properties, as well as the reduction potentials for the various metal centers of these two enzymes, are summarized in Table I.

The ligand environments of the type 1 coppers of tree and fungal laccase are likely to be similar to that of the type 1 copper of plastocyanin, which has been determined by X-ray crystallography and consists

Table I. Optical, EPR and Electrochemical Data on the Laccases[a] and Cytochrome c Oxidase[b].

Enzyme	Optical Bands (nm) and ε_{mM}'s			g_z	g_y	g_x	$A_z(cm^{-1})$	ε^o(mv)
Fungal laccase (*Polyporus versicolor*)								
Type 1 Cu^{+2}	719(2.0)	610(4.6)	440(0.8)	2.19	2.05	2.03	.0090	785[c]
Type 2 Cu^{+2}	-			2.24	2.05		.0194	
Type 3 Cu	330(3.0)			2.27[d]	2.15[d]	2.02[d]	.0115[d]	782[c]
Tree laccase (*Rhus vernicifera*)								
Type 1 Cu^{+2}	787(0.9)	614(5.2)		2.30	2.05		.0037	394[e]
Type 2 Cu^{+2}	-			2.24	2.05		.0178	365[e]
Type 3 Cu	330(2.6)			2.30[d]	2.15[d]	2.05[d]	.0072[d]	434[e]
Cytochrome c Oxidase (bovine)								
Cu_a^{+2}	830(1.5)			2.18	2.03	1.99	.0030[f]	230[g]
$Cu_{a_3}^{+2}$	-			2.28[d]	2.11[d]	2.05[d]	.0094[d]	380[g]
Cytochrome a^{+3}	598(16)[h]	418(150)[h]		3.03	2.21	1.45	-	230[g]
Cytochrome a_3^{+3}	603(44)[i]	520(weak)[i]	444(240)[i]	2.0	~6.0		-	380[g]

[a]ref. 6, [b]ref. 13, [c]pH 5.5, [d]ref. 8; the type 3 site is EPR silent in the fully oxidized enzyme. [e]pH 7.5, [f]ref. 29, [g]pH 7.0, [h]oxidized, sum of both cytochromes, [i]reduced, sum of both cytochromes.

of two histidine nitrogens, a cysteine sulfur, and a methionine sulfur ligated to the copper in a distorted tetrahedral geometry (4). The optical band near 600 nm which gives these proteins their blue color has been assigned to a $\sigma S(cys) \rightarrow Cu(II)$ charge transfer transition. There must, however, be some difference in the ligand environments of the type 1 coppers in tree and fungal laccase to account for the large difference in their reduction potentials (Table I), but at present the precise nature of these differences remains unknown.

The EPR signal exhibited by the type 2 copper center of the laccases suggests that its structure most likely consists of two to three nitrogen ligands (such as histidine) and one or two oxygen ligands (such as tyrosine) as the strong-field ligands in a tetragonal arrangement about the copper ion (5). One of the axial ligands is probably hydroxide or water, which can be displaced to allow binding of externally added ligands such as cyanide and fluoride (6).

Little is known structurally about the type 3 copper center of the laccases. The copper ions are strongly antiferromagnetically coupled in the oxidized enzyme (7), and the EPR signal observed in the partially oxidized enzyme from a single type 3 copper (8) is consistent with nitrogen ligation (5).

As to the mechanism of oxygen reduction as catalyzed by the laccases (6,9), it is reasonably certain that the initial reduction of the enzyme occurs at the type 1 copper site, followed by reduction of the type 2 copper. Two electrons are then passed simultaneously to the type 3 copper site, allowing an oxygen molecule to bind. It is believed

that the last two electrons are then passed to the bound oxygen molecule via the type 1 copper. It has been shown that of the two water molecules produced by the reduction of oxygen, one is released to the bulk water within five minutes, and the other remains bound to type 2 Cu(II) (10, 11).

Cytochrome c oxidase is the last member of the oxidase family that this thesis is concerned with. Cytochrome c oxidase is found in the mitochrondria of all aerobic organisms, and is directly responsible for the utilization of more than 90% of the oxygen consumed by life on Earth (12). The enzyme has a molecular weight of about 140,000 and spans the mitochondrial membrane (13). It catalyzes specifically the reaction

$$4 \text{ cytochrome } \underline{c}^{+2} + O_2 + 4\ H^+ \rightarrow 4 \text{ cytochrome } \underline{c}^{+3} + 2\ H_2O \quad . \qquad (2)$$

The turnover rate is about 400 s^{-1} in the cell, similar to that for the laccases. Part of the energy released in reaction (2) is used by the enzyme to create a proton gradient, the energy from which is then used to drive the phosphorylation of ADP to produce ATP. Among the major goals of studying cytochrome c oxidase are to elucidate the precise mechanism of oxygen reduction as catalyzed by the enzyme, and to understand the details of how this reduction is coupled to oxidative phosphorylation.

The structure of cytochrome c oxidase has been reviewed recently by Malmström (13). The enzyme contains two copper atoms, neither of which fits neatly into the categories of type 1, 2, or 3 copper ions, and two iron atoms in the form of heme a. Starting with the oxidized

enzyme, each of the four metal centers may be reduced by one electron. The two copper centers are distinct chemically, as are the two hemes. The optical and EPR properties of the metal centers of cytochrome c oxidase, as well as their reduction potentials, are given in Table I.

The two hemes are designated cytochrome a and cytochrome a_3, and the copper centers will be referred to here as Cu_a and Cu_{a_3}. Cytochrome a and Cu_a are somewhat analogous to the type 1 and 2 copper centers of the laccases, being the initial electron acceptors from cytochrome c in the catalytic cycle. Cytochrome a_3 and Cu_{a_3}, on the other hand, resemble the type 3 copper center of the laccases in that they are in close proximity and serve as the oxygen-binding site.

Cytochrome a and Cu_a do not bind externally added ligands. Both give rise to EPR signals in the oxidized enzyme. The signal from cytochrome a is that of a low-spin, heme iron, and is most consistent with both axial ligands being imidazole nitrogens (14). The EPR signal from Cu_a is unusual, both in the small hyperfine splitting along g_z, which is not resolved in the X-band EPR spectrum, and in having one of its g-values smaller than $g_e = 2.0023$, the free-electron g-value. The unusual EPR signal led Peisach and Blumberg (5) to propose that the unpaired spin might actually reside on a sulfur radical. This and other considerations led Chan et al. (15,16) to propose a specific model for the structure of the Cu_a center, the essential features of which consisted of two histidine nitrogens and two cysteine sulfurs bound to copper in a nearly tetrahedral geometry, so that the oxidized Cu_a center is best

represented as Cu(I) bound to a sulfur radical. Other workers have since suggested that the coordination between copper and sulfur in the Cu_a center is highly covalent (17), which is equivalent to ascribing some Cu(I)-S· character to the site.

Cytochrome a_3 is high-spin in both the oxidized and reduced enzyme. One of the axial ligands is a histidine nitrogen, as has been shown by isotopic substitution using ^{15}N-labeled histidine (18), and the other axial site is occupied by a labile ligand, so that the heme iron binds externally added ligands such as F^-, CN^-, CO, NO, N_3^-, and others. The labile ligand is probably not exactly the same for all of the enzyme molecules in a given preparation of the oxidized enzyme, as discussed in Chapter 4.

Cu_{a_3} has at least one, and probably two sites available for coordinating exogenous ligands (19,20). This indicates that the coordination environment about the copper is most likely tetragonal, as proposed by Chan et al. (21). The EPR parameters (8) suggest the absence of sulfur ligands to this copper (5), but the parameters are unusual enough that this cannot be assumed with certainty.

Until fairly recently, whether the available coordination site of cytochrome a_3 to which oxygen binds in the catalytic cycle was on the same or opposite side of the heme plane as Cu_{a_3} was completely a matter of speculation. However, Stevens et al. (19) showed in 1979 that it was possible for an externally added ligand, NO, to bridge between cytochrome a_3 and Cu_{a_3}. More recently, further experiments have indicated that

other externally added ligands may also bridge between the two metal centers and mediate the antiferromagnetic coupling between them in the resting, oxidized enzyme (20). How this large coupling ($J > 200\ cm^{-1}$) between the S = 5/2 heme iron and S = 1/2 copper is mediated is unknown.

Once it had been discovered that externally added ligands could bind to cytochrome a_3 and Cu_{a_3} simultaneously, it seemed obvious that oxygen would also bind in this way. Presumably, by bridging between two metal centers in cytochrome c oxidase as well as in the other oxidases, oxygen can be reduced to water without release of intermediates such as peroxide or superoxide. Although there must be a sizeable barrier to the release of these bound intermediate species, there can be only a slight barrier to the subsequent reduction of these species to water in order for catalysis to proceed at a reasonable rate. A mechanism for the reduction of oxygen by cytochrome c oxidase, incorporating these considerations, in which only the roles of cytochrome a_3 and Cu_{a_3} are indicated, is shown in Fig. 1 (from Ref. 22). Experiments in which intermediates in the catalytic cycle are trapped at low temperature and monitored by optical and EPR spectroscopy have been instrumental in uncovering the mechanism of oxygen reduction by the enzyme, and continue to be an area of active investigation.

The work in this thesis is directed towards understanding the nature of the oxygen-binding sites of proteins which are involved in oxygen storage or reduction. The approach used has been to investigate the interactions with these proteins of small molecules, other than oxygen, which can bind or react at the oxygen-binding sites. Comparing

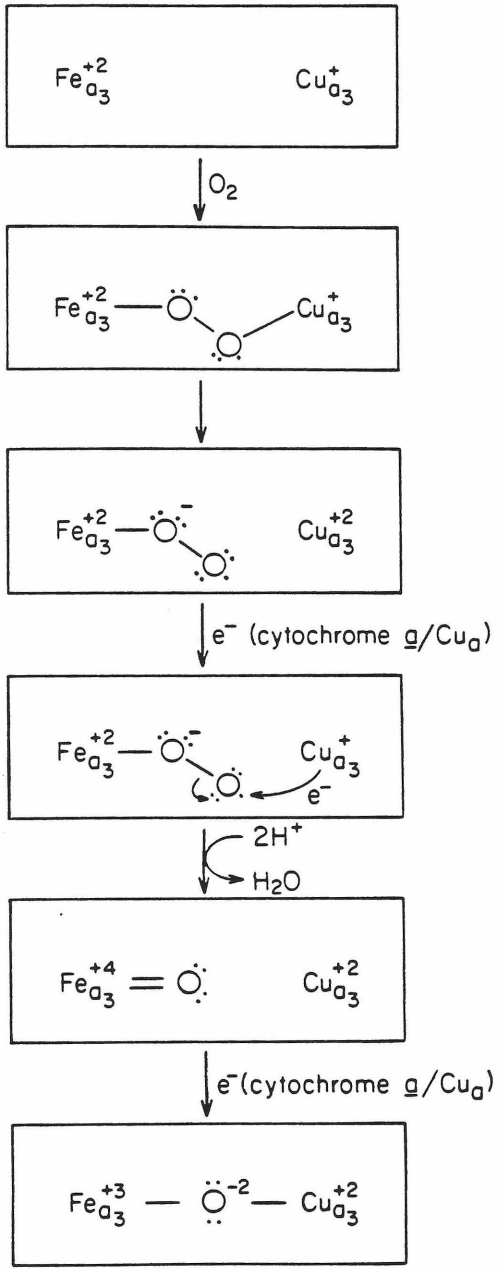

Figure 1. Proposed mechanism for the reduction of oxygen to water by cytochrome c oxidase (from Ref. 22).

the physical and chemical properties of such ligand adducts among various oxygen-utilizing proteins can help in understanding the differences and similarities in the oxygen-binding sites, and how structure influences function in these proteins. I will now outline the way in which this approach was used in the work described in the succeeding chapters of this thesis.

The studies described in Chapter II germinated with our interest in the detailed electronic structure of the oxyheme unit in reduced cytochrome c oxidase. Considerable effort has been invested in constructing a model for the bonding of oxygen to ferrous heme (23-26). It seems now to be accepted that oxygen binds to ferrous hemes in a bent geometry, as first proposed by Pauling (27). The bonding is accompanied by some transfer of electron density from Fe(II) to O_2 (23), although there is still some disagreement on this point (28). The bonding is best described as being due to a pairing between a singly occupied π^* orbital of the oxygen and the singly occupied d_{z^2} orbital of the iron, with additional "back-bonding" from the iron d_{yz} orbital, also singly occupied, into a π orbital of the oxygen to form a three-center, four-electron bond (24,25).

Nitric oxide, NO, has been a useful probe of the electronic structure of ferrous hemes. NO binds to ferrous hemes with a bent geometry, as does O_2. Since the resulting stable complex is paramagnetic, it can be studied by EPR spectroscopy. In Chapter II, I report on investigations of the EPR spectra of a variety of nitrosyl ferrous heme complexes. These investigations resulted in the discovery of a delicately

balanced equilibrium between two conformers in the inorganic heme complexes studied and in myoglobin, but not in cytochrome c oxidase. The nature of the conformational equilibrium, and its implication towards other studies of the structures of oxygen-binding hemeproteins, are discussed.

NO is also a potentially reactive molecule. It can be oxidized to nitrite, NO_2^-, with a reduction potential of about 370 mV at pH 7, and it can be reduced to N_2O with a reduction potential at pH 7, of 1.18 V. Brudvig et al. (22) have found that cytochrome c oxidase catalyzes several reactions of NO, and their findings regarding these reactions have implications for the structure of the oxygen-binding site and the mechanism of oxygen binding and reduction in this enzyme. Chapter III of this thesis describes an analogous study on the reactions of nitric oxide catalyzed by tree and fungal laccase. A catalytic cycle is set up describing the reactions of the laccases with NO, which differs qualitatively from the cycles deduced for the reactions of cytochrome c oxidase with NO.

Studies on the interactions of nitric oxide, in combination with other ligands, with cytochrome c oxidase, also resulted in the finding that three different stable conformations of the oxidized enzyme can be distinguished by EPR spectroscopy (20). Two of the diagnostic EPR signals for these conformations are rather unusual in that they cannot be interpreted simply in terms of normal copper or iron EPR signals. These signals, in view of their complexity, are most likely due to the coupled S = 2 spin center of the oxidized enzyme. Chapter IV describes

calculations of the energy levels of and EPR transitions from the cytochrome $\underline{a}_3$-Cu_{a_3} site under various conditions of exchange coupling, dipolar coupling, and so forth, to facilitate interpretation of these two unusual EPR signals, as well as a third signal arising from a transient species which occurs upon reoxidation of the reduced enzyme by O_2. The studies reported in this chapter are intended to shed further light on the unique features of the oxygen-binding site of cytochrome $\underline{c}$ oxidase.

Finally, Chapter V summarizes the conclusions arrived at in the preceding chapters regarding the nature of oxygen binding and reduction in the oxygen-carrying proteins and in the oxidases.

References

1. Himmelwright, R. S., Eickman, N. C., LuBien, C. D., Lerch, K., and Solomon, E. I. (1980) J. Am. Chem. Soc. 102, 7339-7344.
2. Fee, J. A. (1975) Struct. Bonding (Berlin) 23, 1-60.
3. Kirk, T. K., Harlein, J. M., and Cowling, E. B. (1968) Biochim. Biophys. Acta 165, 134-144.
4. Colman, P. M., Freeman, H. C., Guss, J. M., Murata, M., Norris, V. A., Ramshaw, J. A. M., and Venkatappa, M. P. (1978) Nature 272, 319-324.
5. Peisach, J. and Blumberg, W. E. (1976) Arch. Biochem. Biophys. 165, 691-708.
6. Reinhammar, B. (1979) Adv. Inorg. Biochem. 1, 91-118.
7. Dooley, D. M., Scott, R. A., Ellinghaus, J., Solomon, E. I., and Gray, H. B. (1978) Proc. Natl. Acad. Sci. U.S.A. 75, 3019-3022.
8. Reinhammar, B., Mulkin, R., Jensen, P. Karlsson, B., Andréasson, L.-E., Aasa, R., Vänngård, T., and Malmström, B. (1980) J. Biol. Chem. 255, 5000-5003.
9. Malmström, B. G. (1981) in "Oxidases and Related Redox Systems", T. E. King, H. S. Mason, and M. Morrison, eds., Oxford Press, in press.
10. Brändén, R., Deinum, J., and Coleman, M. (1978) FEBS Lett. 89, 180-182.
11. Brändén, R., and Deinum, J. (1977) FEBS Lett. 73, 144-146.

12. Slater, E. C., Van Gelder, B. F., and Minnaert, K. (1965) in "Oxidases and Related Redox Systems", T. E. King, H. S. Mason, and M. Morrison, eds., John Wiley and Sons, pp. 639-656.

13. Malmström, B. G. (1979) Biochim. Biophys. Acta 549, 281-303.

14. Blumberg, W. E. and Peisach, J. (1970) Wenner-Gren Cent. Int. Symp. Ser. 18, 219-225.

15. Chan, S. I., Bocian, D. F., Brudvig, G. W., Morse, R. H., and Stevens, T. H. (1978) in "Frontiers of Biological Energetics", vol. 2, P. L. Dutton, J. S. Leigh, Jr., and A. Scarpa, eds., Academic Press, pp. 883-888.

16. Chan, S. I., Bocian, D. F., Brudvig, G. W., Morse, R. H., and Stevens, T. H. (1979) in "Cytochrome Oxidase", T. E. King, Y. Orii, B. Chance, and K. Okunuki, eds., Elsevier, pp. 177-188.

17. Powers, L., Blumberg, W. E., Chance, B., Barlow, C. H., Leigh, J. S., Jr., Smith, J., Yonetani, T., Vik, S., and Peisach, J. (1979) Biochim. Biophys. Acta 546, 520-538.

18. Stevens, T. H. and Chan, S. I.(1981) J. Biol. Chem. 256, 1069-1071.

19. Stevens, T. H., Brudvig, G. W., Bocian, D. F., and Chan, S. I. (1979) Proc. Natl. Acad. Sci. U.S.A. 76, 3320-3324.

20. Brudvig, G. W., Stevens, T. H., Morse, R. H., and Chan, S. I. (1981) Biochemistry 20 (in press).

21. Chan, S. I., Stevens, T. H., Brudvig, G. W., and Bocian, D. F. (1980) in "Proceedings of the International Symposium on Frontiers in Protein Chemistry", T. Liu, K. T. Yasunobu, and G. Mamiya, eds., Elsevier, in press.

22. Brudvig, G. W., Stevens, T. H., and Chan, S. I. (1980) Biochemistry 19, 5275-5285.

23. Collman, J. P., Halbert, T. R., and Suslick, K. S. (1980), in "Metal Ion Activation of Dioxygen", T. G. Spiro, ed., Wiley-Interscience, pp. 1-72.

24. Olafson, B. D. and Goddard, W. A. III (1977) Proc. Natl. Acad. Sci. U.S.A. 74, 1315-1319.

25. Olafson, B. D. (1979) PhD Thesis, Caltech.

26. Reed, C. A. and Cheung, S. K. (1977) Proc. Natl. Acad. Sci. U.S.A. 74, 1780-1784.

27. Pauling, L. (1949) in "Haemoglobin", F. J. W. Roughton and J. C. Kendrew, eds., Butterworths Scientific Publications, pp. 57-65.

28. Desbois, A., Lutz, M., and Banerjee, R. (1979) Biochemistry 18, 1510-1518.

29. Van Camp, H. L., Wei, Y. H., Scholes, C. P., and King. T. E. (1978) Biochim. Biophys. Acta 537, 238-246.

CHAPTER II: EPR STUDIES OF NITROSYL FERROUS HEME COMPLEXES. DETERMINATION OF AN EQUILIBRIUM BETWEEN TWO CONFORMATIONS.*

Introduction

An understanding of the bonding of ligands, and oxygen in particular, to ferrous hemeproteins such as hemoglobin, cytochrome P-450, and cytochrome c oxidase, is prerequisite to elucidating the mechanisms by which they carry out their biological functions. In particular, a detailed description of ligand binding is critically necessary in the study of intermediates produced in the reduction of oxygen as catalyzed by one of these hemeproteins, cytochrome c oxidase.

The electronic environments of various hemeproteins and of model heme complexes have been investigated with some success using the ligand nitric oxide as a paramagnetic probe (1 - 17). NO forms a low-spin, six-coordinate complex as does O_2, and binds in a bent fashion as does O_2 (6,18 - 21). Furthermore, since the NO adducts of ferrous heme compounds are paramagnetic, unlike the oxygen and carbon monoxide adducts, they are amenable to study by EPR spectroscopy. Various authors have studied the dependence of the EPR spectra of the NO adducts of hemeproteins and inorganic heme complexes upon variation of the ligand trans to NO (1 - 3, 17), and upon variation of the heme environment (2,4,5,17). Although these studies have increased our understanding of the bonding and stereochemistry in these systems, many of the details of the electronic

*This chapter has appeared in slightly altered form in *J. Biol. Chem.* 255, 7876-7882 (1980).

structure of the NO-bound species remain unclear. In part, this lack of definitive conclusions is due to the difficulty in unambiguously interpreting EPR signals as complex as those observed for these species. However, a second obstacle to meaningful interpretation of the EPR spectra observed for nitrosyl heme compounds, which has been largely ignored, is the presence of at least two distinct signals in the spectra of most of these compounds.

The presence of a second distinct signal can be inferred from the observation of a fourth g-value, distinct from the three g-values assigned g_x, g_y and g_z, which arise from anisotropy in the g-tensor. This fourth g-value was originally labeled $g_?$ (4) and remained unexplained until very recently. Yoshimura et al. (3), in an excellent study, investigated the Q-band (35 GHz) and X-band (9 GHz) EPR spectra of the nitric oxide derivative of Fe(II)-(PPDME) in chloroform, using several imidazole derivatives as the second axial ligand. They varied the temperature and the imidazole base concentration, and concluded that the absorption previously called $g_?$ at g = 2.03, along with another absorption at g = 1.99, constitutes a second EPR signal which is favored at high temperature. The two signals were interpreted in terms of two different structures of base-heme-NO, varying in iron-NO and iron-base distances, and in the Fe-N-O angle. However, it was not determined whether the temperature dependence of the spectra reflected motional/relaxation effects or a chemical equilibrium.

To settle this point, and to characterize these species more

definitively, we have investigated the temperature dependence of the EPR spectra of the NO derivatives of Fe(II) protoporphyrin IX in dimethylsulfoxide (Me_2SO) and dimethylformamide (DMF), of myoglobin, of cytochrome c, and of cytochrome c oxidase. The spectra have been deconvoluted using the technique of factor analysis (25, 26), and the results demonstrate that the variation of the EPR spectra with temperature is due to an equilibrium between two species. Interpretation of the EPR signals then provides some information on the geometries and electronic structures of the complexes. Finally, the unusual behavior of the EPR spectra of the NO adduct of cytochrome c oxidase suggests a structural anomaly which is also discussed.

Experimental Procedures

Materials. Myoglobin from equine skeletal muscle (Sigma), horse heart cytochrome c (Sigma), and bovine hemin chloride (Aldrich) were used without further purification. DMF (Matheson, Coleman and Bell) was dried and distilled before use. All other chemicals used were obtained in reagent grade quality and used without further purification.

Beef-heart cytochrome c oxidase was isolated by the procedure of Hartzell and Beinert (22), and was stored at -85°C until used. The preparation contained 9 nmole heme a/mg protein as measured by the pyridine hemochromagen assay (23). The purified protein was dissolved in 0.5% Tween 20/50 mM Tris·NO_3/pH 7.4 buffer. Protein concentration was determined by the method of Lowry et al. (24).

Sample Preparation. The Fe(II) protoporphyrin IX samples were prepared according to the method of Kon and Kataoka (1). A few mg of the Fe(III) hemin chloride were first dissolved in either Me_2SO or DMF nearly saturated with imidazole. The solution was then transferred to an EPR tube and NO (Matheson) was added anaerobically to a pressure slightly under 1 atm. The samples were made anaerobic by at least two cycles of evacuation and flushing with argon. The samples were then allowed to incubate 40 - 60 minutes, during which reduction of the iron takes place. Excess NO was then removed and replaced by argon (Linde).

Myoglobin was dissolved in 10 mM sodium phosphate, pH 6.0, and was reduced anaerobically by addition of a few grains of sodium dithionite from a sidearm on the EPR tube. The protein solution was then allowed to incubate for at least 30 minutes to allow complete reduction before anaerobic addition of NO.

Cytochrome c (10 mg/ml = 0.7 mM), dissolved in 50 mM Tris·NO_3, pH 7.4 buffer, was reduced anaerobically by addition of excess sodium ascorbate (0.6 M, in 4 mM EDTA, pH 7.4 buffer) from a sidearm on the EPR tube and allowed to incubate 20 minutes before adding NO.

Cytochrome c oxidase was reduced by anaerobic addition of an excess of a solution of paraphenylene diamine and ascorbic acid from a sidearm in the EPR tube, NO was added anaerobically, and the enzyme was allowed to incubate for 60 minutes. Following this, the solution was frozen and the excess NO was evacuated and replaced by argon.

A second preparation of the NO adduct of cytochrome c oxidase was prepared according to the method of Yonetani et al. (4). A solution of

cytochrome c oxidase in an EPR tube with a sidearm containing an excess of $NaNO_2$ in solution was degassed, then the EPR tube was opened long enough to add an excess of paraphenylene diamine and either cytochrome c or ascorbate in solution. The sample was then immediately degassed again, argon was added, and the sample was shaken to mix the $NaNO_2$ with the reduced enzyme. The sample was then allowed to incubate for about 60 minutes. In this procedure, reduction of NO_2^- to NO occurs via the reaction

$$NO_2^- + 2H^+ + e^- \rightarrow H_2O + NO$$

where the electron is provided by reduced cytochrome c oxidase. The EPR spectrum shows that only the NO adduct of cytochrome c oxidase is formed, even in the presence of equimolar reduced cytochrome c, demonstrating that the formation of NO must occur at or near the binding site (cytochrome a_3) of cytochrome c oxidase, and that only one molecule of NO is formed per enzyme molecule.

All sample incubations described above were at room temperature, and protein samples were stored at -85^oC if the EPR spectra could not be obtained immediately.

EPR Spectra. EPR spectra were recorded on a Varian E-line Century series X band spectrometer equipped with an Air Products Heli-Trans low-temperature system. All spectra were obtained at microwave frequencies from 9.246 to 9.251 GHz, and at non-saturating microwave powers. The temperature of the cavity was measured immediately before and after obtaining each spectrum by inserting a calibrated thermocouple [chromel vs. gold (0.07 mole % Fe)] wire into the cavity.

Data Analysis. The EPR spectra obtained for most of the complexes studied varied with temperature. Each set of temperature-dependent spectra was then deconvoluted by using the technique of factor analysis (25,26). This technique may be used to extract the number of components, or factors, contributing to a given set of spectra (or other data). The factorization of data into its component parts will succeed only if the data are indeed factorable, and if whatever error is present is random.

We begin the analysis of the EPR data for a given complex by digitizing the spectra obtained at each of n temperatures. An m x n data matrix $\hat{D}$ may then be constructed whose columns comprise the digitized (m points) EPR spectra at each temperature. If the data are factorable, a given element of $\hat{D}$ may be written as

$$(1) \quad d_{ij} = \sum_{k=1}^{f} (r_{ik})(c_{kj}).$$

In this equation, f is the number of contributing factors (contributing EPR signals in the present instance). The elements r_{ik} belong to $\hat{R}$, an m x f matrix called the row matrix whose f columns comprise the digitized EPR signals contributing to the original data. The elements c_{kj} belong to $\hat{C}$, called the column matrix. According to equation (1), then, the f elements in the jth column of $\hat{C}$ tell how much each of the f columns of $\hat{R}$ contribute to the jth column (or spectrum) in the original data matrix, $\hat{D}$.

Equation (1) may be rewritten as a matrix equation:

$$(2) \quad \hat{D} = \hat{R}\hat{C}$$

In order to find $\underset{\wedge}{R}$ and $\underset{\wedge}{C}$, we must first calculate the covariance matrix Z, where

(3) $\underset{\wedge}{Z} = \underset{\wedge}{D}^T\underset{\wedge}{D}$

$\underset{\wedge}{D}^T$ being the transpose of $\underset{\wedge}{D}$. The eigenvalues of $\underset{\wedge}{Z}$ are then used to find the number of factors contributing to the original data. If there were no errors in the original data, the number of non-zero eigenvalues of $\underset{\wedge}{Z}$ would equal the number of contributing factors. However, error in the data causes all the eignevalues to be non-zero. The largest of these eigenvalues are associated with the eigenvectors contributing to the data; the eigenvectors associated with the smaller eigenvalues contain contributions from experimental error. Standard procedures are available for deciding which of the eigenvalues correspond to eigenvectors representative of the "true" data (25). Probably the most definitive method of assessing which of the original eigenvectors contribute significantly to the original data matrix is to reproduce the data using first the eigenvector associated with the largest eigenvalue, then the two largest, and so forth, until a good reproduction is obtained. In other words, we attempt to reproduce $\underset{\wedge}{D}$ by using equation (1), where f, the number of contributing factors, is varied (f = 1,2,3, ...). Continuing this procedure beyond the correct number of factors should not improve the data reproduction significantly.

Results

Temperature Dependence of EPR Spectra. The EPR spectra of Im-Heme-NO

in Me_2SO and of MbNO showed a temperature dependence similar to that observed by Yoshimura et al. (3) (Fig. 1.). The NO complex of ferrocytochrome c and Im-Heme-NO in DMF, not shown, exhibited similar behavior. We also found that the signals were fairly easily saturated at low temperatures (<20 K), and that the two distinct signals present (see below) exhibited different saturation behavior.

In order to determine whether the temperature dependence observed was due to the disappearance of a signal or signals with increasing temperature, we measured the area of each first derivative spectrum obtained by numerical double integration of the spectra. We found that the areas for all species examined, when corrected for power, gain and temperature, remained constant over the temperature range studied. This demonstrates that the temperature dependent changes observed in the EPR spectra of these compounds must be accounted for in terms of paramagnetic species which exhibit EPR signals throughout the range of temperatures studied.

Deconvolution of EPR Spectra. We next sought to determine how many distinct signals contributed to each spectral series and to deconvolute the spectra into the component signals. To accomplish this we applied the technique of factor analysis, which was described in the previous section.

The analysis was carried out using the EPR spectra obtained at various temperatures of MbNO, and of Im-Heme-NO in DMF and in Me_2SO, and we found that the data could in every case be accurately reproduced

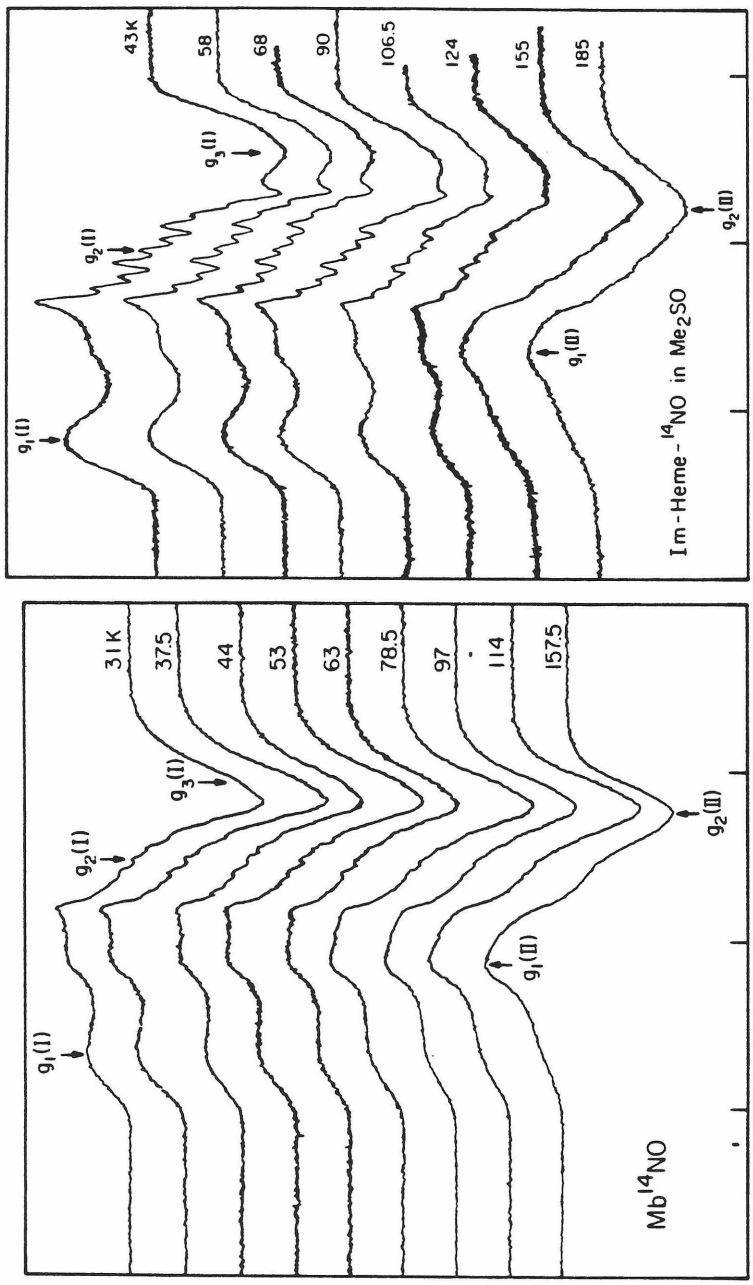

Figure 1. Temperature dependence of the EPR spectra of NO-ferroheme complexes. Left, MbNO; right, Im-Heme-NO in Me_2SO. All spectra were obtained at non-saturating microwave power, and the modulation amplitude used was 2.0 G for MbNO and 1.0 G for Im-Heme-NO in Me_2SO.

using only two row and column vectors. This confirmed the interpretation of Yoshimura et al. (3), i.e. that the EPR signals observed are due to contributions from two species. Furthermore, since the lineshape of the two signals remains constant, it is clear that the variation in the EPR spectra with temperature is due to an equilibrium between two species rather than to motional/relaxation effects. A few representative spectra are plotted in Fig. 2, along with the "spectra" generated by using two row and column vectors to reproduce the original data.

The row and column matrices resulting from the application of factor analysis represent abstract mathematical solutions and cannot, in general, be identified directly with physically significant quantities (the "true" component signals of the EPR spectra, in this case). Therefore, once these matrices have been obtained, the proper physically meaningful linear combinations of row vectors and of column vectors must be obtained.

Although there is no generally applicable method of finding the proper linear combinations, since it depends on the physical nature of the problem under investigation, two circumstances greatly simplified this task in the present instance. The first was that since there were only two contributing factors, the linear combinations could be effected by a simple two-dimensional rotation of the appropriate matrices. In addition, we were provided with a "target" EPR signal by the EPR spectrum of cytochrome c oxidase-NO shown in Fig. 3. This species, prepared by a method similar to that used by Yonetani et al. (4) (see Experimental

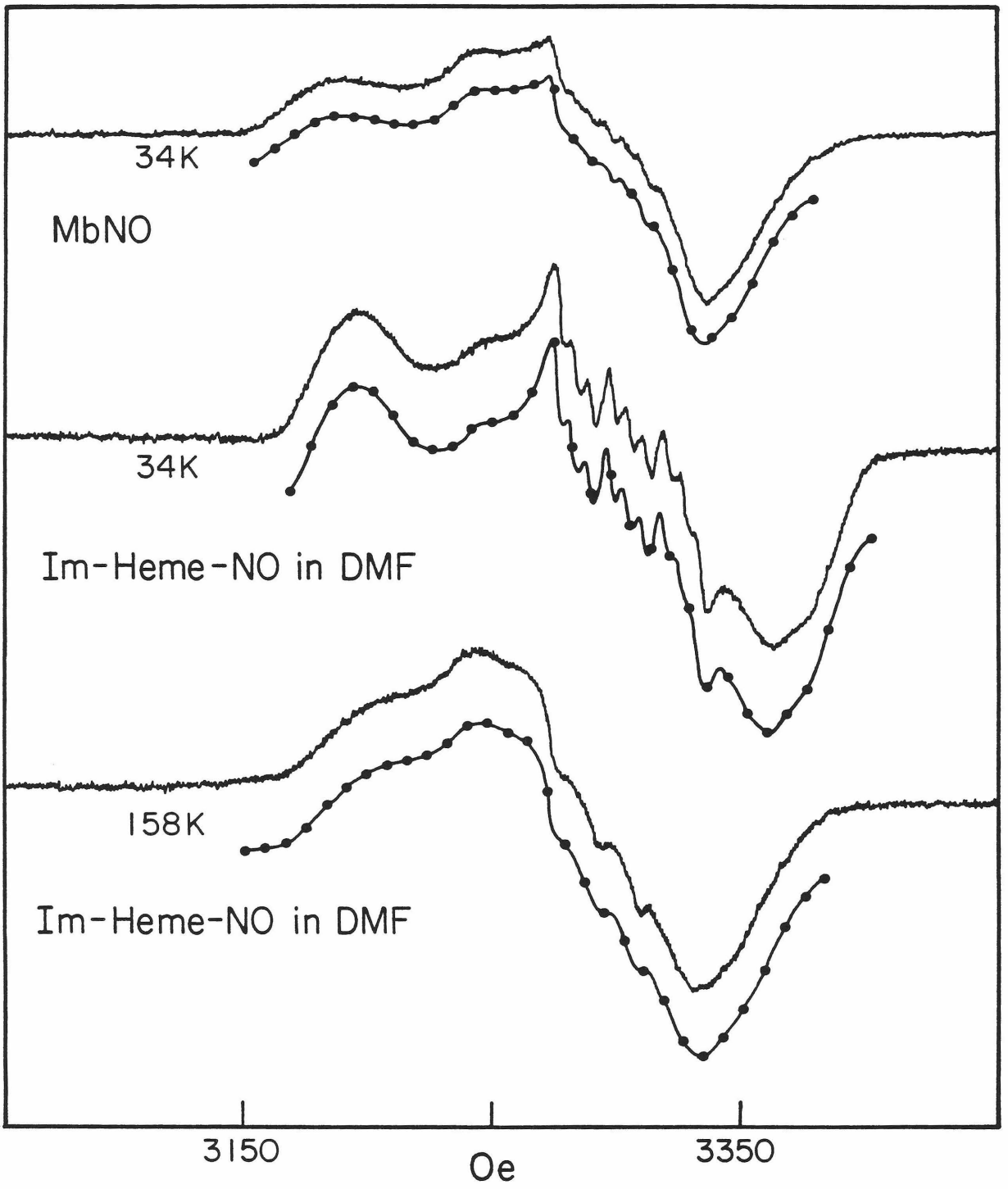

Figure 2: Reproduction of spectra using two component signals. Upper traces are original EPR spectra; lower traces were made by plotting digitized reproduced spectra (filled circles) and tracing original spectra through these points. Top, MbNO at 34 K; center and bottom, Im-Heme-NO in DMF at 34 K and 158 K, respectively.

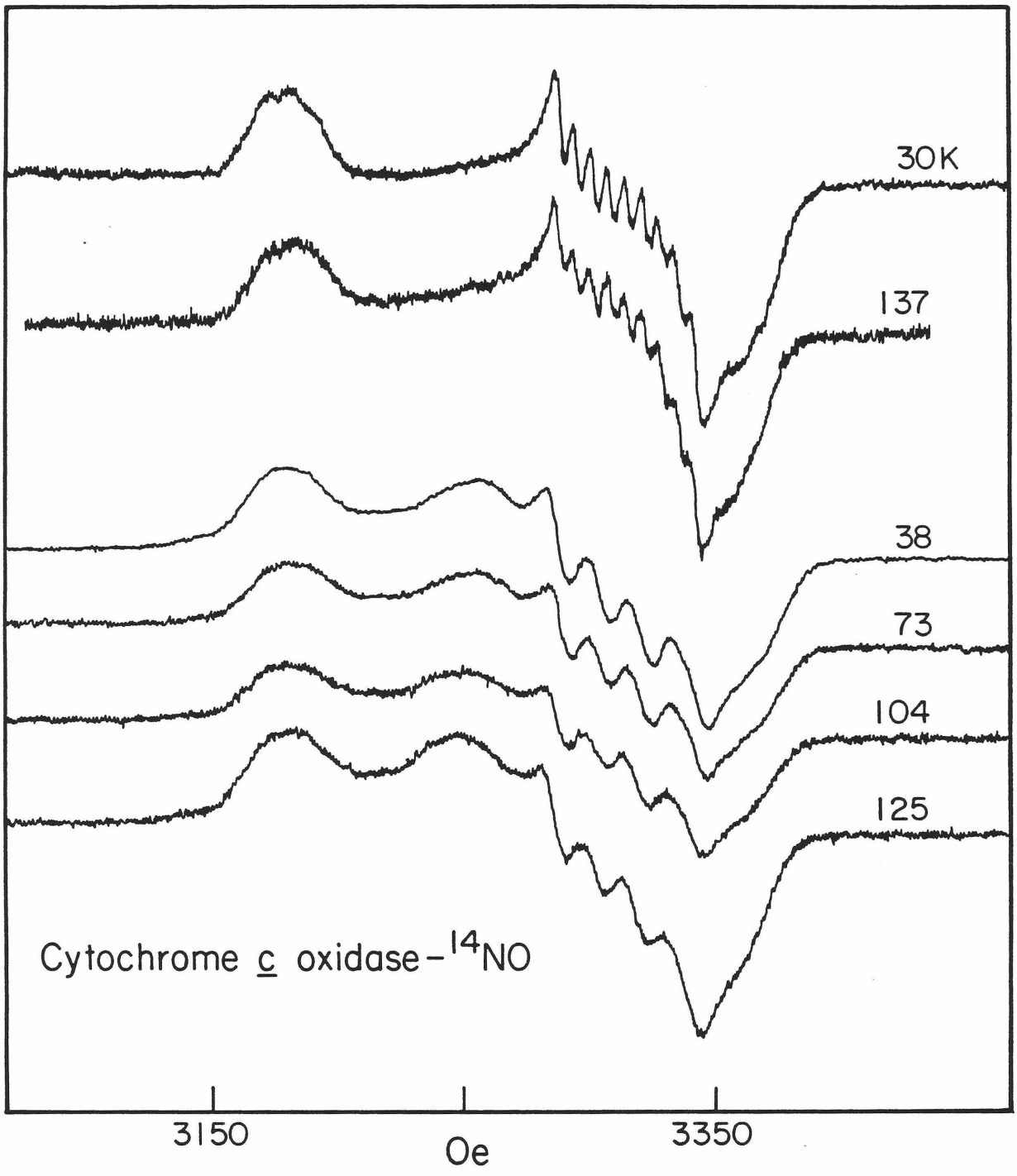

Figure 3: EPR spectra of cytochrome c oxidase-^{14}NO. The sample exhibiting the upper spectra was prepared by the method of Yonetani et al. (4); the lower spectra are due to a sample prepared by anaerobic addition of NO gas to the reduced enzyme. The modulation amplitude in the upper spectra was 2.0 G; in the lower spectra, 10 G.

Procedures), exhibits only three g-values. We interpreted this and the temperature independence of the spectrum as indicating that only one species was present in this preparation, and therefore used the signal seen in Fig. 3 as an approximation of one of the true contributing signals, or row vectors.

The row vectors we obtained for one of the two contributing signals of each species proved to be similar to the cytochrome c oxidase-NO EPR spectrum. The row vectors corresponding to the true contributing signals were chosen on the basis of providing the most reasonable EPR signals, and of giving the best fits to the thermodynamic equations discussed below. These artificially generated signals were graphed in Fig. 4, and their g-values and hyperfine splittings are given in Table I.

Thermodynamic Analysis: The elements of the "true" column matrix give the ratio in which the contributing EPR signals combine to give the observed EPR spectra at each temperature, for each complex examined. Since we normalized the contributing signals, the ratios provided by the column matrix must give the equilibrium constant K(T) at each temperature used for the equilibrum

$$I \rightleftharpoons II$$

where I is the species with EPR signal R_1 and II the species with EPR signal R_2 (see Fig. 4). The temperature dependence of the equilibrium constant then affords a means of investigating the thermodynamics of the system under consideration.

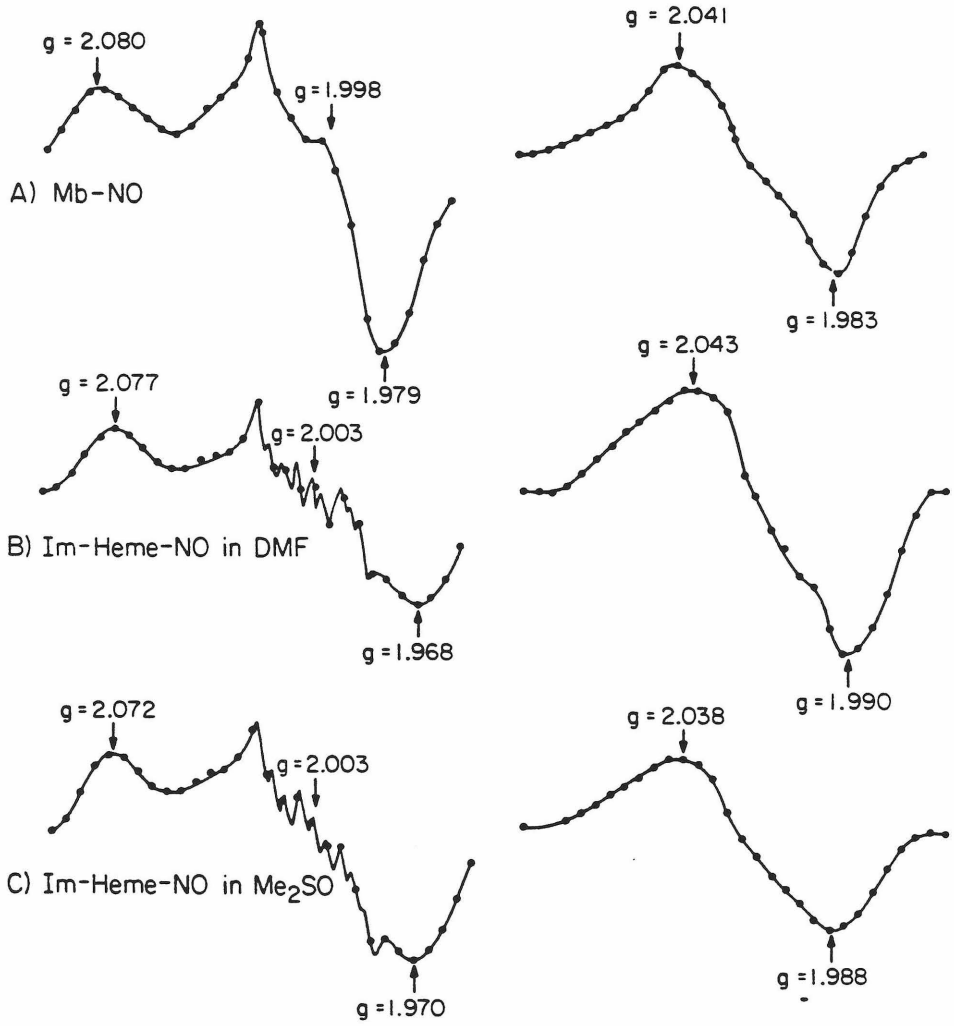

Figure 4: The two component signals present in the EPR spectra of NO-ferroheme complexes. The curves on the left are designated R_1 in the text and assigned to species I; those on the right are called R_2 and assigned to species II. (A) MbNO; (B) Im-Heme-NO in DMF; (C) Im-Heme-NO in Me_2SO. The hyperfine splittings in R_1 of (B) and (C) were added in accordance with the hyperfine splittings observed in the original spectra.

TABLE I

EPR Parameters for Five- and Six-Coordinate Nitrosyl Ferroheme Complexes

	g_1	g_2	g_3	A_1(G)	A_2(G)
Type I	2.07	2.004	1.97	21	7
Type II	2.03	1.99	-	16	
Type III[a]	2.09	2.06	2.010	15.8[b]	

[a] Ref. (3).

[b] A_{iso}

The simplest form that K(T) can take is

$$\ln K(T) = - \frac{\Delta H^o}{RT} + \frac{\Delta S^o}{R}$$

where the entropy change ΔS^o and enthalpy change ΔH^o associated with the interconversion of species I and II are assumed to be independent of temperature. However, the graph of ln K(T) vs. 1/T did not yield a linear plot for any of the complexes examined. Considering the large temperature range studied, this nonlinearity was not surprising. A more general form for the temperature dependence of K(T) is

$$(4) \quad \ln K(T) = - \frac{\Delta H^o(0)}{RT} + \frac{\Delta a}{R} \ln T + \frac{\Delta b}{2R} T + \frac{\Delta S^o(0)}{R}$$

where it has been assumed that

$$(5) \quad \Delta H^o(T) = \Delta H^o(0) + \int_0^T \Delta C_p(T')dT'$$

and

$$\Delta C_p(T) = \Delta a + (\Delta b)T \ .$$

We were able to fit the K's obtained from the column matrices to equation (4) within reasonable error limits, as shown in Fig. 5. Due to the inherent uncertainty in the generation of the column matrices, the parameters obtained do not provide exact thermodynamic data, but rather are only indicative of the magnitudes of these quantities. It turns out that Δa and Δb are both very small, as expected, and $\Delta H^o(0)$ for this equilibrium is on the order of a few kcal/mole or less.

Cytochrome c oxidase. The EPR spectrum of the NO adduct of reduced

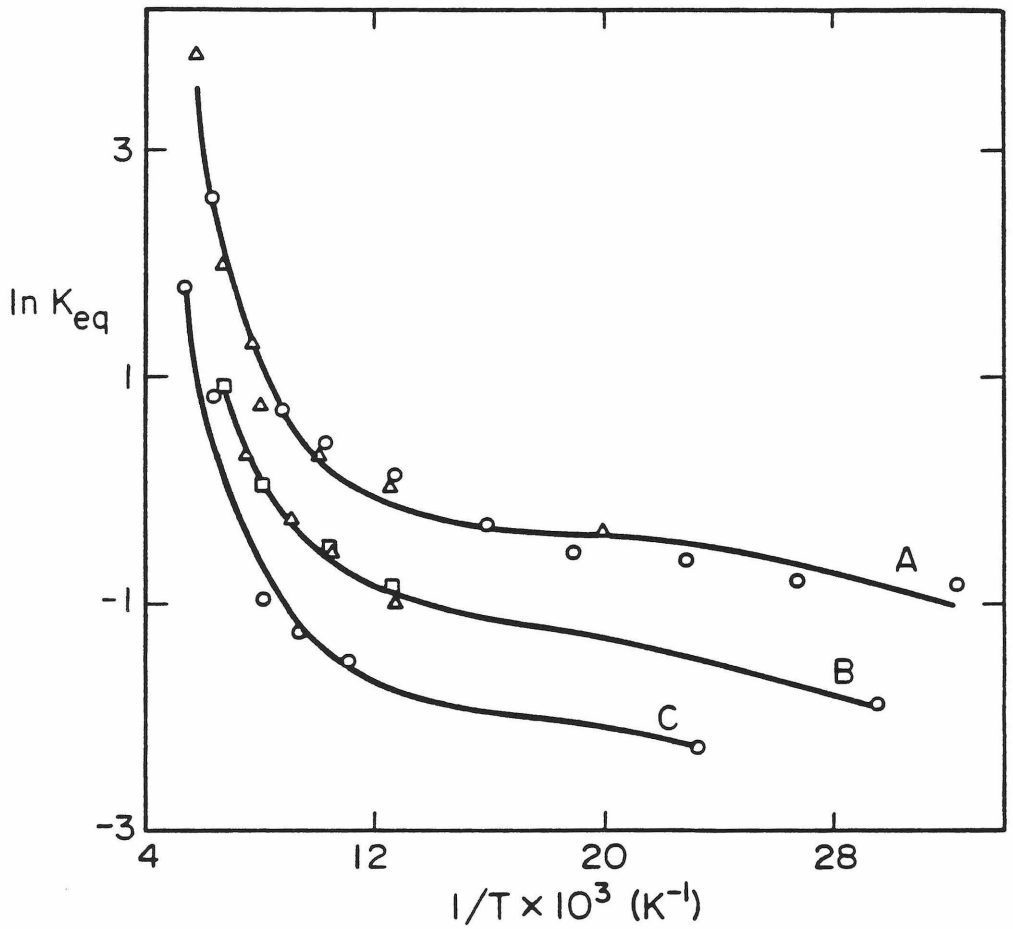

Figure 5: Graph of ln K_{eq} vs 1/T for the reaction I ⇌ II. In curves A and B, the two symbols present are for data from two separate experiments. The solid lines are theoretical fits using eq. (5) in the text. (A) MbNO: Δa = - 25 cal K^{-1} mol^{-1}, Δb = 0.5 cal K^{-1} mol^{-1}, $\Delta H^o(0)$ = 720 cal mol^{-1}, and $\Delta S^o(0)$ = 100 cal K^{-1} mol^{-1}. (B) Im-Heme-NO in DMF; Δa = -17 cal mol^{-1}, Δb = 0.3 cal K^{-1} mol^{-1}, $\Delta H^o(0)$ = 570 cal mol^{-1}, and $\Delta S^o(0)$ = 70 cal K^{-1} mol^{-1}. (C) Im-Heme-NO in Me_2SO; Δa = -23 cal mol^{-1}, Δb = 0.4 cal K^{-1}, $\Delta H^o(0)$ = 730 cal mol^{-1}, and $\Delta S^o(0)$ = 90 cal K^{-1} mol^{-1}.

cytochrome c oxidase, prepared by the method of Yonetani et al. (4) described in the Experimental Procedures section, is shown in Fig. 3. Clearly, only three g-values are exhibited in the spectrum, independent of temperature. Other preparations of this species, particularly those prepared by anaerobic addition of NO gas to the reduced enzyme, exhibit varying amounts of a second signal resembling R_2 along with the signal seen in Fig. 3. However, an important difference between these latter preparations of cytochrome c oxidase and the other complexes studied is that the ratio between the two signals exhibits no variation with temperature for the cytochrome c oxidase preparations.

Discussion

We have shown that the temperature dependence of the EPR spectra exhibited by various nitrosylferroheme compounds is consistent with a thermal equilibrium between two species with EPR signals approximated by R_1 and R_2 (Fig. 4 and Table I). It is likely that both species I, with EPR signal R_1, and species II, with EPR signal R_2, are six-coordinate. The EPR spectrum of five-coordinate HbNO has been recently obtained by Hille et al. (15) and is shown in Fig. 6. The spectrum is similar to the known five-coordinate complex NO-Fe(II) (PPDME) (12), and is clearly different from both the Type I and II EPR signals. The characteristic g-values and hyperfine splittings of this signal, which we call Type III, are tabulated in Table I. A Type III signal is also exhibited by HbNO Milwaukee in the presence of inositol hexaphosphate (5), and by

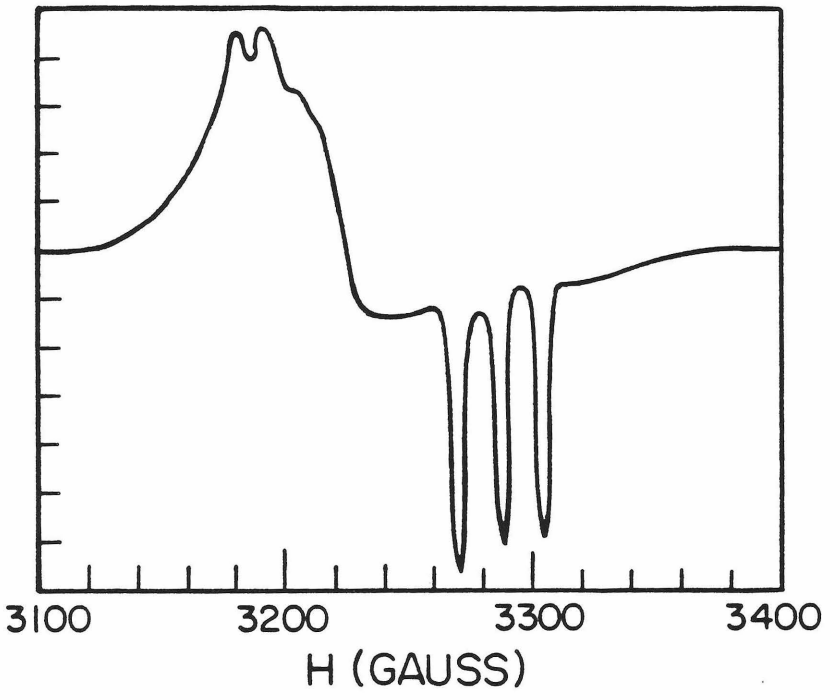

Figure 6: Standard spectrum of five-coordinate, or Type III, nitrosylferroheme. The spectrum was obtained from HbNO by a subtraction procedure, and is redrawn from Hille et al. (15).

NO-Fe(II)(PPDME) in the presence of bases such as quinoline derivatives, 2,6-xylidine (4), and hindered imidazole bases (3). The former compound has been implicated as being five-coordinate in the presence of inositol hexaphosphate on the basis of infrared measurements of NO stretching frequencies (16), and the bases used in the latter compounds as potential sixth ligands are likely to be non-coordinating due to steric repulsions. Furthermore, the three-line hyperfine splitting indicates that there is essentially no delocalization of the unpaired spin onto the imidazole nitrogen. Hence, the Type III signal, in which all three g-values are greater than g_e, is seen to arise from five-coordinate NO-ferroheme complexes.

Our assignment of species I and II follows the arguments of Yoshimura et al. (3). These authors have observed that the equilibrium constant at room temperature for the reaction

$$\text{NO-Fe(II)(PPDME)} + \text{NMeIm} \rightleftharpoons \text{NO-Fe(II)(PPDME)-NMeIm}$$

is small ($K \sim 2\ M^{-1}$), indicating that the iron-base bond in species II is relatively weak. This is consistent with available X-ray crystallographic data obtained at room temperature; the displacement of the iron atom from the heme plane in the NO-Fe(TPP) complexes with 1-methylimidazole (20) and 4-methylpiperidine (18) is towards NO by 0.07 and 0.11 Å, respectively. Also, the 9-line hyperfine splitting observed in the Type I signal of most species, originating from the interaction of the unpaired electron with the ^{14}NO nitrogen and the ^{14}N nucleus of the axial base trans to NO, suggests that the unpaired electron has considerable interaction with the

axial base nitrogen in species I and very little with that nitrogen nucleus in species II.

These observations suggest that the bond distance between iron and base nitrogen is greater in II than in I, and that the iron-NO distance is greater in I than in II. We have depicted schematically the two species in Fig. 7. The equilibrium between them could reasonably occur in frozen solution, and the estimates obtained for $\Delta H^{o}(0)$ ($\lesssim$3 kcal/mol) and the parameters $\Delta\underline{a}$ and $\Delta\underline{b}$ giving ΔC_p as a function of temperature (eq. 6) ($|\Delta a| \lesssim 40$ cal/mol; $|\Delta b| \lesssim 1$ cal mol^{-1} K^{-1}) are consistent with what one might expect for this equilibrium. Moreover, X-ray crystallographic data indicate that the heme iron can indeed be on opposite sides of the heme plane for similar compounds. For example, room temperature measurements show that the iron atom in O_2-Fe(II)(TPivPP)-1-MeIm is displaced 0.03 Å towards oxygen (21), whereas at -12°C the iron atom in oxygenmyoglobin is displaced 0.33 Å towards the coordinated imidazole (27).

The bonding of NO to various ferroheme compounds has been discussed by several authors, but it is now clear that for most NO-ferroheme complexes there must exist two stable conformations with different bonding characteristics. A number of authors have discussed the bonding of NO-ferroheme complexes in terms of a scheme in which the unpaired electron is localized in the iron d_{z^2} orbital (1,2,8); but, as Dickinson and Chien have pointed out (7), this is inconsistent with the observation of g-values less than g_e. A second possible bonding scheme is that designated Type I by Trittelvitz et al. (2) and represented by the molecular orbital

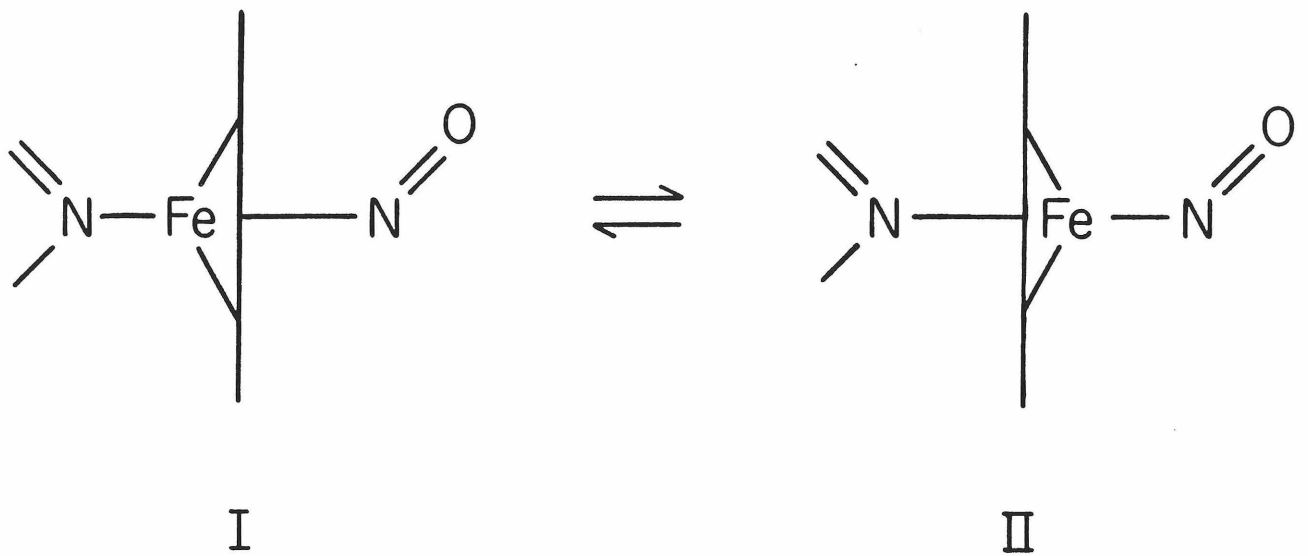

Figure 7: Proposed model for the equilibrium between species predominating at low temperature (I) and higher temperature (II) in base-ferroheme-NO complexes exhibiting temperature dependent EPR spectra. Vertical line represents the porphyrin plane.

diagram of Fig. 8. This scheme corresponds to the configuration $(d_{xz})^2(d_{xy})^2(d_{z2})^2(d_{yz})^1$, which gives rise to the g-values

$$g_{xx} = 2.002 + 6\lambda\beta^2\delta^2/\Delta E_{z^2\rightarrow yz} - 2\lambda\beta^2\varepsilon^2/\Delta E_{yz\rightarrow x^2-y^2}$$

$$(6) \quad g_{yy} = 2.002 + 2\lambda\beta^2\gamma^2/\Delta E_{xy\rightarrow yz}$$

$$g_{zz} = 2.002 + 2\lambda\alpha^2\beta^2/\Delta E_{xz\rightarrow yz}$$

where λ, the one-electron spin-orbit coupling constant for Fe(II), is >0 ($\lambda_o = 390\ cm^{-1}$), and α, β, γ, δ and ε are the "orbital reduction factors" for the d_{xz}, d_{yz}, d_{xy}, d_{z^2}, and $d_{x^2-y^2}$ orbitals, respectively. These factors fall between 0 and 1, and are used to account for reduction in the anisotropy of the g-tensor due to covalency between metal and ligands (28). Second order terms in λ have been neglected. If

$\frac{\varepsilon^2}{\Delta E_{yz\rightarrow x^2-y^2}} > \frac{3\delta^2}{\Delta E_{z^2\rightarrow yz}}$ in eq. (6), then g_{xx} will be less than g_e, as observed. Although this seems a little unlikely in that the separation between the d_{z^2} and d_{yz} energy levels must be greater than that between the d_{z^2} and $d_{x^2-y^2}$ energy levels, it cannot be ruled out entirely. In addition, if this configuration is to represent species I, then g_{yy} or g_{zz} must be very close to g_e, either through a large orbital reduction of the d_{xz} or d_{xy} orbitals, or through a large energy difference between the d_{xz} and d_{yz} orbitals (according to Fig. 8). It is unlikely that either of these effects could account for the observed g-values, and so

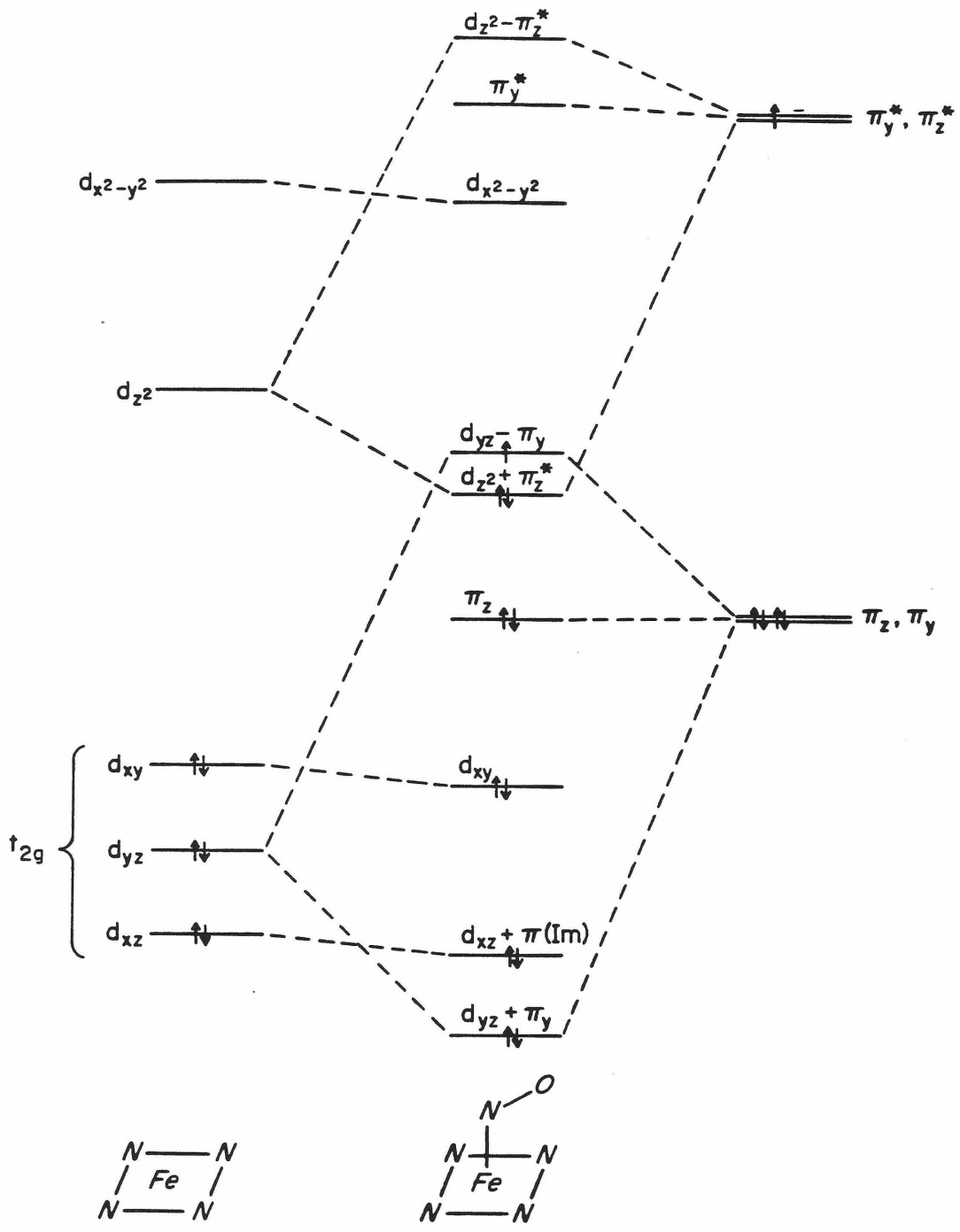

Figure 8: Qualitative molecular orbital diagram for six-coordinate NO-ferroheme-imidazole complexes. This scheme is a modified version of that presented by Trittelvitz et al. (2).

it appears that the g-values of species I cannot be explained on the basis of the configuration $(d_{xz})^2(d_{xy})^2(d_{z^2})^2(d_{yz})^1$. The g-values of species II, however, could be accounted for by this configuration as long as g_{zz} and g_{yy} are almost identical, which could occur of the d_{xz} and d_{xy} orbitals were close enough in energy.

We have also calculated the expressions for the g-values assuming the separation between the $d_{z^2} + \pi_z^*$ and $d_{yz} - \pi_y$ orbitals is on the order of λ, the spin-orbit coupling (see Appendix I). The g-values calculated again fail to satisfactorily account for the observed g-values. Specifically, the values of $\Delta E_{yz \rightarrow x^2-y^2}$ that result from the new expression for g_{xx} are too small to be reasonable (on the order of 1000 cm^{-1}), regardless of which g-value of either species under consideration is assigned to g_{xx}. A similar calculation in which the energies of the $d_{z^2} + \pi_z^*$ and $d_{yz} - \pi_y$ orbitals were reversed also failed to reproduce the experimental g-values of either species.

It may be that mixing of other states, such as a d^5 iron-NO^- configuration, into the ground state must be considered, or that spin-orbit coupling from the NO moiety contributes to the observed g-anisotropy, in which case calculations more detailed than those we have undertaken here would be necessary to calculate g-values. In any case, it is apparent that although the molecular orbital scheme of Fig. 8 may remain intuitively plausible, it is too simple to account for the observed g-values of species I and II.

Although we began this part of the discussion by assuming that

species I and II were similar enough that they might be considered to have identical bonding characteristics, this assumption is clearly a first approximation. We now address the issue of how the two conformations differ significantly in their bonding characteristics.

First, the charge on the iron atom in the two species is likely to be different. The net transfer of charge between iron and NO in either species will be the sum of the NO→iron transfer, through the sigma bond, and the iron→NO charge transfer, through $d\pi - p\pi$ back-bonding. In species I, the $d\pi - p\pi$ interaction between Fe and NO must be reduced far more than is the $d_{z^2} - \pi^*_z$ interaction, compared to species II. Since the $d_{xz} - p\pi$ (imidazole) interaction probably involves little charge transfer, this implies that the iron atom in species II is likely to be more positively charged than in species I. In view of this, it may be that mixing of d^5 iron-NO^- configuration into the ground state must be considered, particularly for species II (see above).

A second obvious difference between the two species can be gleaned from the g-value anisotropy; species I exhibits three distinct g-values, whereas II is apparently of nearly axial symmetry. This could be due to a coincidental near degeneracy of orbital energies in species II, or could arise if the Fe-N-O unit of I were frozen on the EPR time scale and that of II were freely able to rotate. A more nearly linear Fe-N-O conformation in species II could also give rise to its smaller anisotropy. A few nitrosylheme compounds have been studied by X-ray crystallography; for NO-Fe(TPP)-4-methylpiperidine (18), NO-Fe(TPP)-NMeIm (19), and HbNO (20), the Fe-N-O angles at room temperature were found to be 140°, 142°,

and 145°, respectively. Chien found in an EPR study of single crystal MbNO that at 78 K the Fe-N-O angle was only 110° (6). The EPR spectra he obtained indicate that species I was predominant. Thus, from this data it appears that the Fe-N-O unit in species II may be more nearly linear than in species I. This will cause a reduction in the anisotropy by making the iron d_{xz} and d_{yz} orbitals more nearly equivalent in energy.

In summary, three points emerge from the results of this study. First, data on oxyheme complexes have always been interpreted in terms of a single species. However, considering the resemblance of oxyheme complexes to the analogous nitrosylheme complexes, it is entirely conceivable that there exists more than one stable conformation of these as well. Data obtained at different temperatures may not be due to the same species.

The next point is related to the question of biological relevance. Previous studies of nitrosylheme complexes done at low temperatures which were intended to serve as model studies of corresponding oxyheme complexes, we see now, may be deceiving in that they provide information on a conformation unfavored at biologically relevant temperatures. It is likely that species II of the NO-heme complexes, favored at higher temperature, is closer in conformation to the oxyheme complexes near room temperature than is species I. The best evidence for this is that the iron displacement from the heme plane at room temperature for O_2-Fe(II)(TpivPP)-1-MeIm was measured to be 0.03 Å towards oxygen (21), and in NO-Fe(TPP)-4-methylpiperidine it is 0.07 Å towards NO (18). Thus, results obtained at low temperature on the nitrosyl complexes of ferroheme

compounds may not necessarily be as applicable towards understanding the biologically interesting oxygen complexes as was hoped.

A final point stems from the constancy with change in temperature of the EPR spectrum of the NO adduct of cytochrome c oxidase. This anomalous behavior indicates a large relative stabilization of species I over species II.

The heme iron of cytochrome a_3, which is the only heme in cytochrome c oxidase that binds exogenous ligands such as NO, is known to be coordinated to histidine as the sixth axial ligand (29). This makes it similar in this respect to myoglobin, and to the inorganic complexes used in this study, which had imidazole bound as the sixth ligand, so the difference in the temperature dependence of the EPR spectrum must lie elsewhere. It could also be due to the unusual structure of prophyrin A (30), but that seems unlikely in view of the results of Yonetani et al. (4). Their study shows that the EPR parameters of the nitric oxide complexes of ferrous Hb and Mb are not significantly affected by substitution of meso- or deuteroheme for protoheme at 77 K, indicating that the equilibrium between species I and II is insensitive to the porphyrin ring substituents. However, they did not substitute heme a or any other heme containing a formyl group on the porphyrin ring, so this conclusion is not as strong as it might be.

In light of recent results indicating the existence of a nitric oxide bridged species of cytochrome c oxidase, i.e. $Fe^{2+}_{a_3}$ - NO - $Cu^{2+}_{a_3}$, in which only the cytochrome a_3 site is reduced (31), it is interesting to

speculate that the stabilization of species I over II in the NO complex of cytochrome c oxidase may be due to interaction between $Cu^{+}_{a_3}$ and the oxygen of NO. That is, in the reduced enzyme, NO may bridge cytochrome a_3 and Cu_{a_3}, which are known to be the only binding sites in the enzyme for externally added ligands (32). This hypothesis is consistent with models that have been advanced of the initial binding of oxygen to cytochrome a_3, and the subsequent reduction of O_2 to water (33,34). Although some preparations of the NO adduct of reduced cytochrome c oxidase exhibit some of the Type II EPR signal, we believe this is due to an NO complex involving the enzyme in a different conformation. The Type II EPR signal is more predominant in preparations made by addition of NO gas than in preparations made by adding solubilized nitrite to the enzyme, and the former procedure is a harsher treatment. As noted earlier, these preparations also exhibit no variation with temperature in their EPR spectra.

It is interesting to note that the EPR spectra of the nitrosyl adducts of cytochrome c peroxidase and horseradish peroxidase exhibit no Type II signal in their EPR spectra at 77 K (4), and that NO-cytochrome P-450 exhibits almost none of this signal (10). Furthermore, NO-cytochrome c peroxidase exhibits no Type II EPR signal from 93 - 153 K (35). Although these enzymes have no metal center analogous to Cu_{a_3} in cytochrome c oxidase to stabilize species I over species II, it may be that hydrogen bonding from an amino acid side chain to the NO-oxygen could provide such stabilization. Such a hydrogen bond has been proposed for NO-catalase by Schonbaum and Chance (36).

References

1. Kon, H. and Kataoka, N. (1969) Biochemistry 8, 4757-4762.
2. Trittelvitz, E., Gersonde, K. and Winterhalter, K. H. (1975) Eur. J. Biochem. 51, 33-42.
3. Yoshimura, T., Ozaki, T., Shintani, Y. and Watanabe, H. (1979) Arch. Biochem. Biophys. 193, 301-313.
4. Yonetani, T., Yamamoto, H., Erman, J. E., Leigh, J. S., Jr. and Reed, G. H. (1972) J. Biol. Chem. 247, 2447-2455.
5. John, M. E. and Waterman, M. R. (1979) FEBS Lett. 106, 219-222.
6. Chien, J. C. W. (1969) J. Chem. Phys. 51, 4220-4227.
7. Dickinson, L. C. and Chien, J. C. W. (1971) J. Am. Chem. Soc. 93, 5036-5040.
8. Wayland, B. B. and Olson, L. W. (1974) J. Am. Chem. Soc. 96, 6037-6041.
9. Blokzijl-Homan, M. F. J. and Van Gelder, B. F. (1971) Biochim. Biophys. Acta 234, 493-498.
10. O'Keeffe, D. H., Ebel, R. E. and Peterson, J. A. (1978) J. Biol. Chem. 253, 3509-3516.
11. Nagai, K., Hori, H., Yoshida, S., Sakamoto, H. and Morimoto, H. (1978) Biochim. Biophys. Acta 532, 17-28.
12. Yoshimura, T. (1978) Bull. Chem. Soc. Japan 51, 1237-1238.
13. Kon, H. (1968) J. Biol. Chem. 243, 4350-4357.
14. Kon, H. (1969) Biochem. Biophys. Res. Commun. 35, 423-427.
15. Hille, R., Olson, J. S. and Palmer, G. (1979) J. Biol. Chem. 254, 12110-12120.

16. Maxwell, J. C. and Caughey, W. S. (1976) Biochemistry 15, 388-396.

17. Nagai, K., Hori, H., Morimoto, H., Hayashi, A. and Taketa, F. (1979) Biochemistry 18, 1304-1308.

18. Scheidt, W. R., Brinegar, A. C., Ferro, E. B. and Kirner, J. F. (1977) J. Am. Chem. Soc. 99, 7315-7322.

19. Piciulo, P. L., Rupprecht, G. and Scheidt, W. R. (1974) J. Am. Chem. Soc. 96, 5293-5295.

20. Deatherage, J. F. and Moffat, K. (1979) J. Mol. Biol. 134, 401-417.

21. Jameson, G. B., Rodley, G. A., Robinson, W. T., Gagne, R. R., Reed, C. A. and Collman, J. P. (1978) Inorg. Chem. 17, 850-857.

22. Hartzell, C. R. and Beinert, H. (1974) Biochim. Biophys. Acta 368, 318-338.

23. Takemori, S. and King, T. E. (1965) J. Biol. Chem. 240, 504-513.

24. Lowry, O. H., Rosebrough, N. J., Farr, A. L. and Randall, R. J. (1951) J. Biol. Chem. 193, 265-275.

25. Malinowski, E. R. (1977) Anal. Chem. 49, 606-612.

26. Malinowski, E. R. (1977) Anal. Chem. 49, 612-617.

27. Phillips, S. E. V. (1978) Nature 273, 247-248.

28. Owen, J. and Thornley, J. H. M. (1966) Reports Prog. Phys. 29, 675-728.

29. Stevens, T. H. and Chan, S. I. (1981) J. Biol. Chem. 256, 1069-1071.

30. Caughey, W. S., Smythe, G. A., O'Keeffe, D. H., Maskasky, J. E. and Smith, M. L. (1975) J. Biol. Chem. 250, 7602-7622.

31. Stevens, T. H., Brudvig, G. W., Bocian, D. F. and Chan, S. I. (1979) Proc. Natl. Acad. Sci. U.S.A. 76, 3320-3324.

32. Malström, B. G. (1979) Biochim. Biophys. Acta 549, 281-303.

33. Erecinska, M. and Wilson, D. F. (1978) Arch. Biochem. Biophys. 188, 1-14.

34. Ochiai, E. (1975) J. Inorg. Nucl. Chem. 37, 1503-1509.

35. Yonetani, T. (1971) in Probes of Structure and Function of Macromolecules and Membranes (Chance, B., Yonetani, T. and Mildvan, T. S., eds) Vol. 2, pp. 545-552, Academic, New York.

36. Schonbaum, G. R. and Chance, B. (1976) Enzymes 13, 3rd Ed., pp. 363-408, Academic, New York.

CHAPTER III: REACTIONS OF NITRIC OXIDE WITH TREE AND FUNGAL LACCASE.

Introduction

The laccases are copper-containing oxidases which, like cytochrome c oxidase, can reduce dioxygen to two molecules of water (1). The two varieties studied most often are obtained from the oriental lacquer tree Rhus vernicifera and from the white-rot fungus Polyporus versicolor. They both contain four copper ions per molecule. In the oxidized enzymes, two of these ions (types 1 and 2 Cu^{+2}), are detectable by EPR. The type 1 Cu^{+2} ions are characterized by unusually strong optical absorptions around 600 nm, which disappear on reduction, and by EPR spectra with small hyperfine splitting constants ($|A_z| < 0.010$ cm^{-1}). The type 2 Cu^{+2} ions have more normal EPR spectra and, as they lack strong optical bands, these Cu^{+2} ions can only be monitored by EPR. The two EPR-detectable Cu^{+2} ions are the primary acceptors of electrons from the reducing substrates.

The two copper ions which are not detectable by EPR in the oxidized enzymes, called type 3, constitute an antiferromagnetically coupled binuclear Cu^{+2} - Cu^{+2} unit (2,3) which functions as the dioxygen reducing site. Exchange coupled binuclear centers are also found in many other proteins capable of reacting with dioxygen. Thus, binuclear copper centers are present in another blue oxidase, ceruloplasmin; in the mixed-function oxidase, tyrosinase; and in the oxygen-transporting protein, hemocyanin. In cytochrome c oxidase, the dioxygen-reducing site is the copper-heme unit, Cu_{a_3}-cytochrome a_3 (5,6).

Nitric oxide (NO) has been utilized extensively as a spin probe in the study of such dioxygen-reactive centers. For example, direct evidence for the presence of copper pairs has been derived from the investigation of NO complexes with ceruloplasmin (7,8), hemocyanin (9,10) and tyrosinase (9). Furthermore, Brudvig et al. (11) have found that cytochrome c oxidase catalyzes several reactions of NO, and a study of these has yielded significant clues to the mechanisms of dioxygen binding and reduction in this enzyme.

Only limited information is available on the reaction of NO with the laccases. Rotilio et al. (12) have shown that NO reduces the type 1 Cu^{+2} in tree laccase, and Dooley et al. (13) have exploited this result to obtain a pure type 2 Cu^{+2} EPR spectrum. In this paper we describe a detailed examination of the interaction of NO with both tree and fungal laccase, as well as with tree laccase depleted in type 2 copper. It has been found that NO can reduce as well as oxidize tree laccase. Some species observed during the reaction cycle give a type 3 Cu^{+2} EPR signal (14) and a triplet signal of the type also induced by NO in some other proteins having binuclear O_2-binding sites (5,7-9). We have also found that in the presence of NO, the reduced type 1 copper in tree laccase is reoxidized on freezing. The fungal enzyme is also reduced by NO; however, the reduced form is not oxidized by NO, probably because of the extremely high reduction potentials of the copper sites. We will present the evidence suggesting that NO binds to at least one of the reduced copper centers in fungal laccase. These and related findings have enhanced our understanding of the structure and function of the redox

active centers in the laccases.

Materials and Methods

The isolation and purification of laccase from the lacquer tree Rhus vernicifera (15,16) and from the fungus Polyporus versicolor (17) have been described previously. The preparation of tree laccase depleted in type 2 copper has also been described (16). Bovine serum albumin (Sigma, Fraction V) was dialyzed 8 hrs against 5 mM EDTA to remove Mn^{+2} contaminant. All samples were prepared in 25 mM potassium phosphate buffer at the pH's indicated in the figure legends.

Nitric oxide (^{14}NO, Matheson) was purified by condensation in a liquid nitrogen trap and then distilling off only the NO before addition to the samples. ^{15}NO (99.1% isotopic enrichment, Prochem) was found to be essentially free of other nitrogen oxides and was used as received. $Na^{15}NO_2$ (99.1% isotopic enrichment) and $K^{15}NO_3$ (99.1% isotopic enrichment) for use as ^{15}N NMR standards were obtained from Prochem. All other reagents used were of at least reagent grade purity.

In preparing samples of enzyme plus NO, oxygen must be strictly excluded to prevent protein denaturation. To this purpose, all samples to which NO was added were first made anaerobic by three cycles of evacuation and flushing with argon on a vacuum line. NO was then added to the samples through an inlet to the vacuum line so as to exclude oxygen completely. Enzyme samples to which NO had been added were judged to have retained their integrity by checking for optical clarity and for

restoration of their characteristic blue color upon removal of NO and reoxidation by air.

For recording the time course of the optical changes upon addition of NO to the oxidized laccases, enzyme samples were prepared in quartz optical cuvettes fitted with a ground glass stopcock. NO was added, as described previously, to a 100 ml bulb above the evacuated sample. To initiate the reaction, a valve between the bulb and cuvette was opened, the sample was mixed quickly, and the spectrum was run immediately.

For freezing optical samples, we used quartz 2 mm pathlength cuvettes fitted with glass sidearms. Solutions were collected in the sidearm and frozen by slow immersion in liquid nitrogen, then thawed and shaken into the quartz cell for collecting optical data.

For the EPR time course studies with the oxidized laccases, samples were prepared in 5 mm EPR tubes fitted with a ground glass vacuum joint. NO was added directly to the samples. Within two minutes the samples were removed from the vacuum line and mixed, since in the absence of mechanical mixing, the rate at which NO goes into solution has been found to be extremely slow (11). The reaction was then quenched by immersing the tube in liquid nitrogen. The samples of reduced enzyme plus NO were prepared as above, except that the enzyme was first degassed once and a solution of 40 mM sodium ascorbate and 4 mM PPD was added from a sidearm on the EPR tube. The samples were then made anaerobic as before and NO added.

Optical spectra were recorded at room temperature on a Cary 219 spectrometer. EPR spectra were recorded on a Varian E-line Century

Series X-Band spectrometer equipped with an Air Products Heli-Trans low temperature system. For integration or spectral subtractions, spectra obtained under nonsaturating conditions were collected on a Spex Industries SC-32 SCAMP data processor interfaced to the spectrometer. EPR spectra were recorded at 40 K unless otherwise noted, since at this temperature the EPR signal at g = 2 due to matrix-bound NO is not observed (5).

For NMR and mass spectroscopy, samples were prepared in a 5 ml glass bulb fitted with a ground glass stopcock. A magnetic stir bar was included to continuously mix the sample with the NO gas. For mass spectroscopy, the gas above the sample was fed directly through a ground glass inlet into a Du Pont 21-492B mass spectrometer. With this procedure, only the gaseous nitrogen compounds NH_3, N_2, NO and N_2O could be monitored, since other gaseous nitrogen compounds, in particular NO_2, are not stable at room temperature in the presence of water. In these experiments, atmospheric CO_2 is the major contaminant and would have interfered with the observation of the $^{14}N_2O$ parent peak. To alleviate this problem, and to allow ^{15}N NMR determination of the soluble products, we used ^{15}NO in our experiments. In each experiment, a blank was also prepared which was identical to the sample except that enzyme was omitted. Quantitation of $^{15}N_2O$ produced was determined relative to the ^{15}NO parent peak.

After mass spectral analysis, the degassed solutions were transferred to 10 mm NMR tubes for complementary analysis of soluble products by ^{15}N NMR. D_2O (15%) was added as an internal lock. The ^{15}N NMR spectrum

of the solution was recorded at 25°C with a Bruker WM500 NMR spectrometer. Precise quantitation of $^{15}NO_2^-$ and $^{15}NO_3^-$ was not possible because the spectra were acquired under partially saturating conditions.

Results

The type 1 and type 3 copper centers of the laccases may be monitored by the optical absorbances near 610 and 330 nm, respectively. EPR spectroscopy allows complementary monitoring of the oxidation state of the type 1 and type 2 copper centers. The reduced forms of all three copper centers are optically and EPR silent. We have used both techniques to follow the changes in the copper centers when the reduced and oxidized laccases are incubated with NO.

Reduced Fungal Laccase Plus NO. Reduction of anaerobic fungal laccase by ascorbate with PPD as a mediator is rapid and complete. Addition of NO to the fully reduced enzyme results in no change in absorbance at either 610 or 330 nm, even after 10 hrs. However, a weak absorption band at 420 nm (ε = 400 M^{-1} cm^{-1}) appears rapidly and does not change with time.

The EPR spectra of reduced fungal laccase and of reduced fungal laccase incubated with 1 atm NO for 1 hr at 0°C are shown in Figure 1. The type 1 and type 2 copper centers remain reduced. However, in the presence of NO, a new signal appears near g = 2, representing one to two spins per enzyme molecule. This signal reaches full intensity within 1 min and does not change with time thereafter. Furthermore,

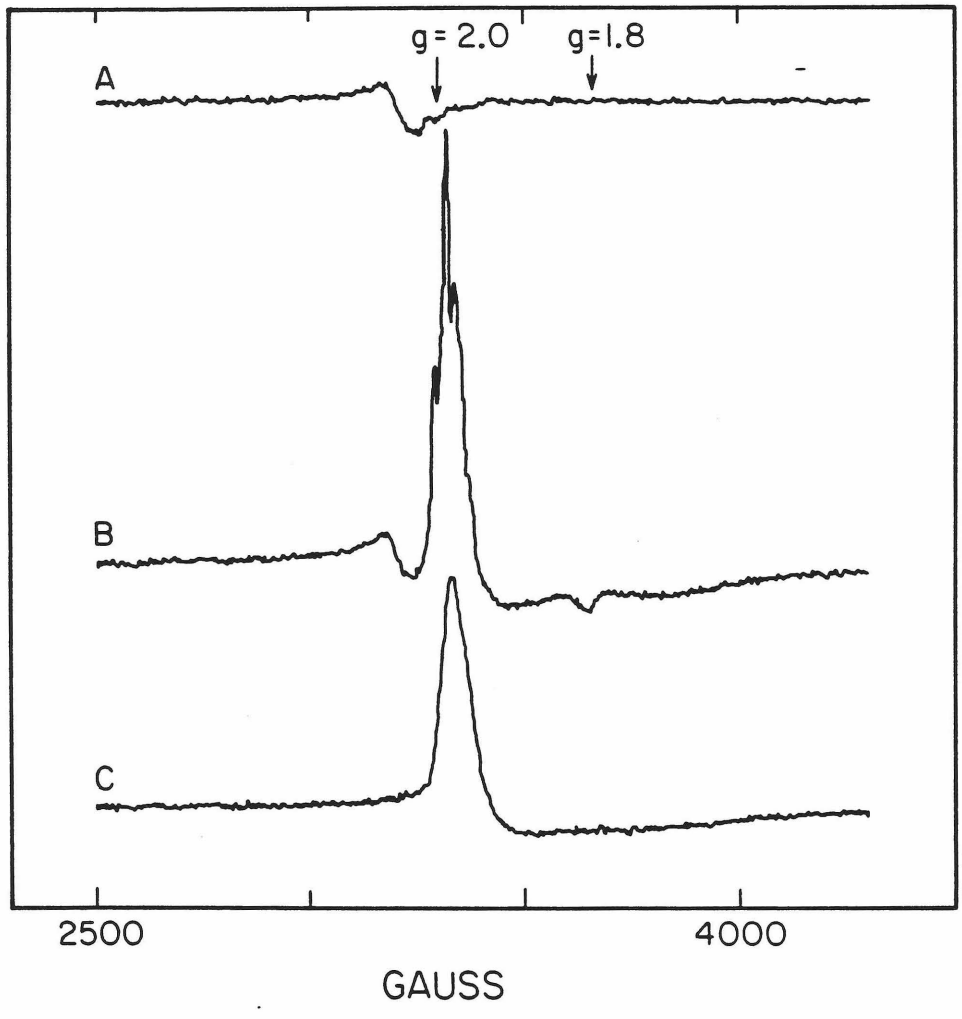

Figure 1: Reduced fungal laccase plus NO. (A) 0.35 mM fungal laccase reduced with 4.0 mM ascorbate and 0.4 mM PPD, pH 6.0; (B) Sample A incubated 10 min with 1 atm NO; (C) 0.30 mM BSA incubated 10 min with 1 atm NO. The conditions were temperature, 40 K; microwave power, 0.2 mW; modulation amplitude, 10 G; and microwave frequency, 9.22 GHz.

degassing of NO from the solution results in complete loss of this signal (spectrum identical to Figure 1A). NO added to a blank without enzyme yields no EPR signals at 40 K. However, a 0.30 mM solution of bovine serum albumin (BSA), which contains no metal centers, when incubated with 1 atm NO shows an EPR signal (Figure 1C) very similar to that exhibited by reduced fungal laccase plus NO, but lacking any resolvable structure. Again, this signal represents one to two spins per protein molecule and disappears upon degassing of NO.

To determine the origin of this new EPR signal, we examined the EPR spectra of the reduced enzyme with isotopically substituted nitric oxide. As seen in Figures 2A and 2B, substitution of ^{15}NO (I = 1/2) for ^{14}NO (I = 1) results in distinct changes in the structure of the new peak. The spectrum of BSA incubated with ^{14}NO is shown in Figure 2C for comparison. Substitution of ^{15}NO for ^{14}NO in the BSA sample resulted in a very slight narrowing of the signal near g = 2 (not shown).

Oxidized Fungal Laccase Plus NO. Anaerobic incubation of oxidized fungal laccase with NO at pH 6.0 results in the reduction of the type 1 and type 3 copper centers as followed optically at 610 and 330 nm, respectively. The reduction of both centers follows pseudo-first order kinetics at room temperature, with $t_{1/2}$ = 2 min, as shown in Figure 3. A weak absorption band at 420 nm is seen as the enzyme becomes reduced.

The EPR spectra obtained at various times after addition of NO to the anaerobic enzyme solution are shown in Figure 4. The rapid reduction of the type 1 copper observed optically is also seen by EPR

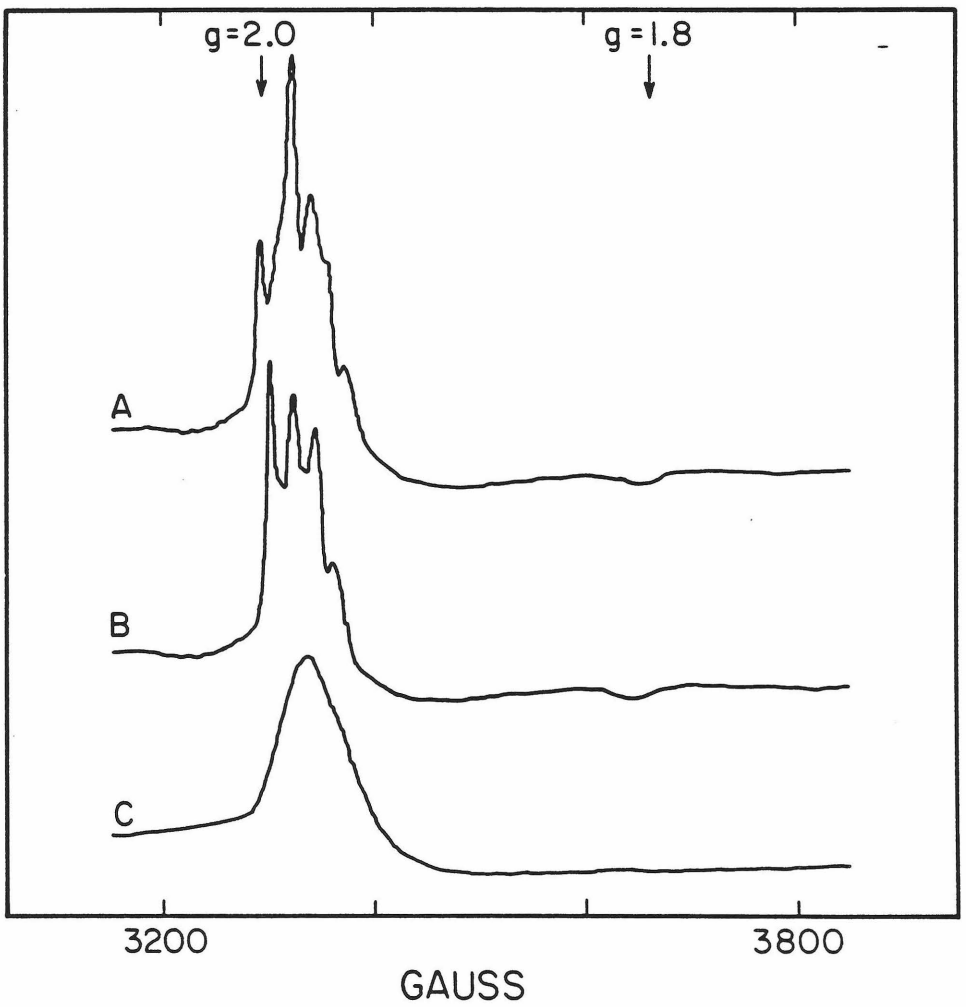

Figure 2: EPR spectra of (A) 0.35 mM fungal laccase, pH 6.0, reduced with 4.0 mM ascorbate and 0.4 mM PPD, then incubated 10 min with 1 atm ^{14}NO; (B) fungal laccase prepared as in (A), but incubated with 1 atm ^{15}NO; (C) 0.30 mM BSA incubated 10 min with 1 atm ^{14}NO. The conditions were temperature; 40 K; microwave power, 80 mW; modulation amplitude, 5 G; and microwave frequency, 9.22 GHz.

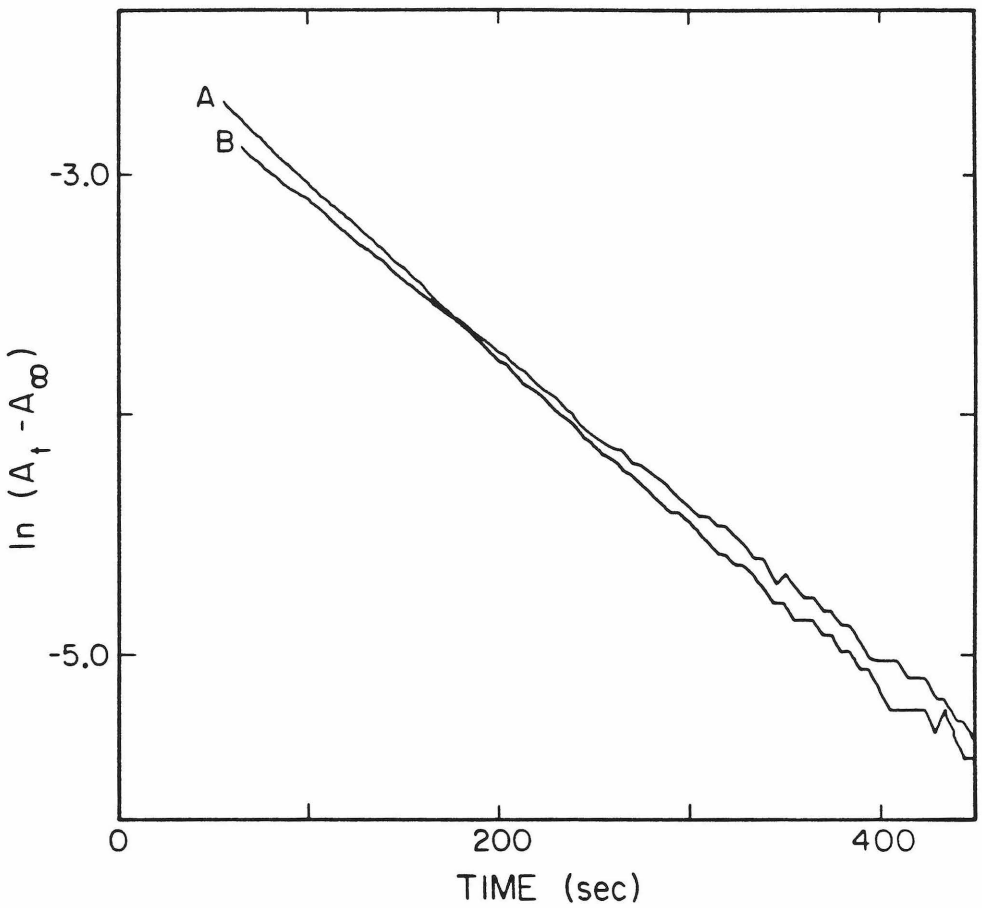

Figure 3: Kinetics of anaerobic reduction of the type 1 and type 3 copper centers of fungal laccase by NO, as followed by optical spectroscopy. (A) absorption at 610 nm; (B) absorption at 330 nm. Spectra were recorded of 0.03 mM samples at 20^{o}C and pH 6.0.

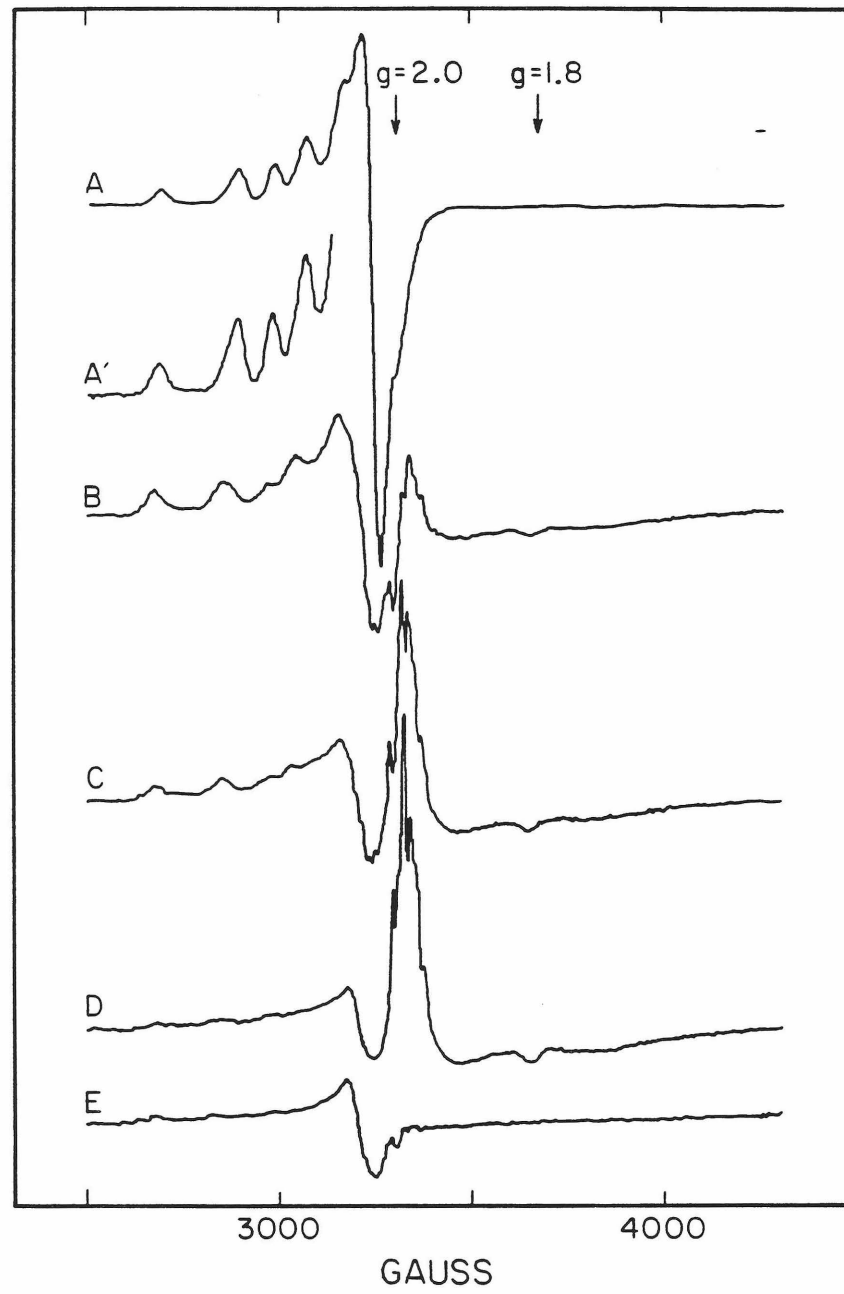

Figure 4: EPR spectra of oxidized fungal laccase incubated with 1 atm NO for various lengths of time. (A, A') 0.35 mM oxidized fungal laccase, pH 6.0; (B) sample (A) made anaerobic, then mixed with NO for 30 sec; (C) sample B mixed and incubated 90 sec longer; (D) sample (C) mixed and incubated 2 hrs; (E) sample D degassed and NO replaced by Ar. The conditions are temperature, 40 K; microwave power, 0.2 mW; modulation amplitdue, 10 G; and microwave frequency, 9.22 GHz. Spectrum (A) was recorded at half the gain of the other spectra.

spectroscopy. The type 2 copper site is also reduced, but more slowly ($t_{1/2} \approx 10$ min). Additionally, the new signal near g = 2 seen in the reduced enzyme plus NO also appears slowly with time. After about 1 hr of incubation, the type 1 and type 2 copper centers appear almost completely reduced, and the new signal reaches a maximum, as seen in Figure 4D. Subsequent degassing of NO from this sample results in complete loss of the new NO signal with no increase in the copper signals (Figure 4E). Finally, admission of air to the degassed sample results in the complete reoxidation of all four copper centers as measured by both EPR and optical spectroscopy (data not shown).

Essentially the same results were obtained at pH 5 and 7.4. However, at the latter pH, we have sometimes observed an EPR signal attributable to type 3 copper (14), after about 1 hr of incubation with NO. This signal becomes about equal in intensity to the type 2 copper signal, but never exceeds 10% of the type 3 copper centers, and its appearance is not reproducible. Incubation of the enzyme with either 1 equivalent or 25 equivalents of fluoride, which is known to bind tightly to the type 2 copper, prior to addition of NO, did not affect the reduction of type 1 copper seen by EPR. The type 2 copper was reduced more slowly in the presence of fluoride.

Oxidized Tree Laccase Plus NO. As with oxidized fungal laccase, NO can reduce the oxidized lacquer tree enzyme, as seen by optical spectroscopy. Reduction of the type 1 and type 3 copper centers again occurs simultaneously and follows pseudo-first order kinetics. However,

the reaction is much slower than that of the fungal enzyme, with $t_{1/2}$ = 70 min (data not shown). As with the fungal laccase, a weak absorbance appears at 420 nm as the enzyme is reduced; this band is also observed when NO is added to the reduced tree laccase.

Attempts to follow the time course of the reaction by EPR spectroscopy were complicated by the fact that the freezing of the sample causes partial bleaching of the residual type 1 blue copper color. The EPR spectra shown in Figure 5 confirm that the reduction of the type 1 copper upon freezing is greater than that observed at the same time point in the optical studies. Subsequent thawing of the EPR samples results in the reappearance of the type 1 blue color. As with the fungal enzyme, EPR studies show a slow reduction of the type 2 copper; for the tree laccase, the time course of the type 2 copper reduction corresponds fairly closely to that of the type 1 copper.

Also seen in Figure 5 is a broad, structureless EPR signal near g = 2. This signal resembles that seen in the spectrum of the fungal enzyme with NO, but is featureless. After 20 hrs incubation of tree laccase with NO without mixing, the NO signal near g = 2 completely disappears, as seen in Figure 5E. EPR spectra at 20 K (not shown) display no signal from matrix-bound NO (see Methods section). The type 1 copper signal also increases, after long incubation of tree laccase with NO, to about 50% of the intensity exhibited by the oxidized enzyme (Figure 5E). The type 2 copper remains mostly reduced. Thawing of this sample, followed by brief mixing (about 1 min), results in the return of the NO signal to full intensity (Figure 5F). This is accompanied by a

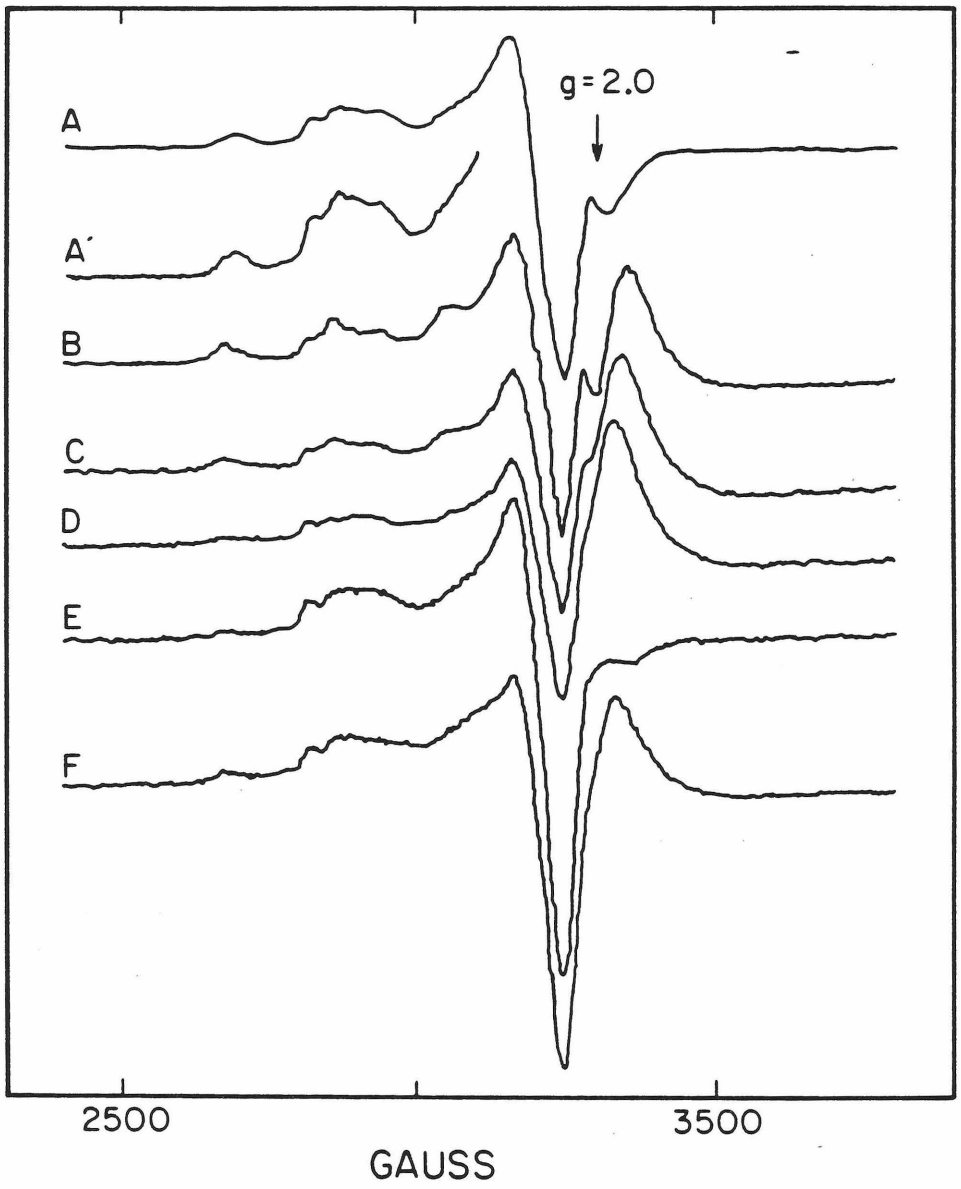

Figure 5: EPR spectra of oxidized tree laccase incubated with 1 atm NO for various lengths of time. (A, A') 0.25 mM oxidized tree laccase, pH 7.0; (B) sample (A) made anaerobic, mixed with NO, and incubated 5 min; (C) sample (B) mixed and incubated 30 min; (D) sample (C) incubated with occasional mixing for 4 hrs; (E) as in (B), but incubated 20 hrs without mixing; (F) sample (E) mixed briefly. The conditions were temperature, 40 K; microwave power. 0.2 mW: modulation amplitude, 10 G; and microwave frequency, 9.22 GHz. Spectrum (A) was recorded at half the gain of the other spectra.

small increase in the type 2 copper EPR signal and a slight decrease in the type 1 copper signal.

To determine whether the depletion of NO in solution upon long incubation with tree laccase is due to a turnover of the enzyme similar to that which has been observed for cytochrome c oxidase (11), we looked for evidence of products due to the oxidation and reduction of NO. NO can be oxidized by either the one- or two-electron process shown below:

(1) $NO + H_2O \rightarrow NO_2^- + 2H^+ + e^-$

(2) $NO + H_2O \rightarrow NO_2 + 2H^+ + 2e^-$

NO_2 is unstable, however, in the presence of water and readily disproportionates via the following reaction:

(3) $2NO_2 + H_2O \rightarrow NO_2^- + NO_3^- + 2H^+$

Accordingly, the production of nitrite and/or nitrate was examined by incubating 2.0 ml of tree laccase with ^{15}NO as described in the Methods section. After incubation of the enzyme with NO at 0^oC for 73 hrs, ^{15}N NMR spectroscopy of the sample solution and the appropriate blank showed substantial production of $^{15}NO_2^-$ relative to the blank. Only a small amount of $^{15}NO_3^-$ was detected (less than 10% of the $^{15}NO_2^-$ produced). The amount of $^{15}NO_2^-$ produced is too great to be accounted for by a single reduction of the enzyme, and must therefore be explained on the basis of enzyme turnover.

The only likely pathway for reoxidation of the enzyme is via the two-electron reduction of NO given by

(4) $2NO + 2H^+ + 2e^- \rightarrow N_2O + H_2O$

To ascertain whether any N_2O had been produced by the enzyme's reaction with NO, we analyzed the atmosphere above the NMR samples by mass spectroscopy. The only significant difference between the mass spectra of the enzyme sample and the blank was a large parent peak at m/e = 46, confirming production of $^{15}N_2O$ in the former (Table I).

Reduced Tree Laccase Plus NO. To confirm the reduction of NO to N_2O by the reduced enzyme, we incubated 1.0 ml of tree laccase with ^{15}NO as before, but with the addition of 4 mM ascorbate and 0.4 mM PPD to provide rapid reduction of the enzyme. After 26 hrs of incubation of the enzyme with NO, mass spectral analysis confirmed the production of $^{15}N_2O$ (Table I). Quantitation of the mass spectral data (see Table I) indicates that the rate of production of $^{15}N_2O$ is two to three times faster in the presence of external reductant than in its absence. The half-time for the reaction in which N_2O is produced, assuming that the reduction of the enzyme by ascorbate and PPD is much faster than its reoxidation by NO, is calculated from the mass spectra data to be about 90 min.

Optical spectroscopy of the reduced tree enzyme in the presence of NO shows that the bands at 330 and 610 nm are absent. However, upon freezing of this sample (either in liquid nitrogen or at -20°C), the type 1 blue color returns to about full intensity. EPR spectroscopy verifies that reoxidation of the type 1 copper center has taken place and is complete (Figure 6A). Note that in this experiment a pure type 1 copper EPR spectrum has been observed from native tree laccase without interference

TABLE I.

$^{15}N_2O$ Seen by Mass Spectroscopy upon Incubation of ^{15}NO with Tree Laccase[a]

	Oxidized[b]	Reduced[c]
Enzyme	.085	.025
Blank	.002	.009

[a] Numbers given are p_{N_2O}/p_{NO}.

[b] 73 hrs incubation.

[c] 26 hrs incubation.

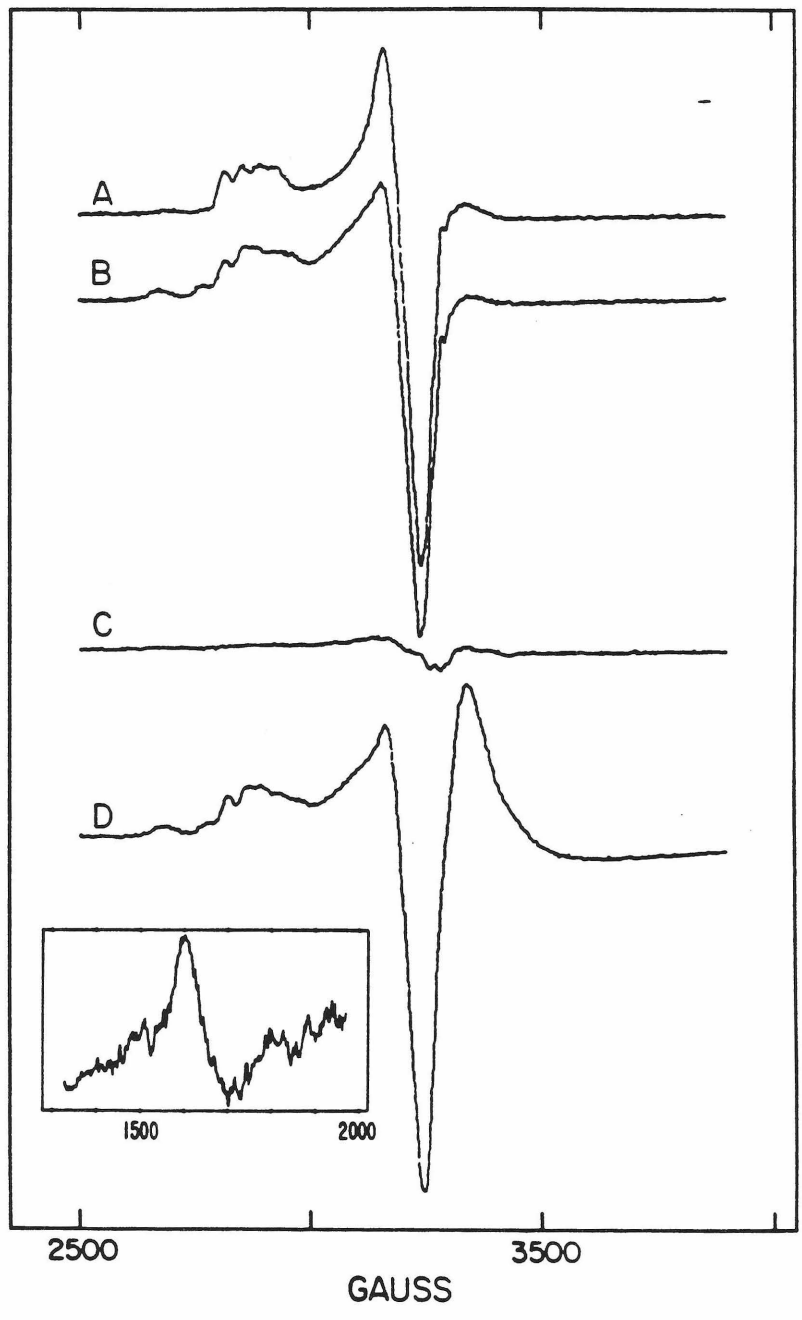

Figure 6: EPR spectra of reduced tree laccase incubated with 1 atm NO for various lengths of time. (A) 0.25 mM tree laccase, pH 7.0, reduced with 4.0 mM ascorbate and 0.4 mM PPD, then mixed with 1 atm NO and incubated 1 min; (B) sample (A) incubated for 30 min without mixing. (C) sample (B) incubated 21 hrs without mixing; (D) sample (C) mixed briefly. The conditions were temperature, 40 K (A and B) and 20 K (C and D); microwave power, 0.2 mW; modulation amplitude, 10 G; microwave frequency, 9.22 GHz; and gain, 1.0×10^4 (A and B) and 8.0×10^3 (C and D). The inset shows the low field region of D, averaged over 10 scans, with conditions as above except: temperature, 11 K, microwave power, 20 mW; and gain, 2.5×10^4.

from the other copper centers! Upon thawing, the type 1 copper center is completely reduced again within 1 min, as monitored optically at 610 nm. It was not possible to monitor the type 3 copper absorbance at 330 nm due to the appearance of a large absorption band (ε = 20,000 M^{-1} cm^{-1} relative to enzyme concentration) centered at 352 nm. This absorption was also observed in an identical blank without enzyme, if a small amount of O_2 was admitted; therefore, it was not studied further.

To see whether the oxidation of the type 1 copper upon freezing of the reduced enzyme with NO might be due to a change in solution pH upon freezing, we repeated this experiment substituting Hepes buffer (25 mM) for phosphate. Hepes buffer has been reported to minimize pH changes upon freezing of solutions (18). The same EPR spectrum, identical to that of Figure 6A, is observed for two different preparations of the enzyme in either 25 mM Hepes, pH 7.0, or 25 mM phosphate, pH 7.0; an identical EPR spectrum is seen for a sample at pH 6.0 in 25 mM phosphate buffer. However, when the enzyme solution is frozen as a glass, using 30% ethylene glycol, no reoxidation of the type 1 copper takes place; the frozen solution remains colorless. (We should also note that when oxidized tree laccase is frozen as a glass, the EPR spectrum is the same as when the enzyme is frozen in buffered solution.)

The reduced enzyme solution plus NO can be frozen and thawed many times, and the same effects observed. However, if a sample of reduced tree laccase plus NO is incubated on ice without mixing, some changes are seen in the EPR spectrum. The NO peak, whether observed at 40 or 20 K, gradually decreases; at the same time, EPR signals of approximately equal intensity appear gradually from the type 2 and 3 coppers (Figure 6B).

Eventually, the NO peak disappears completely, as seen in Figure 6C; concomitantly, the type 1 and 2 copper centers are almost totally reduced. At this stage, the solution is colorless (except for some blue color near the meniscus), and it remains colorless when frozen. When a sample which has been incubated for a long time without mixing is then thawed and briefly shaken to dissolve NO in solution again, an EPR spectrum such as that shown in Figure 6D results. The NO peak is restored to full intensity, and the type 1, 2 and 3 coppers exhibit signals of intensity ranging from 30 - 100% of full intensity (70% for type 1, 100% for type 2 and 30 - 50% for type 3 copper, approximately). Furthermore, a weak signal is now observed at g = 4.0, as shown in the inset to Figure 6. We have also sometimes observed this signal in the samples after long incubation but before remixing. The signal at g = 4.0 is most easily observed at low temperature (<20 K) and high power, and is not saturated at 80 mW at 20 K (in contrast, at 20 K the copper signals in the oxidized enzyme show the onset of saturation at 0.2 mW power).

If the reduced tree laccase turns over in the presence of NO, the reductant should eventually be consumed. This was found to be the case; when the reduced enzyme plus NO is incubated at $0^{o}C$ and mixed frequently to keep NO in solution, the enzyme solution eventually turns blue and remains so thereafter. EPR spectroscopy shows that, at this point, the sample behaves identically to one made by adding NO to the oxidized tree laccase.

Three-Copper Tree Laccase Plus NO. We also examined the interaction

with NO of tree laccase depleted of type 2 copper. As with the oxidized native enzyme, NO reduced the type 1 copper center with $t_{1/2} \approx 40 - 50$ min. EPR spectra (not shown) show that the type 1 copper is rapidly reduced on freezing, similarly to the native tree laccase plus NO. However, the type 3 copper center does not appear to be reduced by NO, as seen optically, and no absorption band is seen at 420 nm. After 21 hrs incubation with NO without mixing, the type 1 copper is completely reduced, as in the native tree laccase, but in contrast to the results obtained with the native enzyme. there is no observable depletion of NO under these conditions (Figure 7).

The type 1 copper center of three-copper tree laccase can be reduced readily by PPD and ascorbate; however, the type 3 copper center requires about 24 hrs incubation for complete reduction (16). The partially reduced species can therefore be made by short incubation with reductant. Addition of NO to this species again results in no significant reduction of type 3 copper, as seen optically. Furthermore, freezing of this sample does not result in any significant oxidation of type 1 copper (Figure 7C) as seen with the fully reduced native enzyme.

The fully reduced three-copper enzyme incubated with NO also shows no significant oxidation of the type 1 copper, either at room temperature as monitored optically, or when frozen as observed by EPR spectroscopy (Figure 7D). Again, no absorption band is visible at 420 nm in this sample. It is also interesting to note that this product shows very little enzyme-bound NO EPR signal near g = 2. Incubation of the fully reduced species with NO for 21 hrs without mixing (Figure 7E) again shows

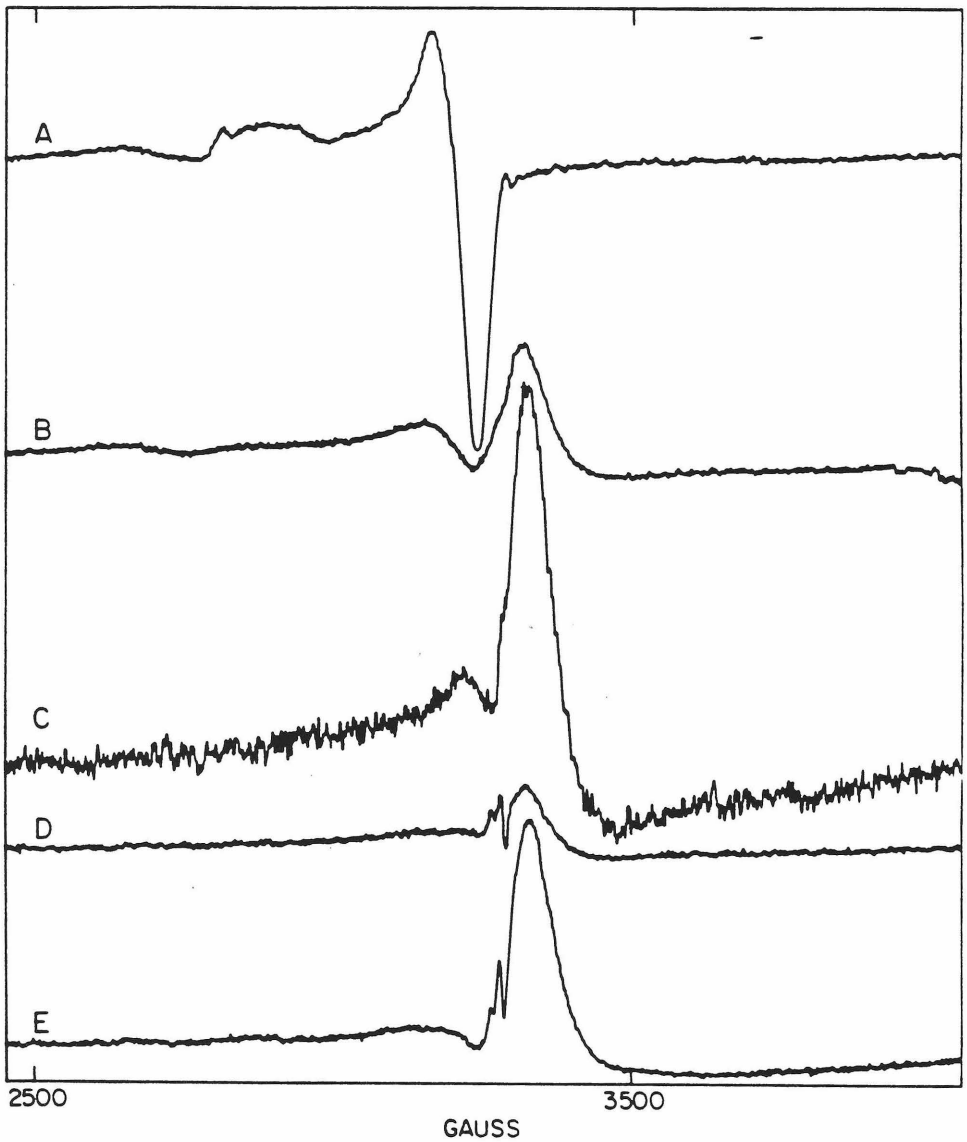

Figure 7: EPR spectra of (A) 0.25 mM oxidized tree laccase depleted of type 2 copper in 25 mM phosphate, pH 7.0; (B) sample (A) with 1 atm NO mixed in, then incubated 21 hrs without mixing; (C) as in (A), but reduced 1 min with 0.7 mM ascorbate and 0.07 mM PPD, then NO added and mixed 2 min; (D,E) as in (A), but reduced 40 hrs with 0.7 mM ascorbate and 0.07 mM PPD, then NO added, mixed and incubated 21 hrs without further mixing. The conditions were temperature, 40 K (A - D) and 20 K (E); microwave power, 0.2 mW; modulation amplitude, 10 G; and microwave frequency, 9.22 GHz. Spectrum (C) was recorded with a 4-fold higher gain than the other spectra.

no depletion of the EPR signal due to NO in solution.

From equation (1), it might be expected that NO_2^- would react with the reduced laccases to produce the NO derivatives. However, no change was seen in the EPR spectra of either reduced fungal laccase (pH 6.0) or reduced tree laccase (pH 7.0) after 16 hrs incubation with 2 mM NO_2^- at 0^oC.

Discussion

The reaction of NO with oxidized tree laccase has been studied previously by Rotilio et al. (12), who observed only reduction of the type 1 copper. However, as they did not report the lengths of incubation of the enzyme with NO, it is difficult to compare their results with our own.

The EPR experiments summarized in Figures 5 and 6 demonstrate that oxidized tree laccase can be reduced by NO and, conversely, the reduced enzyme can be oxidized by NO. The most likely route for the oxidation of the reduced enzyme is via the reduction of NO to N_2O (reaction (4)). The detection of $^{15}N_2O$ by mass spectroscopy after incubation of reduced tree laccase with ^{15}NO confirms that the oxidation of the reduced enzyme occurs via reaction (4). The reduction of the oxidized tree laccase by NO could occur via the oxidation of NO to NO_2^- (a one-electron oxidation) or to NO_2 (a two-electron oxidation) (reactions (1) and (2)). Since NO_2 in solution disproportionates to NO_2^- and NO_3^- (reaction (3)), the observation by ^{15}N NMR spectroscopy of only a small amount of $^{15}NO_3^-$,

compared to the amount of $^{15}NO_2^-$ observed, as reaction product of oxidized tree laccase with ^{15}NO implies that the reduction of the enzyme occurs primarily in conjunction with the one-electron oxidation of NO to NO_2^-.

Both the oxidation and reduction of tree laccase by NO occur very slowly. The half-time for reduction of the type 1 and type 3 copper centers, as measured by optical spectroscopy, was found to be 70 min; the mass spectroscopy data on the reaction of reduced tree laccase with NO, which indicate about 15 turnovers in 26 hrs, imply that $t_{1/2}$ for the reaction in which N_2O is produced is about 90 min, on the same order as for the reaction of the oxidized enzyme with NO.

The reaction of oxidized fungal laccase with NO, on the other hand, is much faster. The optical data show that the type 1 and type 3 copper centers are reduced with $t_{1/2}$ = 2 min, and the EPR data indicate that the type 2 copper is reduced with $t_{1/2} \approx 10$ min. Furthermore, in contrast to the tree laccase, the reduced fungal enzyme gives no indication of a reaction with NO, even after long incubation. We ascribe this difference in reactivity of the reduced laccases with NO to the difference in their reduction potentials. Fungal laccase, with its extremely high reduction potentials, is a much poorer reductant than tree laccase, so it is not surprising that reduced fungal laccase cannot be oxidized by NO.

Because the reduced fungal laccase did not react with NO, no cyclic reaction analogous to those observed with the tree laccase (in which NO served as oxidant and either NO or ascorbate served as reductant) could take place. Hence, although it seems likely that the reduction of fungal laccase by NO is also accompanied by production of NO_2^-, we were

unable to verify this directly.

We also investigated the interactions of NO_2^- with both laccases. Nitrite is known to be reduced to NO by cytochrome c oxidase (11) and nitrate reductase (19); however, we found no evidence for this reaction with reduced tree or fungal laccase. The lack of reactivity of the laccases with NO_2^- is more likely due to kinetic rather than thermodynamic constraints.

In addition to the reaction of NO with tree and fungal laccase, we have also obtained evidence for the specific binding of NO, particularly to fungal laccase. The peak observed by EPR spectroscopy at g = 2 upon addition of NO to reduced fungal laccase is somewhat similar to that seen in a sample of NO dissolved in buffer solution. The signal differs, however, in that with fungal laccase (1) well-defined hyperfine structure can be seen on the EPR signal at g = 2, (2) there is an inflection at g = 1.8 associated with the peak, and (3) the signal is observed at temperatures as high as 80 K, whereas no EPR signal is observed from NO dissolved in buffer solution at 40 K. In contrast to the NO signal seen with fungal laccase, the corresponding signal seen with tree laccase is featureless and resembles that seen upon addition of NO to a BSA solution. This latter signal differs, however, from that of NO dissolved in buffer solution, in that it is observable at 40 K. This featureless NO peak, which probably also contributes to the NO signal seen with fungal laccase, is most likely due to a weak association of NO with the protein, perhaps at a hydrophobic region.

The NO signal seen with fungal laccase exhibits structure which

changes upon substitution of ^{15}NO for ^{14}NO (Figure 2). The observed structure is thus due to hyperfine interaction between the unpaired electron spin and the NO nitrogen nuclear spin. The signal is remarkably similar to one seen upon addition of NO to soybean lipoxygenase (20), which contains a single iron atom per enzyme molecule, and also bears some resemblance in its structural features to an immobilized nitroxide spin label (21). We assign the signal in Figure 2 to NO bound to a reduced copper site. The observed g-anisotropy is not inconsistent with a bound NO molecule of this structure. The high potential of the fungal laccase copper centers (whichever one the NO is bound to) would prevent a charge transfer from copper to NO, which might otherwise be expected to lead to oxidation of the copper center, as is the case for the tree enzyme.

It is most likely that the NO is bound to the reduced type 2 copper center, as the EPR signal due to this center is observed to decrease concomitantly with the increase in the EPR signal due to the specifically bound NO. The reduction of the type 1 and 3 copper centers by NO occurs considerably more quickly than the appearance of the new NO signal. The type 2 copper center is known to bind exogenous ligands such as F^- and CN^- (1), so it is not surprising that it could bind NO. The 420 nm band we observed when NO was present with either reduced tree or fungal laccase may also be due to an association of NO with the type 2 copper, as the band does not appear in the type 2 copper-depleted enzyme plus NO.

The reductions of the type 1 and 3 copper centers by NO occur simultaneously, in both the tree and fungal laccases. In contrast, when

fungal laccase is reduced by hydroquinone or ascorbate, the type 1 copper is reduced considerably faster than the type 3 copper, and the rate-limiting step in the latter reduction appears to be an intramolecular electron transfer (22). Similar results have been obtained for the anaerobic reduction of tree laccase by hydroquinone (23). The slow and simultaneous reduction of the type 1 and 3 copper sites by NO indicates that the first step in the reaction, whether it be reduction of the type 1 or 3 copper center, must be the slow step; the reduction by NO of the second site then follows rapidly. Such a sequence might occur in a number of ways, but the results of adding NO to oxidized, type 2 copper-depleted tree laccase suggest a particular mechanism. In the latter experiment, only the type 1 copper center was reduced by NO, with $t_{1/2}$ slightly less than with the normal oxidized enzyme; the type 3 copper center remained oxidized even after long incubation with NO. The simplest mechanism that can account for the observations made with the normal and type 2 copper-depleted tree laccase (and the fungal laccase) is shown in Figure 8. The first steps are the slow reduction of the type 1 copper center, probably by an outer-sphere electron transfer, followed by the fast reduction of the type 3 copper site. Apparently the reduction of the type 3 copper center requires the presence of the type 2 copper center. It may be that, following the reduction of the type 1 copper, two NO molecules in succession are rapidly oxidized to NO_2^- at the type 2 copper, and two electrons are quickly transferred to the type 3 site. Alternatively, the two electrons can be transferred to the type 3 site from the type 1 and type 2 coppers immediately after

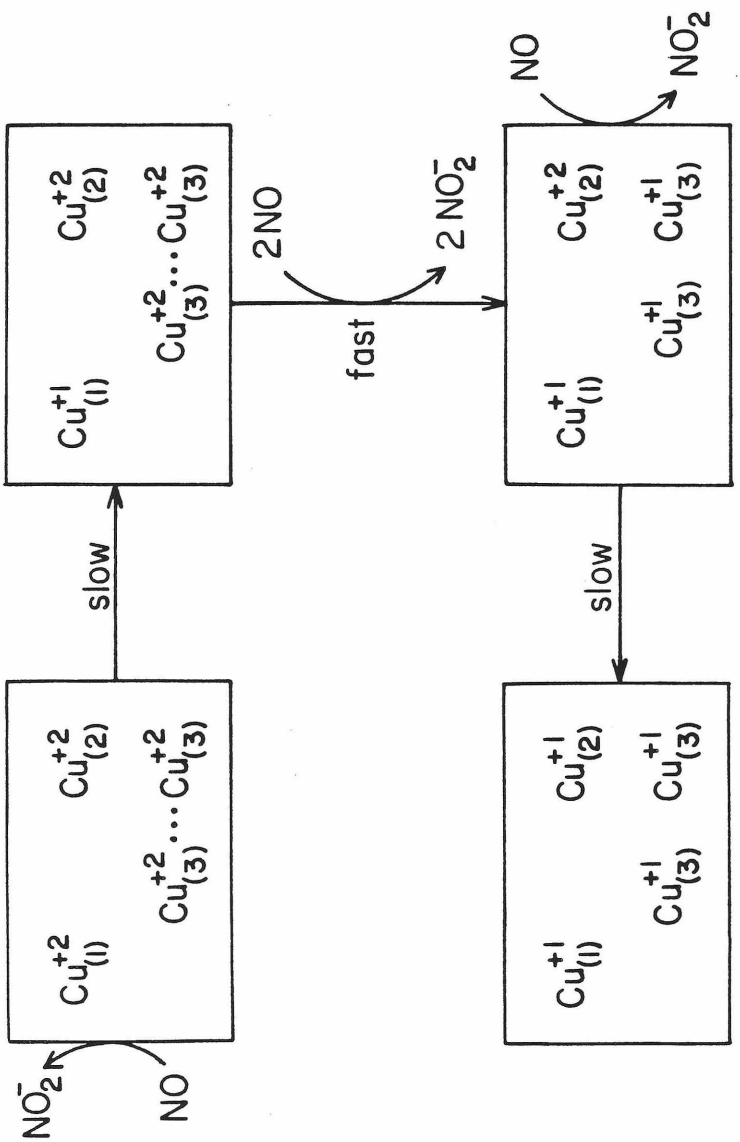

Figure 8: Proposed mechanism for the reduction of tree or fungal laccase by NO.

one NO molecule is oxidized to NO_2^- at the type 2 site. Our data do not permit us to distinguish between these two pathways. In any event, it is likely that after the initial reduction of the type 1 site, the next two electrons enter via the type 2 copper, as there is no precedent for the reactivity of the type 1 site varying with the redox states of the type 2 or 3 sites. On the other hand, stopped-flow experiments on the anaerobic reduction of tree laccase indicate that the reactivity of the type 2 copper site varies with the redox state of the type 1 copper (23). We find that the reactivity of the type 2 copper is dependent on the redox states of both the type 1 and 3 coppers. The final reduction of the type 2 center was found to be quite slow, in agreement with earlier kinetic experiments showing that anaerobic reduction of the type 2 copper becomes much slower once the type 1 and 3 copper centers have been reduced in either tree laccase (23) or fungal laccase (24).

The foregoing scheme deals only with the reduction of the oxidized tree (or fungal) laccase by NO. We have shown, however, that NO can also oxidize the reduced tree laccase. We now develop a scheme for the complete cyclic reaction in which tree laccase is both oxidized and reduced by NO. Such a scheme must embrace the following observations: (1) when ascorbate is used as reductant with PPD as mediator, $t_{1/2}$ for the reaction in which N_2O is produced is about 90 min; (2) in the absence of ascorbate or PPD, so that the enzyme is reduced by NO, the production of N_2O is two to three times slower; (3) the blue color remaining in the oxidized tree laccase plus NO after long incubation accounts for 10 - 15% of the original optical absorbance at 610 nm in

the oxidized enzyme (when the enzyme is kept at $4^{o}C$); (4) upon long incubation with NO, the reduced enzyme exhibits small type 2 and type 3 copper EPR signals of about equal intensity; (5) only the type 1 copper of the type 2 copper-depleted tree laccase is reducible by NO; and (6) reduced type 2 copper-depleted tree laccase gives no indication of being oxidized by NO, even after long incubation.

A simple reaction scheme which accounts for the above observations is depicted in Figure 9. This scheme emphasizes the requirement for the type 2 copper in both the oxidation and reduction of laccase by NO, as dictated by the results obtained using the type 2 copper-depleted tree laccase. Beginning with the fully reduced enzyme, we show in steps (1), (2) and (3) the binding of NO to reduced type 2 (species I) and 3 (species II) copper sites and the reaction to produce N_2O, respectively. At least one of these steps, most likely (3), must be slow. The reaction of step (3) almost certainly involves two bound molecules of NO, as shown. First, we know that the type 2 copper is required for this step from the results obtained with the type 2 copper-depleted enzyme. Second, there is no precedent for an exogenous ligand binding to a type 1 copper in any enzyme, and it is unlikely that the second molecule of NO could come from solution, as this would result in a two-electron reduction taking place at a single copper atom.

Species III, shown in Figure 9 following step (3), in which the type 2 copper and one type 3 copper are oxidized, is most likely responsible for the type 3 EPR signals that we have observed (Figure 6). A molecule of NO binding to the type 3 site in this half-oxidized

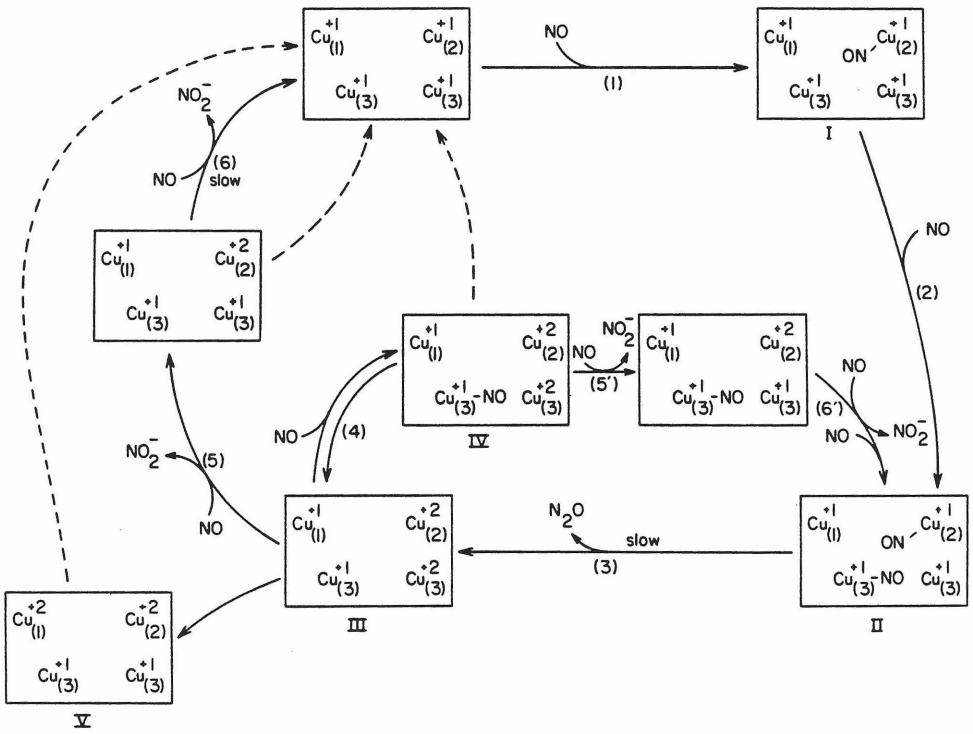

Figure 9: The proposed reaction cycle which occurs when tree laccase is incubated with NO. The dotted lines show paths which may be taken in the presence of ascorbate.

enzyme would result in the appearance of Species IV, which could be expected to exhibit, in addition to a type 2 EPR signal, a triplet EPR signal due to a weak coupling between the NO moelcule bound to the reduced type 3 copper and the remaining oxidized type 3 copper atom. This triplet species would account for the "half-field" EPR signal observed at g = 4.0. Compared to the type 3 signal exhibited by reduced tree laccase in the presence of NO, which is almost as large as the type 2 signal, the triplet signal is quite small (Figure 6), suggesting that Species IV accounts for only a small fraction of the enzyme molecules. From this result, we infer that the equilibrium III $\rightleftharpoons$ IV is towards the left. Presumably this equilibration is rapid.

Both forms of the half-oxidized enzyme, namely Species III and IV, are expected to be reduced in two successive one-electron oxidations of NO (steps (5), (5'), (6) and (6')) to give the fully reduced enzyme and complete the reaction cycle. Steps (5) and (5'), which result in the enzyme being three-quarters reduced, should be fast, to maintain consistency with our earlier results on the reduction by NO of the oxidized enzyme (Figure 8). The relatively high reactivity of the redox state of the enzyme in which the type 3 site is only half-reduced is probably related to the specific function of that site, which is to react with O_2, when both coppers are reduced, to yield peroxide as the first intermediate in oxygen reduction (25). The reduction of the type 2 copper shown in steps (6) and (6') again is presumably slow.

Finally, to account for the 10 - 15% of the blue copper observed even after long incubation of the oxidized tree enzyme with NO, we

introduce Species V. Since both the type 1 and type 2 coppers are oxidized in this species, the type 2 copper center is expected to be relatively inert towards NO; hence, Species V is not shown to be active in the redox cycle.

The observations made upon freezing reduced tree laccase in the presence of NO can also be rationalized by this scheme. If ascorbate is present, the half-oxidized enzyme will be reduced rapidly, so that Species I and/or II in the reaction cycle predominates in the steady state. Upon freezing the solution, we propose that the Species I and II of the enzyme undergo a conformational change which increases the relative reduction potential of the type 2 copper center and facilitates electron transfer between the type 1 and 2 copper sites.

Transfer of an electron from the reduced type 1 copper site to the NO which is bound to the type 2 copper, as shown in Figure 10, would result in the restoration of the type 1 copper EPR signal to full intensity. Note that this observation implies that step (1) of Figure 9 is fast. When the solution is thawed again, the enzyme slowly returns to its original conformation, so that after about 90 s the solution again becomes colorless. The involvement of the type 2 copper center is implicated by studies on the reduced type 2 copper-depleted enzyme, which remains colorless upon freezing. Here, of course, there can be no $[Cu^{+1}_{(2)}$ - NO] unit to which an electron can be transferred. Furthermore, when a solution of reduced native tree laccase plus NO is frozen as a glass, the type 1 copper remains reduced. This could be due to our hypothesized conformational change being induced by a reordering of the

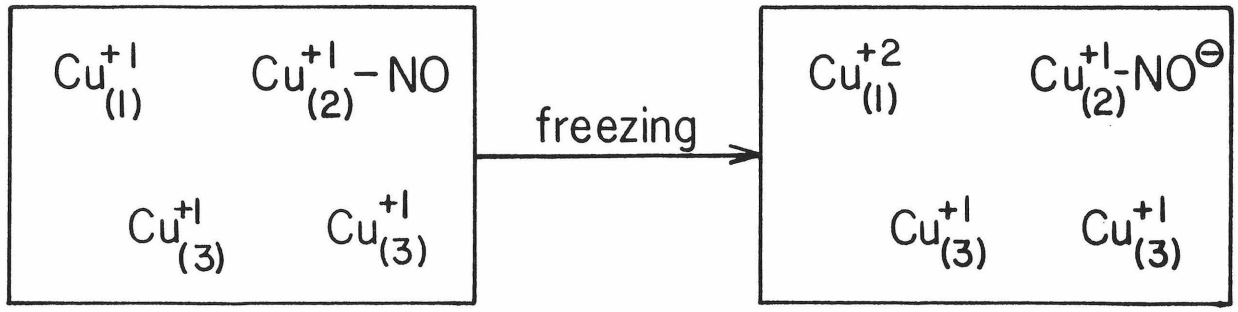

Figure 10: Proposed mechanism for the oxidation of the type 1 copper of tree laccase upon freezing the reduced enzyme in the presence of NO.

liquid water solvent structure around the enzyme upon freezing, whereas the solvent structure in the frozen glass is not expected to induce this same conformational change.

Morpurgo et al. (26) have recently shown by EPR spectroscopy that the hyperfine splitting and principal g-values of the type 1 and 2 coppers in tree laccase are different at room temperature and 77 K. Their results demonstrate that the geometry of the ligand field about these coppers changes between room temperature and 77 K. A change in geometry of this sort would change the reduction potentials of the type 1 and 2 copper sites, and could give rise to the color change seen upon freezing the reduced enzyme in the presence of NO. However, the color change is not seen when the enzyme is frozen as a glass, whereas the EPR spectrum of the oxidized enzyme is the same whether it is frozen as a glass or in buffered solution. It would appear, then, that our proposed conformational change of the enzyme upon freezing is not primarily a change in ligand field geometry about the coppers, although this still cannot be entirely ruled out.

The schemes of Figures 8, 9 and 10 contain certain structural implications. First, the type 2 and 3 copper centers must be close, to allow the reaction of two bound NO's to produce N_2O as in Figure 9, step (3). These two copper centers must act in concert in the oxidation of tree laccase by NO. Secondly, NO appears able to bind at the type 2 copper site, as in Figure 10, and at the type 3 site, as indicated by the appearance of the triplet EPR signal in the experiments with reduced

tree laccase plus NO, but we have obtained no evidence that NO binds at the type 1 copper.

The interactions of tree and fungal laccase with nitric oxide show some similarities, but also some substantial differences from those which have been made with other copper proteins. We may compare the results obtained here on laccase with those obtained for some other copper proteins, and for cytochrome c oxidase. Of the metalloproteins containing only copper, hemocyanin, which contains only a type 3 copper site, has been the most thoroughly studied with regard to its interactions with NO. A triplet absorption has been observed upon treatment of reduced hemocyanin with NO in the absence of ascorbate, and was interpreted as being due to dipole-dipole interactions between the two Cu(II) ions in the active site (9,27). Computer simulation of the EPR spectrum showed that the Cu(II)-Cu(II) distance is about 6 Å (28). More recently, Van der Deen and Hoving (29) have shown that the active site can be singly oxidized by reaction with either nitrite or nitric oxide in the presence of ascorbate, and Verplaetse et al. (10) have shown that the oxidation of reduced hemocyanin from Helix pomatia is accompanied by production of N_2O. In the latter study, it was also shown that NO can bind to the active site in the oxidized hemocyanin. Tyrosinase resembles hemocyanin in possessing just a single type 3 copper site: mushroom tyrosinase exhibits a triplet EPR signal upon brief incubation of the oxygen-binding form of the enzyme with NO, and Neurospora tyrosinase exhibits a similar EPR signal upon brief mixing of the deoxygenated enzyme with NO and a small amount of O_2 (30). Ceruloplasmin, which

contains type 1, 2 and 3 copper centers, exhibits a triplet EPR signal upon addition of NO to either the oxidized enzyme (8) or the reduced enzyme (7). Thus, these type 3 copper-containing proteins resemble tree laccase in that NO is capable of "uncoupling" the type 3 copper centers, but they differ in the precise mechanism by which the magnetic coupling is broken. Furthermore, in contrast to hemocyanin, the oxidation of the type 3 site in reduced tree laccase requires the presence of another copper center (the type 2 site). Fungal laccase differs in this respect in that there is no evidence for any reaction or charge transfer between NO and the reduced type 3 copper center; again, this is probably related to the extremely high reduction potentials of the copper centers associated with this enzyme.

The type 1 copper of ceruloplasmin is reduced by NO; the reduction is reversible upon degassing if the incubation with NO is short (5 min), but reoxidation after longer incubation requires admission of oxygen (8). The interpretation made was that a charge transfer complex between NO and the type 1 copper accounts for the early decrease in the 600 nm optical absorbance, whereas reduction of the site occurs upon longer incubation. EPR spectroscopy showed no changes in copper signal intensity between 5 min and 2 hrs.

The effect upon freezing of reduced tree laccase plus NO in our study is unique among the blue copper proteins. No such effect is seen with fungal laccase, but it may be that the much higher reduction potentials of the copper centers in the fungal laccase preclude an electron transfer similar to that of Figure 10.

Finally, cytochrome c oxidase is remarkably similar to tree laccase in its reactions with NO (11). In the presence of reductant, both cytochrome c oxidase and tree laccase are oxidized by NO to the half-oxidized state. In cytochrome c oxidase, the oxidized enzyme is also slowly reduced by NO and slowly reoxidized to form a cycle similar to that of Figure 9 deduced for tree laccase. However, all four metal centers of tree laccase (and fungal laccase), as we have seen, are completely reduced by NO, whereas only Cu_{a_3} and cytochrome a_3 of cytochrome c oxidase are reduced by NO. Furthermore, in the cyclic reaction of oxidized tree laccase with NO, all three copper centers are involved (Figures 8 and 9), whereas only the oxygen-binding site is involved in the analogous cycle of oxidized cytochrome c oxidase with NO. The similarity of cytochrome c oxidase to the laccases in its reactions with NO is undoubtedly related to its similar function of catalyzing the four-electron reduction of oxygen to water. The differences, on the other hand, may reflect the unique role of cytochrome c oxidase as an energy-conserving protein with proton pumping capabilities (31) to create a trans-membrane proton gradient during its catalytic cycle (32).

References

1. Reinhammar, B. (1979) Adv. Inorg. Biochem. 1, 91-118.
2. Petersson, G., Ångström, J. and Ehrenberg, A. (1978) Biochim. Biophys. Acta 526, 311-317.
3. Dooley, D. M., Scott, R. A., Ellinghaus, J., Solomon, E. I. and Gray, H. B. (1978) Proc. Natl. Acad. Sci. U.S.A. 75, 3019-3022.
4. Mason, H. S. (1976) in Iron and Copper Proteins (Yasunobu, K., Mower, H. F. and Hayaishi, O., Eds) pp. 464-469, Plenum, New York.
5. Stevens, T. H., Brudvig, G. W., Bocian, D. F. and Chan, S. I. (1979) Proc. Natl. Acad. Sci. U.S.A. 76, 3320-3324.
6. Malmström, B. G. (1979) Biochim. Biophys. Acta 549, 281-303.
7. Van Leeuwen, F. X. R., Wever, R. and Van Gelder, B. F. (1973) Biochim. Biophys. Acta 315, 200-203.
8. Van Leeuwen, F. X. R. and Van Gelder, B. F. (1978) Eur. J. Biochem. 87, 305-312.
9. Schoot Uiterkamp, A. J. M. and Mason, H. S. (1973) Proc. Natl. Acad. Sci. U.S.A. 70, 993-996.
10. Verplaetse, J., Van Tornout, P., Defreyn, G., Witters, R. and Lontie, R. (1979) Eur. J. Biochem. 95, 327-331.
11. Brudvig, G. W., Stevens, T. H., and Chan, S. I. (1980) Biochemistry 19, 5275-5285.
12. Rotilio, G., Morpargo, L., Graziani, M. T. and Brunori, M. (1975) FEBS Lett. 54, 163-166.
13. Dooley, D. M., Rawlings, J., Dawson, J. H., Stephens, P. J., Andréasson, L.-E., Malström, B. G. and Gray, H. B. (1979) J. Am. Chem. Soc. 101, 5038-5046.

14. Reinhammar, B., Malkin, R., Jensen, P., Karlsson, B., Andreásson, L.-E., Aasa, R., Vänngård, T. and Malmström, B. G. (1980) J. Biol. Chem. 255, 5000-5003.

15. Reinhammar, B. (1970) Biochim. Biophys. Acta 205, 35-47.

16. Reinhammar, B. and Oda, Y. (1979) J. Inorg. Biochem. 11, 115-127.

17. Fåhraeus, G. and Reinhammar, B. (1967) Acta Chem. Scand. 21, 2367-2378.

18. Williams-Smith, D. L., Bray, R. C., Barber, M. J., Tsopanakis, A. D. and Vincent, S. P. (1977) Biochem. J. 167, 593-600.

19. Wharton, D. C. and Weintraub, S. T. (1980) Biochem. Biophys. Res. Commun. 97, 236-242.

20. Galpin, J. R., Veldink, G. A., Vliegenthart, J. F. G. and Boldingh, J. (1978) Biochim. Biophys. Acta 536, 356-362.

21. Williams, J. C., Mehlhorn, R. and Keith, A. D. (1971) Chem. Phys. Lipids 7, 207-230.

22. Andréasson, L.-E., Malmström, B. G., Strömberg, C. and Vänngård, T (1973) Eur. J. Biochem. 34, 434-439.

23. Andréasson, L.-E. and Reinhammar, B. (1979) Biochim. Biophys. Acta 568, 145-156.

24. Brändén, R. and Reinhammar, B. (1975) Biochim. Biophys. Acta 405, 236-242.

25. Malmström, B. G. (1981) in Oxidases and Related Redox Systems (King, T. E., Mason, H. S. and Morrison, M., Eds.) Oxford Press, London, in press.

26. Morpurgo, L., Calabrese, L., Desideri, A. and Rotilio, G. (1981). Biochem. J. 193, 639-642.

27. Schoot Uiterkamp, A. J. M. (1972) FEBS Lett. 20, 93-96.

28. Schoot Uiterkamp, A. J. M., Van der Deen, H., Berendsen, H. J. C. and Boas, J. F. (1974) Biochim. Biophys. Acta 372, 407-425.

29. Van der Deen, H. and Hoving, H. (1977) Biochemistry 16, 3519-3525.

30. Himmelwright, R. S., Eickmann, N. C., LuBien, C. D., Lerch, K. and Solomon, E. I. (1980) J. Am. Chem. Soc. 102, 7339-7344.

31. Chan, S. I., Bocian, D. F., Brudvig, G. W., Morse, R. H. and Stevens, T. H. (1979) in Cytochrome Oxidase (King, T. E., Orii, Y., Chance, B. and Okunuki, K., Eds.) pp. 177-188, Elsevier, Amsterdam.

32. Wikström, M. and Krab, K. (1979) Biochim. Biophys. Acta 549, 177-222.

Chapter IV. Exchange- and Dipolar-Coupled Cupric and High-Spin Ferric Ions in Cytochrome c Oxidase. Origin of the Unusual EPR Signals Exhibited by the Oxidized Enzyme.

Introduction

Cytochrome c oxidase has four metal centers, two coppers and two heme irons. Van Gelder and Beinert (1) first produced evidence that of these metal centers, one copper and one iron (cytochrome a and Cu_a) are magnetically isolated and EPR detectable in the oxidized enzyme, whereas the second iron and copper (cytochrome a_3 and Cu_{a_3}) interact electrostatically and are undetectable by EPR at X-band (9 GHz). Griffith (2) subsequently derived the properties of the antiferromagnetically coupled Fe^{+3}-Cu^{+2} system, assuming the iron to be high-spin, and concluded that the lack of an EPR signal at X-band from this coupled pair was not surprising. More recently, variable temperature magnetic susceptibility measurements have confirmed the presence of an S=2 spin center in the oxidized enzyme (3,4), consistent with an antiferromagnetically coupled Fe^{+3}-Cu^{+2} pair, with $J > 200\ cm^{-1}$.

In a recent publication (5), we reported the identification of four distinct conformations of oxidized cytochrome c oxidase, which differ in the structure of the O_2-binding site. These conformations can be distinguished by EPR spectroscopy. One of these conformations, the "resting" conformation, reveals a rhombic EPR signal at g = 6 when NO is added to the oxidized enzyme. This signal is readily interpreted as being due to magnetically isolated, high-spin cytochrome a_3^{+3}, which

becomes EPR-detectable when NO binds to $Cu^{+2}_{a_3}$ and reorients the ligand field about the copper so that the antiferromagnetic coupling between iron and copper is broken.

A second conformation of the enzyme exhibits an EPR signal at g = 12 when measured at X-band. This signal is best seen at low (<30 K) temperatures, and has been noted several times in the literature (5 - 8). Greenaway et al. (6) found that this EPR signal increases in intensity as the enzyme is purified and disappears upon reduction of the enzyme, and they suggested that the signal may arise from the S = 2 center of the enzyme. Work in our laboratory has indicated that this signal is associated with a conformation of cytochrome c oxidase which accounts for up to 70% of the enzyme molecules, depending on the enzyme preparation (5).

A third conformation of cytochrome c oxidase is the so-called "oxygenated" conformation. The cytochrome a_3-Cu_{a_3} site is EPR silent in this conformation. However, upon incubation with 100 mM F^-, it exhibits the fluorocytochrome a_3^{+3} EPR signal, an unusual EPR signal which is characterized by resonances at g = 8.5, 6, 5, 4.3 and 3.2. Brudvig et al. (5) suggested that the complexity of this signal could only arise form a weakly exchanged coupled and/or dipolar-coupled cytochrome a_3^{+3}-$Cu^{+2}_{a_3}$ site, with hydroxide ion as a probable bridging ligand.

Finally, Shaw et al. (9) have reported the transient formation of a fourth conformation of cytochrome c oxidase. This conformation appears

within 5 ms on reoxidation of reduced cytochrome c oxidase by O_2, and is characterized by an EPR spectrum with g-values at g = 5, 1.78 and 1.69. Shaw et al. (9) suggested that the signal most likely arises from cytochrome $\underline{a}_3^{+3}$, and that the high-field resonances may be due to spin-spin interaction between cytochrome $\underline{a}_3^{+3}$ and $Cu^{+2}_{a_3}$. We made a similar suggestion in Ref. (5), viz., that the "g5" EPR signal arises from a dipolar-coupled, and possible weakly exchange-coupled, cytochrome $\underline{a}_3^{+3}$-$Cu^{+2}_{a_3}$ site.

An important common feature of the "g5", "g12" and the fluorocytochrome $\underline{a}_3$ EPR signals is that they cannot be interpreted simply in terms of an isolated high-spin or low-spin ferric heme iron, or to an isolated copper center. Although the suggestions regarding the nature of these unusual EPR signals all seem reasonable, these ideas need to be verified by direct quantum mechanical calculations. This is the objective of this paper.

Theory

The Hamiltonian which describes the system under investigation is

$$H = +J\hat{\underset{\sim}{S}}_1\cdot\hat{\underset{\sim}{S}}_2 + D(\hat{S}^2_{1z} - \frac{35}{12}) + E(\hat{S}^2_{1x} - \hat{S}^2_{1y}) + \beta\underset{\sim}{H}\cdot\underset{\approx}{g}_1\cdot\hat{\underset{\sim}{S}}_1 + \beta\underset{\sim}{H}\cdot\underset{\approx}{g}_2\cdot\hat{\underset{\sim}{S}}_2 + H_{dip} \quad (1)$$

where $\hat{\underset{\sim}{S}}_1$ refers to iron (S_1 = 5/2) and $\hat{\underset{\sim}{S}}_2$ to copper (S_2 = 1/2), D and E are the axial and rhombic zero-field splitting constants for the heme iron, $\underset{\approx}{g}_1$ and $\underset{\approx}{g}_2$ are the g-tensors for the two ions, β is the Bohr magneton, $\underset{\sim}{H}$ is the applied external magnetic field, and H_{dip} is the dipolar

coupling term. Note that we have written the exchange coupling term as $+JS_1 \cdot S_2$, so that J is assumed to be isotropic, and is positive for antiferromagnetic coupling.

There are two natural coupling schemes for our system, the $S_1S_2M_1M_2$ and S_1S_2SM schemes, where S and M are, respectively, the total spin and its projection along the z-axis (perpendicular to the heme plane) for the coupled system. The two representations are related through the Clebsch-Gordon coefficients (10). Specifically,

$$|S_1S_2 3M\rangle = \left(\frac{3+M}{6}\right)^{\frac{1}{2}} |S_1S_2 M - \tfrac{1}{2},\tfrac{1}{2}\rangle + \left(\frac{3-M}{6}\right)^{\frac{1}{2}} |S_1S_2 M + \tfrac{1}{2},-\tfrac{1}{2}\rangle$$

$$|S_1S_2 2M\rangle = -\left(\frac{3-M}{6}\right)^{\frac{1}{2}} |S_1S_2 M - \tfrac{1}{2},\tfrac{1}{2}\rangle + \left(\frac{3+M}{6}\right)^{\frac{1}{2}} |S_1S_2 M + \tfrac{1}{2},-\tfrac{1}{2}\rangle \qquad (2)$$

Griffith has treated the first three terms of H, assuming that the exchange coupling dominates, and calculated the energies to first order in the coupled representation. The first term in the Hamiltonian gives rise to states having a total spin of S = 2 and 3, with energies

$$W(2) = -\frac{7}{4} J$$

$$W(3) = \frac{5}{4} J \qquad (3)$$

The S = 2 and S = 3 levels are five-fold and seven-fold degenerate, respectively. Inclusion of the D and E terms lifts the degeneracy of the S = 2 and 3 coupled states. Specifically, the S = 2 energy level is split into four sublevels having energies

$$W(M = \pm 2) = 8/3\ D$$

$$W(M = +1) = -4/3\ D + 4E \qquad (4)$$

$$W(M = -1) = -\ 4/3\ D - 4E$$

$$W\ (M = 0) = -\ 8/3\ D$$

Note that the $M_s = \pm 2$ levels are still degenerate within this order of approximation.

If the constraints applied in Griffith's calculations (D/J and E/D small) are relaxed, it becomes necessary to diagonalize the complete 12 x 12 Hamiltonian matrix to solve for the energies and wavefunctions of H. The Hamiltonian matrix including the first three terms of equation 1, and written in the S_1S_2SM representation, is shown in Fig. 1.

The two terms describing the Zeeman interaction of the magnetic field with the individual ions can be most easily written in the coupled representation by first rewriting them as

$$H_{Zeeman} = \beta \underset{\sim}{H} \cdot \underset{\approx}{g}_1 \cdot (\hat{\underset{\sim}{S}}_1 + \hat{\underset{\sim}{S}}_2) + \beta \underset{\sim}{H} \cdot (\underset{\approx}{g}_2 - \underset{\approx}{g}_1) \cdot \hat{\underset{\sim}{S}}_2 \qquad (5)$$

$$= \beta \underset{\sim}{H} \cdot \underset{\approx}{g} \cdot \hat{\underset{\sim}{S}} + \beta \underset{\sim}{H} \cdot \Delta \underset{\approx}{g} \cdot \hat{\underset{\sim}{S}}_2$$

Since the zero-field splitting interaction is large compared to the Zeeman interaction, we expand the Zeeman term in the principal axis system of the zero-field splitting tensor (x,y,z). To do this, $\underset{\approx}{g}_1$ and $\underset{\approx}{g}_2$ must be transformed into this same coordinate system before

	|3 3⟩	|3 2⟩	|3 1⟩	|3 0⟩	|3 -1⟩	|3 -2⟩	|3 -3⟩	|2 2⟩	|2 1⟩	|2 0⟩	|2 -1⟩	|2 -2⟩
⟨3 3|	$\frac{5}{4}J+\frac{10}{3}D$	0	$\frac{2}{3}\sqrt{15}E$	0	0	0	0	0	$-\frac{1}{3}\sqrt{30}E$	0	0	0
⟨3 2|		$\frac{5}{4}J$	0	$\frac{2}{3}\sqrt{30}E$	0	0	0	$\frac{2\sqrt{5}}{3}D$	0	$-\frac{1}{3}\sqrt{30}E$	0	0
⟨3 1|			$\frac{5}{4}J-2D$	0	4E	0	0	0	$\frac{2\sqrt{2}}{3}D$	0	$-\sqrt{2}E$	0
⟨3 0|				$\frac{5}{4}J-\frac{8}{3}D$	0	$\frac{2}{3}\sqrt{30}E$	0	$\frac{1}{3}\sqrt{6}E$	0	0	0	$-\frac{1}{3}\sqrt{6}E$
⟨3 -1|					$\frac{5}{4}J-2D$	0	$\frac{2}{3}\sqrt{15}E$	0	$\sqrt{2}E$	0	$\frac{-2\sqrt{2}}{3}D$	0
⟨3 -2|						$\frac{5}{4}J$	0	0	0	$\frac{1}{3}\sqrt{30}E$	0	$\frac{-2\sqrt{5}}{3}D$
⟨3 -3|							$\frac{5}{4}J+\frac{10}{3}D$	0	0	0	$\frac{1}{3}\sqrt{30}E$	0
⟨2 2|								$-\frac{7}{4}J+\frac{8}{3}D$	0	$\frac{4}{3}\sqrt{6}E$	0	0
⟨2 1|									$-\frac{7}{4}J-\frac{4}{3}D$	0	4E	0
⟨2 0|										$-\frac{7}{4}J-\frac{8}{3}D$	0	$\frac{4}{3}\sqrt{6}E$
⟨2 -1|											$-\frac{7}{4}J-\frac{4}{3}D$	0
⟨2 -2|												$-\frac{7}{4}J+\frac{8}{3}D$

[a] Determined by symmetry

Figure 1. Matrix of $JS_1 \cdot S_2 + D(\hat{S}_{1z} - \frac{35}{12}) + E(\hat{S}^2_{1x} - \hat{S}^2_{1y})$ in the S_1S_2SM representation. Only the values $|SM\rangle$ are indicated.

calculating the elements of $\Delta\underset{\approx}{g}$. In this case, we may assume that $\underset{\approx}{g}_1$ is isotropic with all g-values equal to 2.0, since the high symmetry of the high-spin $\underline{d}^5$ iron results in a nearly zero spin-orbit interaction for these electrons, and in fact the observed EPR signals from high-spin cytochrome $\underline{a}_3^{+3}$ are very nearly isotropic (7). (The EPR signals at g = 6 exhibited by high-spin ferric hemes result not from anisotropy in $\underset{\approx}{g}$, but because the transition occurs between $M_s = \pm 1/2$ states within an S = 5/2 manifold.) The transformation of $\underset{\approx}{g}_2$ from the principal axis system of the copper ion g-tensor (x_2, y_2 and z_2) into that of the zero-field splitting tensor may be related through the direction cosines $l_{i\alpha}$ between the corresponding axes in the two coordinate systems. Thus,

$$g_{ij} = \sum_{\alpha=x_2,y_2,z_2} l_{i\alpha} l_{j\alpha} g_\alpha \qquad (6)$$

and

$$\Delta g_{ij} = \sum_{\alpha=x_2,y_2,z_2} (l_{i\alpha} l_{j\alpha} g_\alpha - 2.0) \qquad (7)$$

The principal g-values for Cu_{a_3} are expected to deviate some from 2.0 due to the spin-orbit interaction of $\underline{d}^9$ copper, but this deviation should be no larger than about 15%. In fact, the measured principal g-values for Cu_{a_3} are 2.28, 2.11 and 2.05 (11), although these exact values may not necessarily pertain to the states of the enzyme we are considering in this work.

Calculation of the matrix elements of the first term of the Zeeman Hamiltonian (equation 3) in the coupled representation is straightforward. The matrix elements of the second term can be readily calculated in the $S_1S_2M_1M_2$ representation, and then transformed into the coupled representation via equation (2). The resulting elements of H_{Zeeman} are shown in Fig. 2.

The last term in equation (1), which represents the dipolar interaction between the two ions, has the form (12)

$$H_{dip} = \hat{\underset{\sim}{S}}_1 \cdot \underset{\approx}{J}_{dip} \cdot \hat{\underset{\sim}{S}}_2$$

where $\underset{\approx}{J}_{dip}$ is the dipolar coupling tensor. This interaction is dependent on the relative orientation of the principal g-tensors of the two ions as well as on the distance between them. The elements of $\underset{\approx}{J}_{dip}$, in the principal axis system of $\underset{\approx}{g}_1$, are given by (12)

$$J_{ij} = \frac{g_{1i}\beta^2}{r^3} \left[\sum_{\alpha=x_2,y_2,z_2} g_{2\alpha} l_{j\alpha} \left(l_{i\alpha} - 3\sigma_i \sum_{k=x_1,y_1,z_1} l_{k\alpha}\sigma_k \right) \right] \quad (8)$$

where the $l_{i\alpha}$ are the direction cosines between the principal axes of the two ions, the σ_i are the direction cosines denoting the orientation of $\underset{\sim}{r}$ with respect to x_1, y_1 and z_1, as shown in Fig. 3; and r is the distance between the two ions. Since we are assuming $\underset{\approx}{g}_1$ to be isotropic, we may replace x_1, y_1 and z_1 in equation 8 with x, y and z, the principal axes of the zero-field splitting tensor; the resulting direction cosines $l_{i\alpha}$ will then be the same as those in equations (6) and (7).

	|3 3⟩	|3 2⟩	|3 1⟩	|3 0⟩	|3 -1⟩	|3 -2⟩	|3 -3⟩	|2 2⟩	|2 1⟩	|2 0⟩	|2 -1⟩	|2 -2⟩
⟨3 3|	$3(Z+\zeta)$	$\frac{\sqrt{3}}{2}(A+\alpha)$	0	0	0	0	0	$\frac{\sqrt{30}}{2}\alpha$	0	0	0	0
⟨3 2|		$2(Z+\zeta)$	$\frac{\sqrt{10}}{2}(A+\alpha)$	0	0	0	0	$-\sqrt{5}\,\zeta$	$\frac{\sqrt{20}}{2}\alpha$	0	0	0
⟨3 1|			$Z+\zeta$	$\sqrt{3}(A+\alpha)$	0	0	0	$-\frac{\sqrt{2}}{2}\bar{\alpha}$	$-2\sqrt{2}\,\zeta$	$\frac{\sqrt{12}}{2}\alpha$	0	0
⟨3 0|				0	$\sqrt{3}(A+\alpha)$	0	0	0	$-\frac{\sqrt{6}}{2}\bar{\alpha}$	-3ζ	$\frac{\sqrt{6}}{2}\alpha$	0
⟨3 -1|					$-(Z+\zeta)$	$\frac{\sqrt{10}}{2}(A+\alpha)$	0	0	0	$-\frac{\sqrt{12}}{2}\bar{\alpha}$	$-2\sqrt{2}\,\zeta$	$\frac{\sqrt{2}}{2}\alpha$
⟨3 -2|						$-2(Z+\zeta)$	$\frac{\sqrt{3}}{2}(A+\alpha)$	0	0	0	$-\frac{\sqrt{20}}{2}\bar{\alpha}$	$\sqrt{5}\,\zeta$
⟨3 -3|							$-3(Z+\zeta)$	0	0	0	0	$-\frac{\sqrt{30}}{2}\bar{\alpha}$
⟨2 2|								$2(Z-\zeta)$	$A-\alpha$	0	0	0
⟨2 1|									$Z-\zeta$	$\frac{\sqrt{6}}{2}(A-\alpha)$	0	0
⟨2 0|										0	$\frac{\sqrt{6}}{2}(A-\alpha)$	0
⟨2 -1|											$-(Z-\zeta)$	$A-\alpha$
⟨2 -2|												$-2(Z-\zeta)$

$\underline{a}$ Determined by symmetry.

Figure 2. Matrix of the Zeeman Hamiltonian (equation 5) in the S_1S_2SM representation. Only the values $|SM\rangle$ are indicated. $Z = \beta H_z g_{1z}$; $A = \beta(H_x g_{1x} - iH_y g_{1y})$;

$$\zeta = \frac{\beta}{6} \sum_{\substack{j=x,y,z \\ \alpha=x_2,y_2,z_2}} H_j(l_{j\alpha}l_{z\alpha}g_\alpha - 2.0); \alpha = \left(\frac{\beta}{6\sqrt{2}}\right)\left[\sum_{\substack{j=x,y,z \\ \alpha=x_2,y_2z_2}} H_j(l_{j\alpha}l_{x\alpha}g_\alpha - 2.0) - iH_j(l_{j\alpha}l_{y\alpha}g_\alpha - 2.0)\right].$$

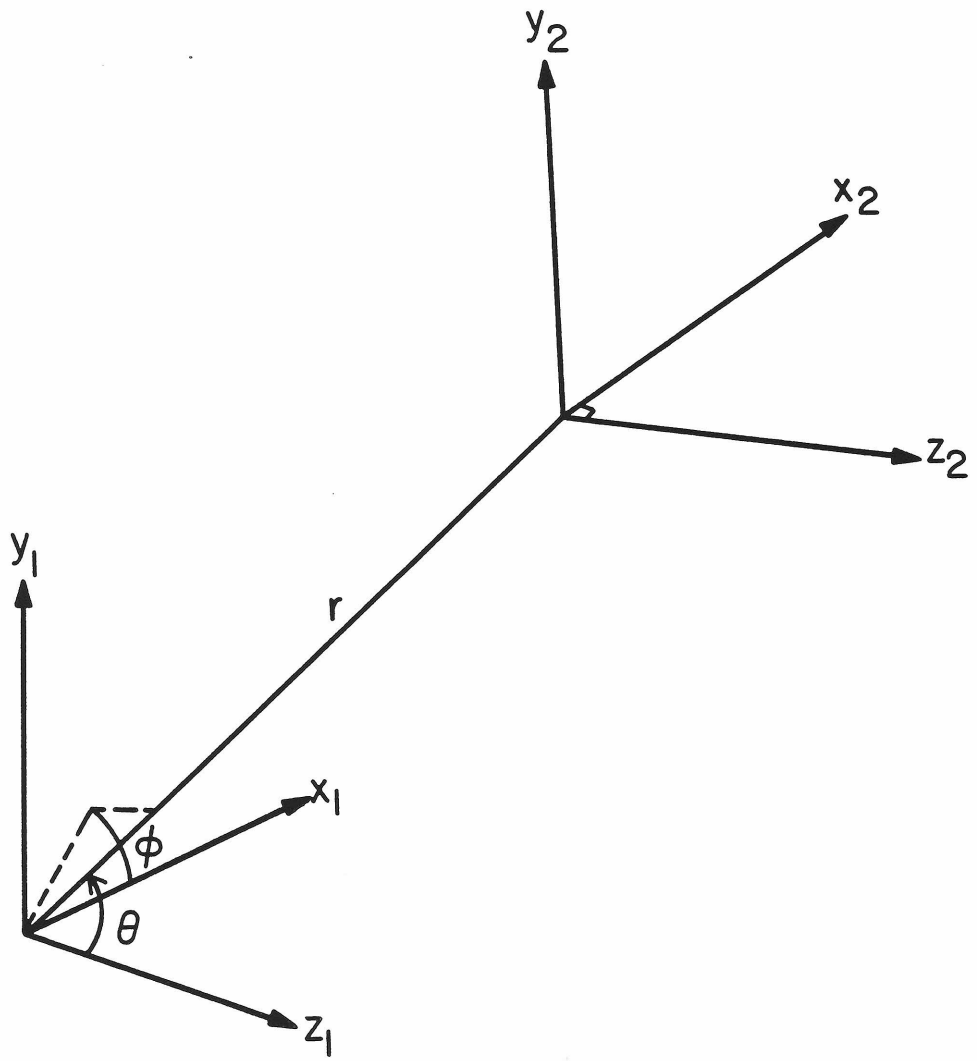

Figure 3. Relative coordinates of the two ions, $Fe_{a_3}^{+3}$ and $Cu_{a_3}^{+2}$.

The matrix elements of H_{dip} are most readily determined in the $S_1S_2M_1M_2$ representation. To obtain the elements of H_{dip} in the coupled representation, they are therefore first calculated in the $S_1S_2M_1M_2$ representation, and then transformed into the coupled representation via equation (2).

By diagonalizing the full 12 x 12 Hamiltonian matrix of H in our calculations, rather than resorting to perturbation theory, we can vary J, D, E, H and the relative orientations of the two ions without regard for the relative contributions of the elements of H. A computer program to diagonalize H was written in Fortran IV and run on Caltech's IBM 370/158 computer. The accuracy of the calculations was checked by running the program with J = 0 and r = 100 Å, in which case the energies and wavefunctions obtained correspond to those of the isolated ions and the allowed EPR transitions occur at the predicted values of the magnetic field. The program was also checked in the limits of small D/J and E/D. The energies calculated corresponded well to those predicted by the first-order calculations (see, for example, Table I); in particular, the low-field EPR transition was split into two resonances above and below g = 6 by 24 E/D, as predicted by theory (13).

Results

With a Hamiltonian as complex as equation (1), the behavior of the energy levels of the coupled cytochrome $\underline{a}_3^{+3}$-$Cu_{a_3}^{+2}$ spin system in a magnetic field might be expected to be complicated. Several of the terms of H are of comparable magnitude for the particular case we are

investigating, and the various terms can have synergistic effects on the energy levels of the system. In particular, the rhombic zero-field splitting, the Zeeman interaction, and the dipolar interaction are of comparable magnitude; furthermore, for a given conformation of the enzyme, the exchange coupling could conceivably be comparable to either the rhombic or axial zero-field splitting, depending on the relative configuration of the cytochrome $\underline{a}_3$ and Cu_{a_3} sites. We will attempt to deal with these inherent complexities by first considering the limiting cases of $J >> D$ and $J = 0$, and examining the way that the various terms of $\mathcal{H}$ other than the exchange coupling term act to generate unusual EPR "spectra". Finally, we will consider the EPR "spectra" that result from the case of small, but nonzero exchange couplings.

J >> D

The effect of J on the energy levels. When $J >> D$, S and M are good quantum numbers, and the energy levels should be close to those of equations (3) and (4) derived using first-order perturbation theory. The calculated splittings between adjacent energy levels of the $S = 2$ manifold for several values of the exchange coupling are shown in Table I for $D = 10\ cm^{-1}$ and $E = 1.0\ cm^{-1}$. There is indeed little deviation from the values predicted by the first-order theory (equations 3 and 4) for large J/D; only for $J/D \lesssim 5$ does the difference between the first-order and exact calculations become appreciable.

Allowed EPR transitions for the case of large J/D. Since the zero-field splitting, D, for a high-spin heme is expected to be $2\ cm^{-1}$ or

Table I. Differences in energy between the S = 2 energy sublevels, in cm^{-1}, as a function of J.

J	Δ_1[a]	Δ_2	Δ_3	Δ_4
10	6.55	7.94	26.77	0.07
25	8.33	8.46	32.85	0.54
50	9.02	8.30	34.71	0.46
200	9.55	8.09	35.73	0.41
500	9.66	8.04	35.89	0.40
Calculated to first order	9.33	8.00	36.00	0.00

[a] Δ_i is the energy difference between the ith and i + 1th energy levels, beginning with the lowest in energy. The values in the Table are for D = 10 cm^{-1}, E = 1 cm^{-1}, H_o = 0, and no dipolar interaction.

more, whereas an X-band EPR spectrometer operates at 9 GHz ($h\nu$ = 0.3 cm^{-1}) with the magnetic field scanned from 0 - 15,000 Gauss, transitions between the levels of the S = 2 manifold for which $\Delta M_s = \pm 1$ should not be observable by X-band EPR spectroscopy. This can be seen easily from equation (4). However, it can also be seen from equation (4) that if E is sufficiently small (E < 0.04 cm^{-1}), a $\Delta M_s = 2$ transition between the $M_s = \pm 1$ levels may be accessible by X-band EPR spectroscopy. Although the $\Delta M_s = 2$ transition is formally forbidden, it may become allowed at low magnetic fields when mixing occurs between the $M_s = \pm 1$ energy levels. The states are coupled only when there exists a component of $\underset{\sim}{H}_0$ directed along the z-axis (normal to the heme plane), and the transition is effected only when H_1, the oscillating magnetic field, also is parallel to H_z. Although a conventional EPR spectrometer has $H_1 \perp H_0$, the $\Delta M_s = 2$ transition could be still observed in a powder spectrum due to molecules for which both H_0 and H_1 have nonzero projections on the appropriate axis of the molecular coordinate system, as is the case for triplet EPR signals observed in frozen solution.

The dependence of the energy of the $\Delta M_s = 2$ transition upon magnetic field is shown in Fig. 4 for J = 200 cm^{-1}, D = 10 cm^{-1}, and a range of E values for which the transition will fall in the X-band region. The resonance condition is approximately described by

$$h\nu = 8E + 2g\beta H_o$$

or

$$g = (h\nu - 8E)/2\beta H_o \ .$$

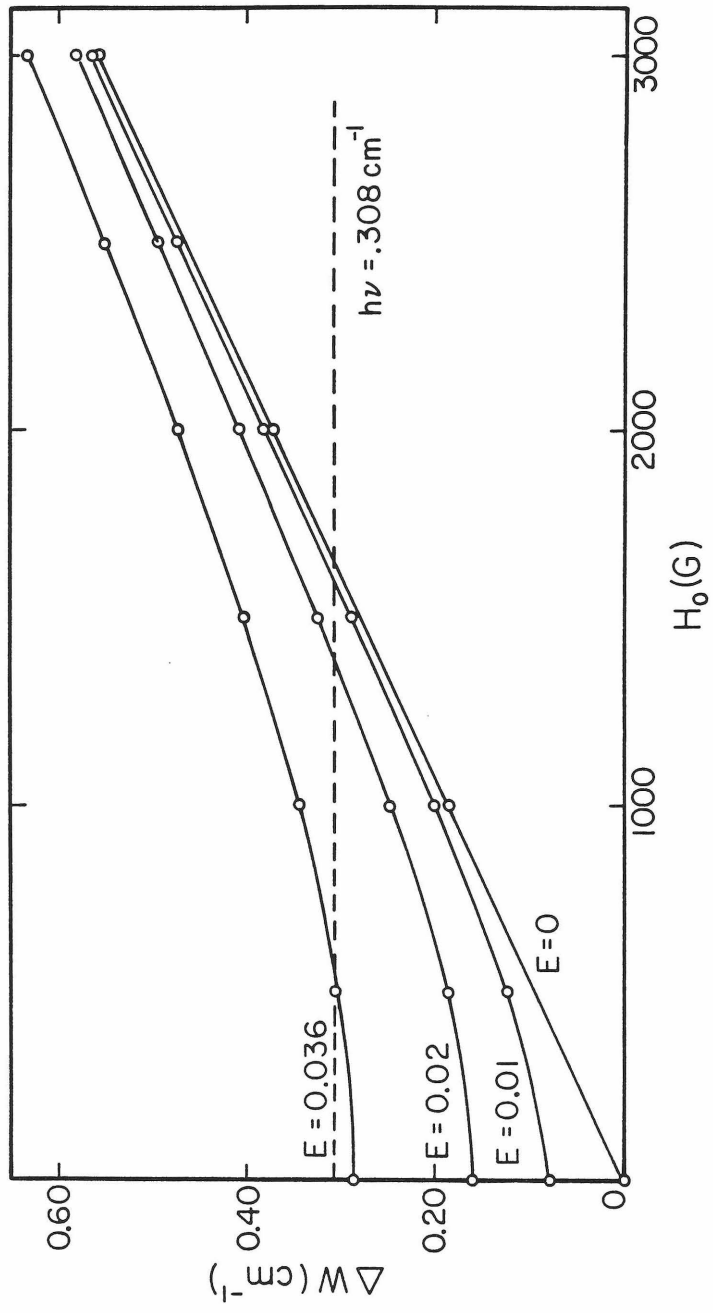

Figure 4. Energy of the $\Delta M_s = 2$ transition, in cm^{-1}, versus H_z, in Gauss, for $J = 200\ cm^{-1}$ and $D = 10\ cm^{-1}$. The values of E for each curve are indicated in the figure, and the dotted line indicates the resonance energy at X-band.

The transition probabilities for the $\Delta M_s = 2$ transition, for the same values of E as shown in Fig. 4, are shown in Fig. 5. These are clearly large enough that at low magnetic field the $\Delta M_s = 2$ transition should be observable.

Similarly to the $\Delta M_s = 2$ transition, a $\Delta M_s = 4$ transition between the $M_s = \pm 2$ sublevels of the S = 2 manifold may become allowed at low magnetic fields when mixing occurs between the $M_s = 2$ and $M_s = -2$ sublevels. Since the splitting between these sublevels is zero to first order (equation 4), for the transition to be observed by EPR spectroscopy at X-band, E must be substantially larger than it was for the $\Delta M_s = 2$ transition to be observed. This is confirmed in Fig. 6, which shows the splitting between the $M_s = \pm 2$ sublevels at $H_0 = 570$ G as a function of E, for J = 200 cm^{-1} and D = 10 cm^{-1}. Again, the transition probabilities at low magnetic field ($H_0 < 1000$ G) are large enough that the transitions would be expected to have appreciable intensity.

Detailed calculations show that, as expected, the dipolar interaction and/or anisotropy in $\underset{\approx}{g}_2$ have virtually no effect on the position of the $\Delta M_s = 2$ or 4 transitions for a given E, provided J/D > 1.

J = 0

For $J \lesssim D$, considerable mixing occurs between the S = 2 and S = 3 manifolds because of the off-diagonal matrix elements of the zero-field splitting terms in equation (1). These states are also mixed by the matrix elements of H_{zeeman} and H_{dip}, so the variation of the energy

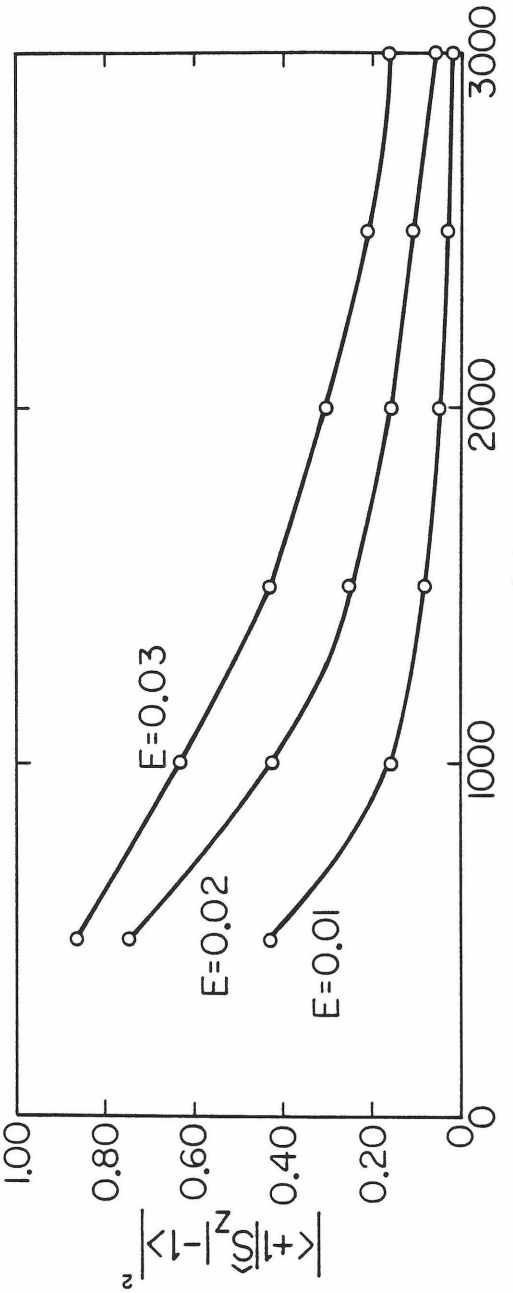

Figure 5. The transition probabilities for the $\Delta M_s = 2$ transition as a function of the magnetic field, in gauss. The transition probabilities were calculated as $|\langle +1|\hat{S}_z|-1\rangle|^2$, where the $M_s = +1$ and $M_s = -1$ eigenstates were solved for at each value of H_z for which a point is indicated in the figure. The values of E for each curve are indicated.

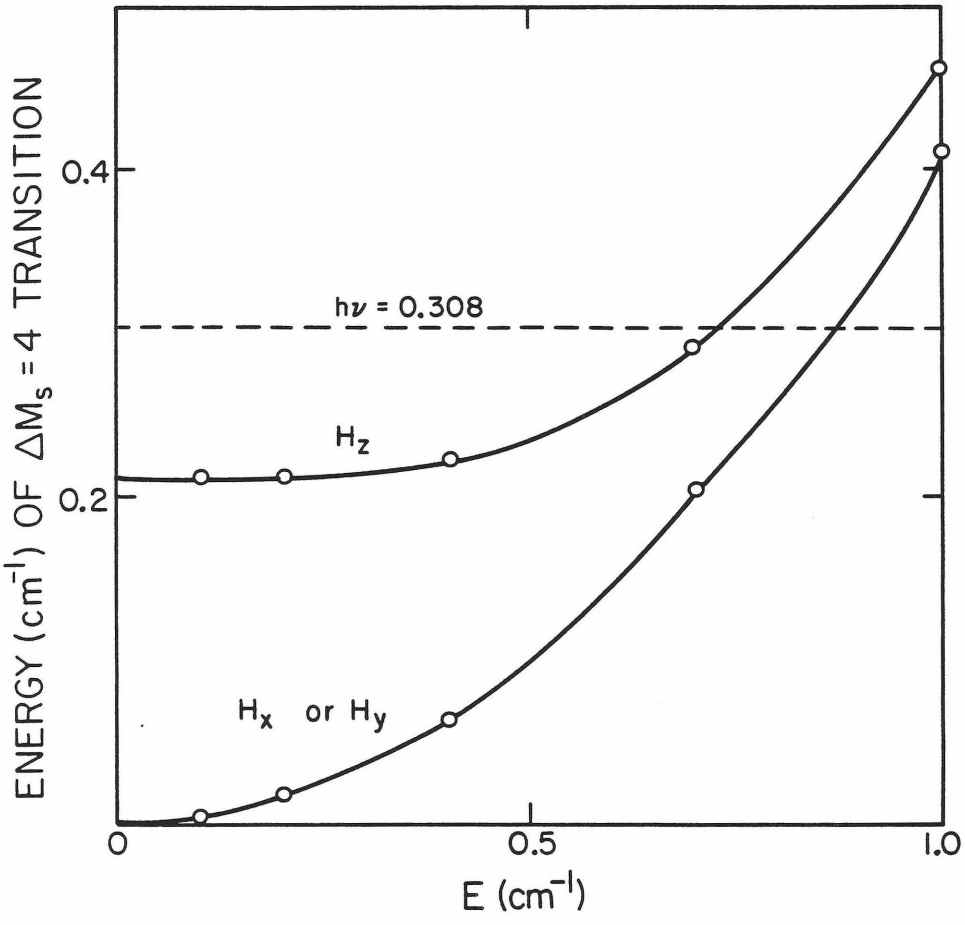

Figure 6. Energy of the $\Delta M_s = 4$ transition, in cm^{-1}, versus the rhombic splitting E, in cm^{-1}, at $H_0 = 750$ G. The dotted line indicates the energy required to observe a transition by X-band EPR spectroscopy.

levels with E, $\mathcal{H}_{zeeman}$ and $\mathcal{H}_{dip}$ for a given D is expected to be complex. The way in which this complexity arises is shown in Fig. 7, and will be discussed in detail below.

J = 0, $r \to \infty$. For J = 0, in the absence of dipolar coupling we have the simplest case of two isolated spins. At r = 100 Å, the dipolar term is negligible and when the magnetic field is turned off, three energy levels are obtained for the two ions, with energies approximately (almost exactly, since E << D) -8/3 D, -2/3 D and 10/3 D, as seen in Table II. Each of the energy levels is four-fold degenerate, since the four wave functions $|\pm M_1, \pm 1/2\rangle$ (where $M_2 = \pm 1/2$) have the same energies when $H_0 = 0$. When the magnetic field is turned on, the energy levels split, the splitting being determined by the summed effect of $\mathcal{H}_{zeeman}$ on the individual ions.

Since D >> hν (for a high-spin ferric heme, D is expected to be in the neighborhood of 2 - 10 cm^{-1}), one observes EPR from the $M_s = \pm 1/2$ Kramer's doublet of the heme iron, and the exact magnitude of D is not so important in determining the resonant field as is that of E/D. For the case of isotropic g-tensors for each of the ions, and no rhombic zero-field splitting for the heme iron (E = 0), the copper ion will exhibit a single resonance at g = 2, and the heme iron will display two resonances between the $M_s = \pm 1/2$ sublevels of the S = 5/2 manifold, at g = 2 ($g_{||}$) and g = 6 ($g_{\perp}$), as depicted in Fig. 7A.

If E is nonzero, then the resonance at g = 6 will be split into two resonances along H_x and H_y, with g-values of 6 ± 24 E/D, as depicted

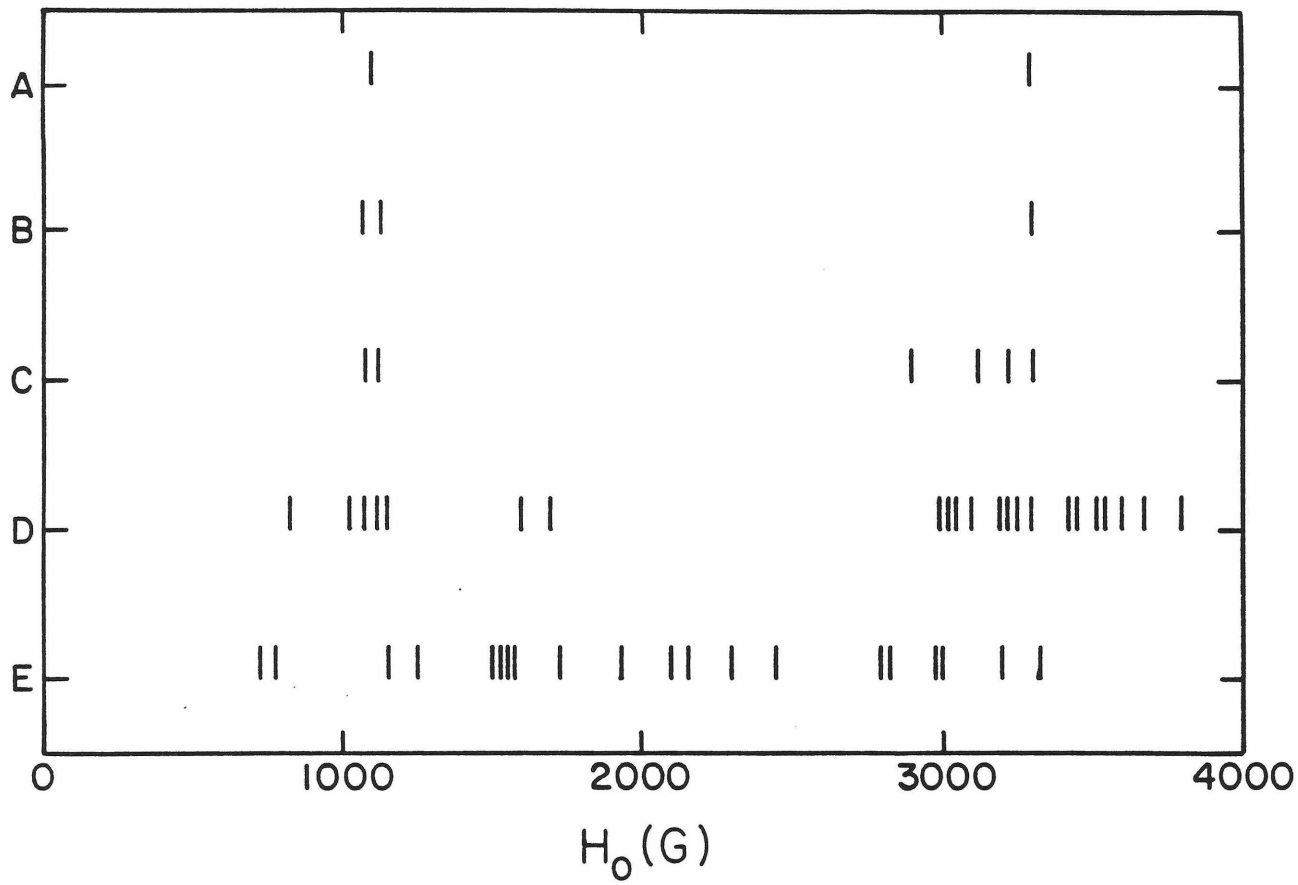

Figure 7. Calculated resonance positions (or turning points in a powder spectrum) at X-band ($h\nu$ = 0.308 cm^{-1}), for a high-spin, ferric iron and a cupric copper. (a) with isotropic g_1 and g_2, and no rhombic zero-field splitting, no dipolar interaction, and no exchange coupling; (b) with E = 0.030 cm^{-1} (E/D = .005); (c) with E = 0.030 cm^{-1} and anisotropic g_2; (d) with E = 0.030 cm^{-1}, isotropic g_2, and a dipolar interaction with r = 5 Å; (e) as in (d), with J = 0.1 cm^{-1}. The value of D used was 6.0 cm^{-1}.

in Fig. 7B. If anisotropy in $\underset{\approx}{g}_2$ is now included, with the spins still isolated, then the g = 2 resonance of the copper ion is correspondingly split into three resonances for a powder, as shown in Fig. 7C; a transition at g = 2 remains due to the heme iron.

J = 0, with dipolar coupling. When r is set at 5 Å, the dipolar interaction is no longer negligible, and the formerly degenerate energy states are now split at zero magnetic field. Concomitantly, as seen in Fig. 7D, the calculated "spectrum" becomes considerably more complicated. This is true even if an isotropic $\underset{\approx}{g}_2$ is assumed. Some of the allowed transitions which were degenerate in the absence of H_{dip}, such as the $|M_1 = -1/2, M_2 = -1/2\rangle \rightarrow |M_1 = 1/2, M_2 = -1/2\rangle$ and $|M_1 = -1/2, M_2 = 1/2\rangle \rightarrow |M_1 = 1/2, M_2 = 1/2\rangle$ transitions (in the uncoupled representation), are split apart slightly by the dipolar coupling. This accounts for the splittings of the transitions around g = 6 and g = 2. Furthermore, some transitions which are forbidden in the absence of dipolar coupling become allowed when H_{dip} is included. This is the origin of the transitions near half-field, as well as of the transition at lowest field.

(a) Effect on the energy levels of anisotropy in $\underset{\approx}{g}_2$.

The effect of including anisotropy in $\underset{\approx}{g}_2$ for the case of dipolar coupling only is shown in Table II, assuming parallel principal axes for $\underset{\approx}{g}_1$ and $\underset{\approx}{g}_2$. It can be seen that the effect of including anisotropy in $\underset{\approx}{g}_2$ is to cause the energy levels to shift, in the same direction as the magnetic field shifts them from their energies at zero field, an additional amount approximately equal to $\Delta g \beta H_0$, where Δg is the

Table II. Effect of varying r upon some selected energies of the dipolar-coupled, cytochrome $\underline{a}_3^{+3}$, $Cu_{a_3}^{+2}$ spin system.[a]

r = 100 Å	-16.002[b]		-4.000[b]		-20.002[b]		$H_o = 0$
	-16.566	-15.464	-4.138	-3.840	19.864	20.144	H_x
	-16.282	-15.722	-4.559	-3.438	19.160	20.841	H_z $H_o = 3000$ G
r = 5 Å	-16.025	-15.968	-4.019	-3.976	19.966	20.034	$H_o = 0$
	-16.563	-15.461	-4.141	-3.835	19.847	20.162	H_x
	-16.288	-15.725	-4.574	-3.452	19.134	20.818	H_z $H_o = 3000$ G
r = 4 Å	-16.048	-15.937	-4.039	-3.954	19.934	20.066	$H_o = 0$
	-16.562	-15.456	-4.150	-3.826	19.828	20.181	H_x
	-16.296	-15.726	-4.589	-3.464	19.109	20.803	H_z $H_o = 3000$ G
r = 5 Å	-16.565	-15.458	-4.143	-3.833	19.845	20.164	H_x
Δg incl.	-16.307	-15.706	-4.594	-3.433	19.115	20.838	H_z $H_o = 3000$ G

[a] Energies (in cm^{-1}) are the highest and lowest in each of the three sublevels (see Fig. 9). Other parameters are: $J = 0\ cm^{-1}$, $D = 6.0\ cm^{-1}$, $E = 0.030\ cm^{-1}$, $A_1 = A_2 = A_3 = 0^o$, $\theta = 30^o$, $\phi = 0^o$.

[b] Four-fold degenerate.

anisotropy in g. The energy levels not given in the table, which are intermediate in each sublevel, are similarly shifted, but by somewhat smaller amounts.

We have also investigated the effect upon the energy levels of including anisotropy in $\underset{\approx}{g}_2$ in the dipolar Hamiltonian. As expected, a change in anisotropy of about 10% of g_e causes the energies to shift by just a few thousandths of a wavenumber, or a few tens of Gauss, at the most.

(b) Effect on the EPR spectrum of varying E.

One might expect subtler effects on the energy levels and calculated transitions upon varying E, r, or the relative orientation between the two ions, in this case (ions interacting via dipolar coupling only). The variation in the calculated EPR "spectra" of the dipolar-coupled spin system with E, for D = 6.0 cm^{-1} and r = 5 Å, is shown in Fig. 8A. We should note that the transitions indicated are all allowed, but that the relative intensities among these transitions, which we have not calculated, are expected to vary. Varying E between 0.030 and 0.1 cm^{-1} has slight effect on the absolute energies of the calculated eigenstates of the coupled spin system, and consequently there is little change in the positions of the calculated resonances. For $E \geq 0.2$ cm^{-1}, the energies of the eigenstates are substantially affected by the rhombic splitting, and the resonance positions are more noticeably affected.

(c) Effect on the energy levels of varying the relative orientation

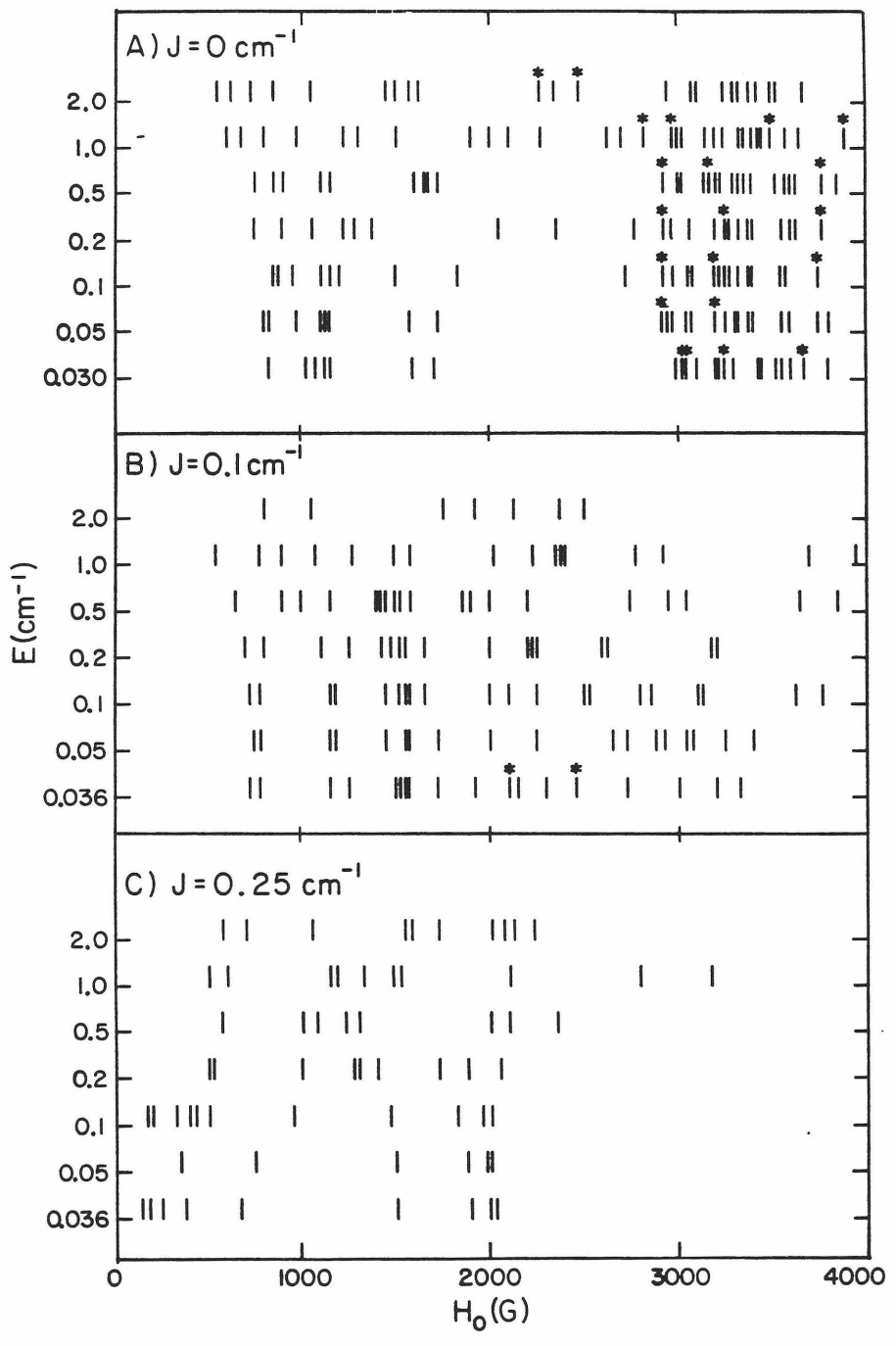

Figure 8. Allowed X-band EPR transitions for the coupled spin system for various values of E, the rhombic zero-field splitting. (A) J = 0, (B) J = 0.1, (C) J = 0.25 cm^{-1}. The values of the other parameters used are: $D \cong 6.0\ cm^{-1}$, $A_1 = A_2 = A_3 = 0^o$, $\theta = 30^o$, $\phi = 15^o$, and r = 5 Å. Transitions marked with an asterisk occur among the highest energy sublevels of the coupled spin system, and would exhibit little intensity at temperatures less than 20 K.

of cytochrome $\underline{a}_3^{+3}$ and $Cu_{a_3}^{+2}$.

The relative orientation of the two ions may be varied by varying θ and ϕ (see Fig. 3), and by varying the Euler angles A_1, A_2 and A_3 (see, for example, Ref. 14, p. 102). We have found that, for J = 0, changing the relative orientation of the two ions has only a small effect on the energy levels at zero magnetic field and at 3000 G. Changing θ or ϕ produces a larger shift in energies than does changing the Euler angles, but in either case the energies change only by a few thousandths of a wavenumber.

The effect of varying r (in the neighborhood of 5 Å) upon the energy levels, and hence upon the calculated EPR transitions, of the dipolar-coupled spin system, is also small. This can be seen from the data in Table II, for r equal to 4 Å and 5 Å. We have assumed r = 5 Å (15) in most of our calculations.

$J \neq 0$, $J \lesssim D$

The effect of small J on the EPR spectrum. We now consider the effect of including a small exchange coupling interaction in addition to the rhombic zero-field splitting and the dipolar interaction, with J larger than the dipolar coupling (J = 0.1 cm^{-1}; the magnitude of H_{dip} at r = 5 Å is about 0.030 cm^{-1}). The result is an increased splitting between the energy levels at zero magnetic field, which causes most of the transitions to be shifted to lower field, as seen in Fig. 7E. Some of the transitions are lost altogether, and at large

enough J, the energy levels are split apart sufficiently far that no transitions can occur except for the formally forbidden $\Delta M_s = 2$ and $\Delta M_s = 4$ transitions, depending on the value of E/D, as has already been discussed. The splitting of the energy levels of the coupled spin system in an applied magnetic field for various values of J is shown in Fig. 9, with D, E, r and the relative orientation between the two ions held constant.

(a) Effect on the energy levels of anisotropy in $\underset{\approx}{g}_2$.

The effect of including a small amount of anisotropy (about 10%) in $\underset{\approx}{g}_2$, in the case of small exchange coupling, is similar to that found for J = 0. A couple of the transitions shift by as much as 100 - 200 G, but most are considerably less affected.

(b) Effect on the EPR spectrum of varying E.

The variation in the EPR "spectra" with E for J = 0.10 and 0.25 cm^{-1} is shown in Figs. 8B and 8C, respectively, for D = 6.0 cm^{-1} and r = 5 Å. It can be seen from Fig. 8B that as E increases from 0.036 to 0.2 cm^{-1}, the high-field transitions are split apart. The reason for this is that these transitions occur among the central set of sublevels shown in Fig. 9 (those transitions occurring among the upper set of sublevels disappear for $E \geq 0.05$ cm^{-1}), and as can be seen from that figure, a slight change in the energies of these sublevels is expected to cause a relatively dramatic shift in the resonance positions of these transitions. No such transitions occur for J = 0.25 cm^{-1}, as seen in Fig. 8C, as only the set of sublevels lowest in energy are split by the Zeeman interaction such that transitions between them can occur at the energies

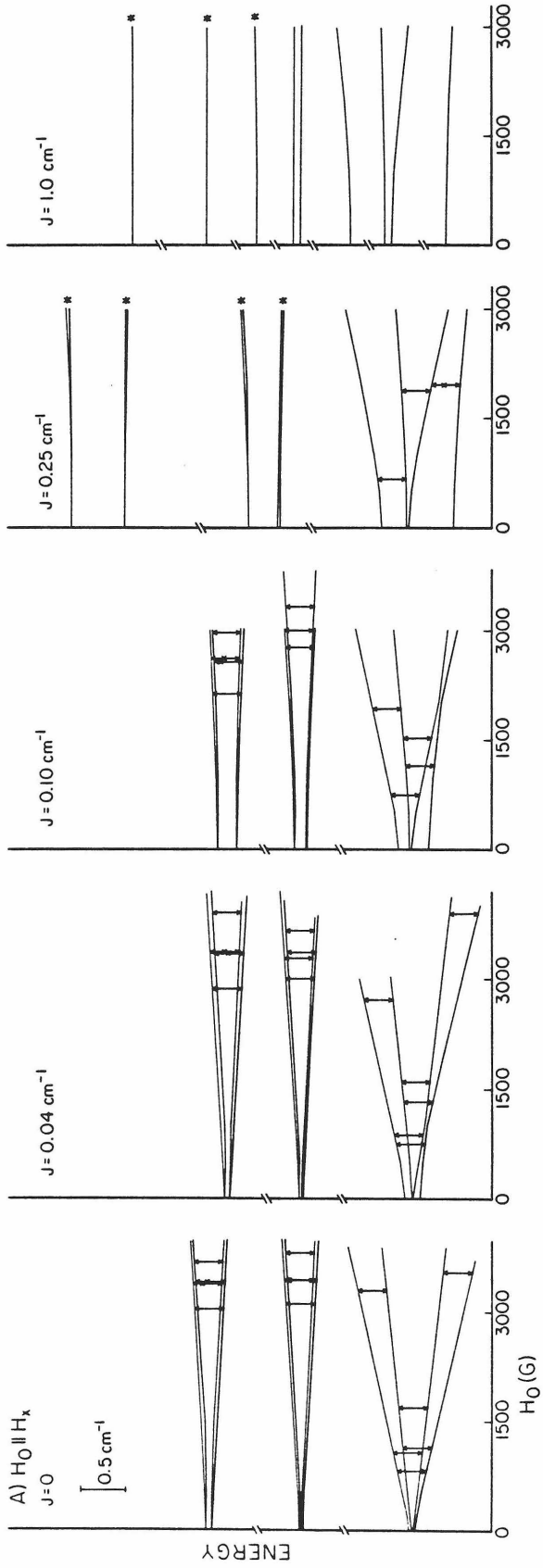

Figure 9(A). Energy levels of the coupled spin system as a function of magnetic field. The transitions accessible to X-band EPR spectroscopy ($h\nu$ = 0.308 cm^{-1}) are indicated; those transitions with near-zero transition probability are marked with an x to indicate that they are not allowed. Energy levels marked with an asterisk are doubly degenerate. From left to right, J = 0, 0.04, 0.10, 0.25 and 1.0 cm^{-1}; (A) $H_0 \| H_x$, (B) $H_0 \| H_y$, (C) $H_0 \| H_z$. The values of the other parameters are: D = 6.0 cm^{-1}, E = 0.036 cm^{-1} (E = 0.030 cm^{-1} for J = 0). $A_1 = A_2 = A_3 = 0^0$, $\theta = 30^0$, $\phi = 0^0$, and r = 5 Å.

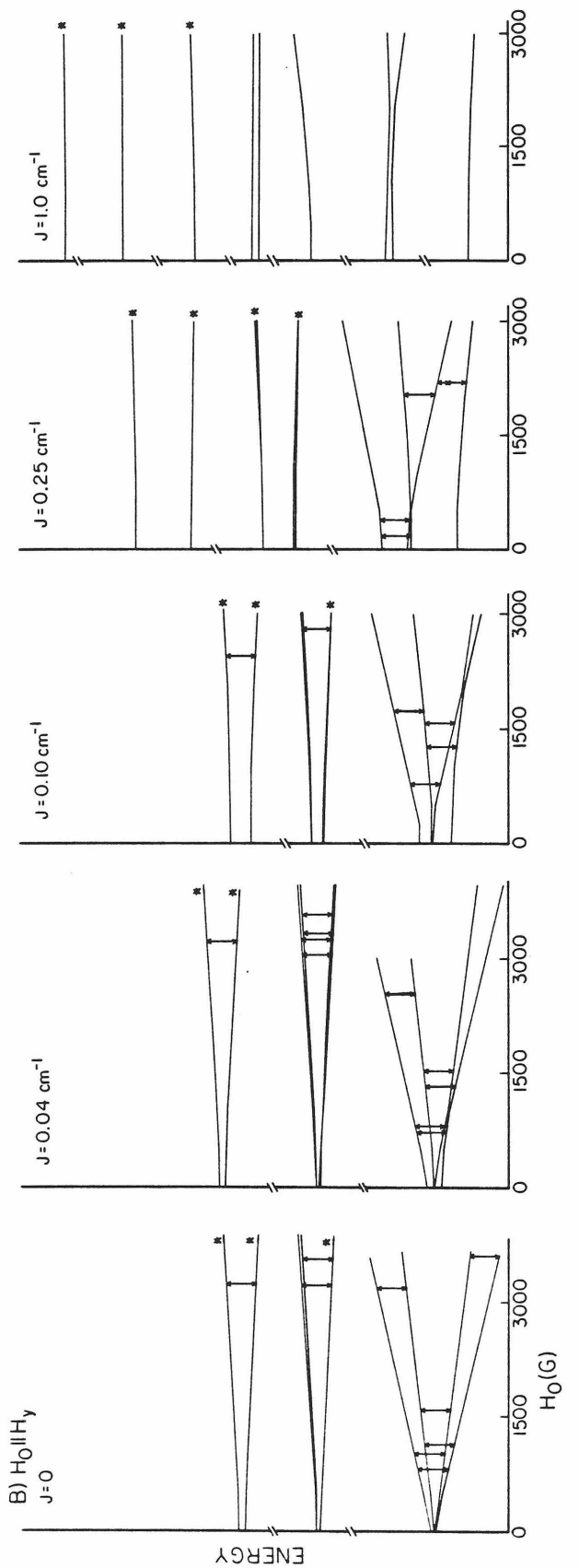
B) $H_0 \| H_y$
J=0
J=0.04 cm^{-1}
J=0.10 cm^{-1}
J=0.25 cm^{-1}
J=1.0 cm^{-1}
ENERGY
0
1500
3000
H_0(G)

Figure 9(B).

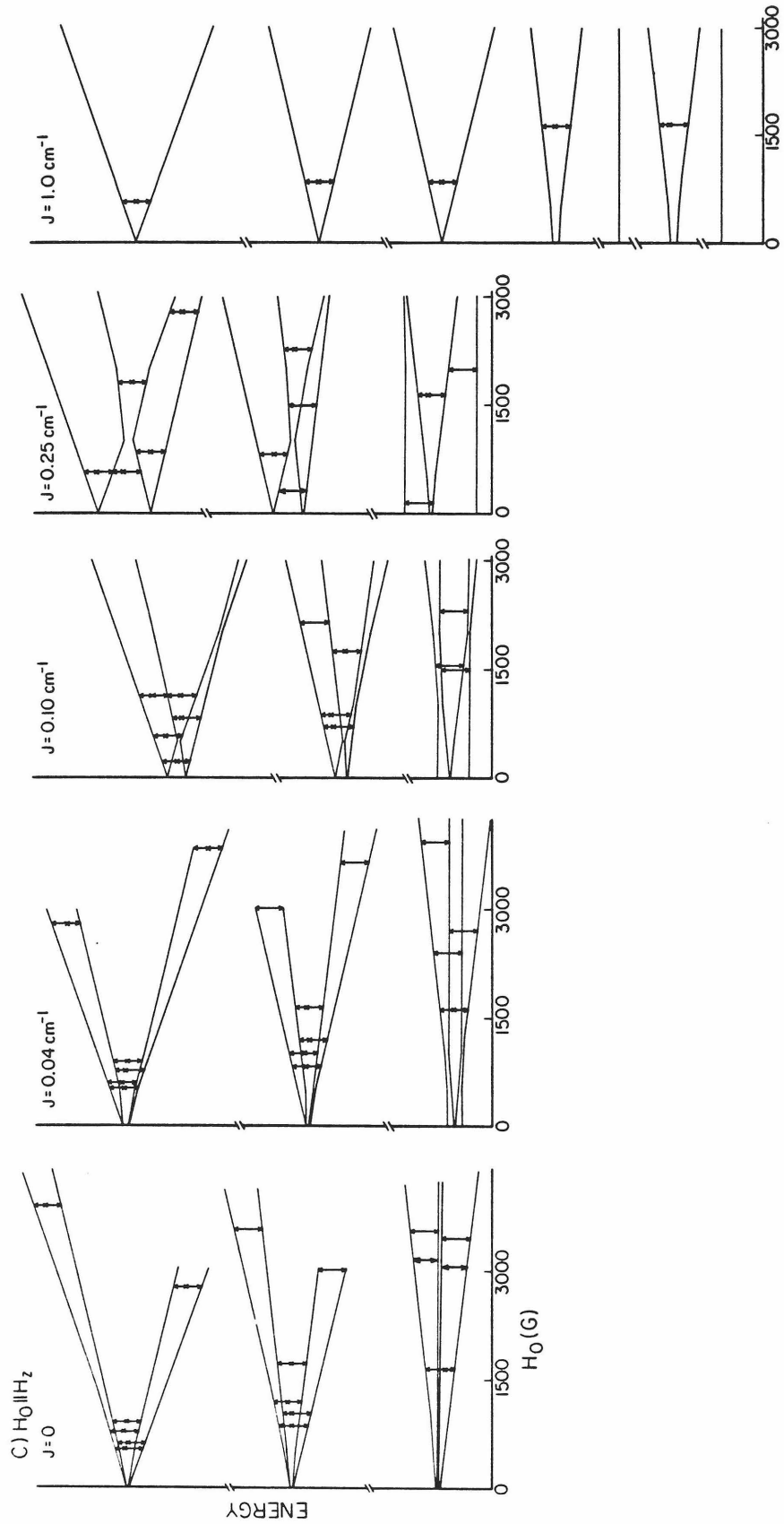
C) $H_0 \| H_z$
J=0
J=0.04 cm^{-1}
J=0.10 cm^{-1}
J=0.25 cm^{-1}
J=1.0 cm^{-1}
ENERGY
H_0(G)
0
1500
3000

Figure 9(C)

used in EPR spectroscopy (Fig. 9). As for the case of no exchange coupling, the transitions at low field are not much affected by varying E if E is fairly small; in the presence of weak exchange coupling, only for $E > 0.2\ cm^{-1}$ are the EPR "spectra" appreciably altered. Furthermore, the overall character of the "spectra" for both J = 0.10 and $0.25\ cm^{-1}$ does not depend much on the value of E, in that transitions are exhibited in the same regions of the EPR "spectra" for all possible values of the rhombic splitting constant.

(c) Effect on the energy levels of varying the relative orientation of cytochrome $\underline{a}_3^{+3}$ and $Cu_{a_3}^{+2}$.

Finally, the effect of varying the relative orientation between the two ions for small J is relatively minor, as it was for J = 0. The energies of the eigenstates change by only a few thousandths of a wavenumber over a range of orientations, so the EPR observable transitions will occur at the same magnetic field, within a few tens of Gauss, regardless of the relative orientation of the two ions.

Discussion

In this section, we will attempt to explain the origin of the unusual "g5", "g12", and fluorocytochrome $\underline{a}_3$ EPR signals, using the results discussed previously. We have shown that the largest changes in the positions of calculated EPR resonances occur upon varying J and E. However, the values of E calculated from the high-spin heme EPR signals exhibited by partially oxidized cytochrome $\underline{c}$ oxidase (7) range

only from 0.01 - 0.2 cm^{-1}. Since varying E in this range has little effect upon the EPR spectrum, the exchange coupling is left as the most important factor in matching the observed and calculated EPR spectra for the coupled spin system. The magnitude of D might also be expected to influence significantly the calculated resonance positions. However, we have assumed $D > 2\ cm^{-1}$, in accordance with measured values for high-spin ferric hemes, and with D this large, only the magnitude of J/D is expected to be important. Hence, we have varied only J, with $D = 10\ cm^{-1}$ or $6\ cm^{-1}$, in accordance with the value determined for oxidized cytochrome $\underline{a}_3^{+3}$ of about $9\ cm^{-1}$ (3,4) and for metmyoglobin fluoride of $6.1\ cm^{-1}$ (16), which is likely to be similar to the value of D for fluorocytochrome $\underline{a}_3$.

We may also note that the effect of anisotropic $\underset{\approx}{g}_2$ would most likely be to induce some broadening in the frozen solution EPR spectrum. Since the spectra we are concerned with display primarily broad features separated by many hundreds of Gauss (Fig. 7 and Ref. 5), we therefore do not believe that the effect of anisotropy in $\underset{\approx}{g}_2$ will be fundamental to explaining the nature of these signals, and so we have used isotropic $\underset{\approx}{g}_2$ for most of our calculations. For the same reason, we have not included the effect of hyperfine interactions in our calculations, either.

The "g12" EPR signal.

The allowed EPR transitions from Fig. 9 are plotted as a function of the magnetic field in Fig. 10, with the observed transitions of the "g12", "g5", and the fluorocytochrome $\underline{a}_3$ EPR signals, as well as the Cu_a signal, shown for comparison. As in Fig. 8, we have indicated only allowed transitions, and not relative intensities. Considering the

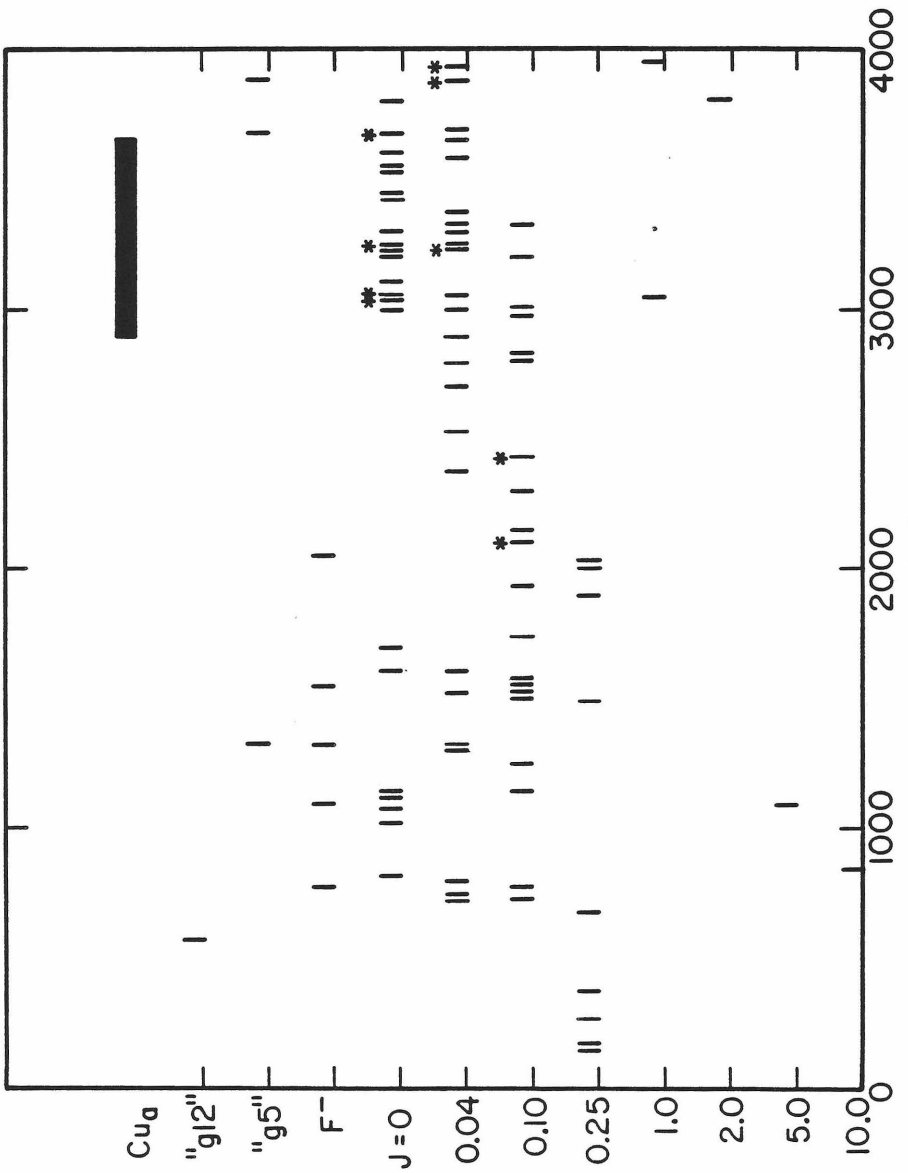

Figure 10. Allowed X-band EPR transitions for the coupled spin system for various values of J, with other parameters as in Fig. 9. The observed transitions for the fluoro-cytochrome a_3 EPR signal (designated by "F$^-$"), the "g5" EPR signal, and the Cu$_a$ EPR signal, are also shown. Transitions marked with an asterisk occur among the highest energy sublevels of the coupled spin system (see Fig. 9), and would exhibit little intensity at temperatures less than 20 K.

"g12" signal first, it is clear from Fig. 10 that this signal could only arise from a conformation with J on the order of 5 cm^{-1} or greater. The transition could either be due to a $\Delta M_s = 2$ transition between $M_s = \pm 1$ sublevels, if E is small, as in Fig. 10, or it could arise from a $\Delta M_s = 4$ transition between $M_s = \pm 2$ sublevels if E is on the order of 0.8 cm^{-1} (Fig. 6). We believe the former possibility is more likely, since the rhombic splitting observed from high-spin cytochrome $\underline{a}_3^{+3}$ EPR signals is small (7). Furthermore, the $M_s = \pm 2$ sublevels are approximately 16/3 D, or about 50 cm^{-1} for cytochrome c oxidase, above the ground state in energy. This means that the intensity of the signal should decrease with decreasing temperature below 30 K, when in fact the opposite is observed (5). For the $\Delta M_s = 2$ transition, the EPR signal intensity should increase with decreasing temperature down to about 12 K, which is not inconsistent with our observations (5). Thus, we assign the g = 12 EPR signal of oxidized cytochrome c oxidase to a $\Delta M_s = 2$ transition between $M_s = \pm 1$ sublevels in the S = 2 manifold, with E = 0.036 cm^{-1} (Fig. 4).

In our experience, when cytochrome c oxidase is isolated by the method of Hartzell and Beinert (17), typically about 30 - 40% of the enzyme molecules are found in the "g12" conformation. Since the magnetic susceptibility measurements (3,4) were done with enzyme isolated by the Hartzell and Beinert procedure, and no non-Curie behavior was found below 200 K (neglecting the effect of D), cytochrome $\underline{a}_3$ and Cu_{a_3} must be strongly exchange-coupled in the "g12" conformation.

The fluorocytochrome a_3 EPR signal. Inspection of Fig. 10 shows that the complexity of this signal requires that there be only a weak exchange coupling, if any, as suggested by Brudvig et al. (5). Although there is not an exact match between observed and predicted g-values, a fairly good match is provided by values of J less than or equal to 0.1 cm^{-1}, with the best fit being for J = 0.1 cm^{-1}. The high-field resonances predicted for this value of J would be obscured by the Cu_a signal near g = 2, whereas for smaller values of J one would expect to observe transitions occurring at higher field than those for Cu_a, when in fact none are observed. We therefore believe that the fluorocytochrome a_3 EPR signal is best assigned to a dipolar-coupled and weakly exchange-coupled high-spin fluorocytochrome a_3^{+3}-$Cu_{a_3}^{+2}$ site.

Inspection of Fig. 8B shows that E must be small ($\leq$ 0.05 cm^{-1}) in order that no high-field resonances be observed, in the presence of Cu_a^{+2}, for J = 0.1 cm^{-1}. This is consistent with the axial character of the high-spin, fluorocytochrome a_3^{+3} EPR signal seen when $Cu_{a_3}^{+2}$ is uncoupled from this center by addition of NO to the enzyme (5,18).

The "g5" EPR signal.

Finally, comparison of the predicted resonances for the values of J in Fig. 10 with the observed resonances of the "g5" signal indicates that none of the coupling schemes with transitions shown in the figure accounts for the observed resonances. When J is less than or equal to about 0.25 cm^{-1}, the calculated EPR "spectra" exhibit too many resonances,

particularly in the low-field region, to mimic the "g5" spectrum. As J is increased, the low-field resonances are first lost, and one or two transitions are calculated to occur at g-values less than g_e. These transitions occur when H_0 is parallel to H_x or H_y. At greater J ($J > 3.0\ cm^{-1}$), a transition is again expected to be seen at low-field, when $H_0 \| H_z$, but the high-field resonances have already been lost when this occurs. Since we have seen that varying E (with $E < 0.2\ cm^{-1}$) or the relative orientation of the two ions has little effect on the character of the EPR spectrum, it appears that the "g5" signal cannot be accounted for by a model including only a weak exchange and/or dipolar interaction between the two ions.

An explanation suggested by Shaw et al. (9) is that the signal at g = 5 could arise from quantum mechanical mixing between a spin 5/2 and spin 3/2 system, as suggested for other heme proteins by Maltempo and Moss (19). In fact, g_x and g_y would be expected to occur near g = 5 if the S = 3/2 and 5/2 states of the heme were nearly equal in energy. The high-field, g_z resonance would be expected to occur near g = 1.7 if the value of E was about $0.09\ cm^{-1}$, not an unreasonable value. The observed splitting of this resonance could be due to a weak interaction with another paramagnetic center, as suggested by Shaw et al. (9). The most likely candidate for this center, based on the magnitude of the splitting (about 200 G) and assuming a dipolar interaction as its cause, is the Cu_{a_3} center. However, this fails to explain why no EPR signal is observed from this latter site, since it would have to be oxidized to induce the observed splitting. It is possible that the interaction of

the $Cu^{+2}_{a_3}$ center with the cytochrome $\underline{a}_3^{+3}$ site in this conformation might cause the EPR signal from the $Cu^{+2}_{a_3}$ site to be obscured by broadening. Further studies, such as investigating the temperature dependence of the "g5" EPR signal, are needed to help settle this matter.

Conclusion

We have calculated the g-values of the allowed transitions that are accessible to energies used in EPR spectroscopy between the energy levels of the dipolar-coupled cytochrome $\underline{a}_3$-Cu_{a_3} spin system of cytochrome $\underline{c}$ oxidase, in the presence of strong, weak and zero exchange coupling. By calculating the effects on the energies of allowed transitions of varying J, D, E, H, r, and the relative orientations between cytochrome $\underline{a}_3$ and Cu_{a_3}, we have been able to suggest that

(1) The "g12" signal exhibited by oxidized cytochrome $\underline{c}$ oxidase at X-band is due to a $\Delta M_s = 2$ transition between $M_s = \pm 1$ levels of the strongly exchange-coupled, S = 2 center that constitutes the oxygen-binding site of the enzyme.

(2) The fluorocytochrome a_3 EPR signal with resonances at g = 8.5, 6, 5, 4.3 and 3.2 is due to a dipolar-coupled, weakly exchange-coupled ($J \simeq 0.1\ cm^{-1}$) fluorocytochrome $\underline{a}_3^{+3}$, $Cu^{+2}_{a_3}$ site.

(3) The "g5" EPR signal seen within 5 ms upon reoxidation by O_2 of the reduced enzyme, with resonances at g = 5, 1.78 and 1.69 is probably due to a quantum mechanically mixed spin state of cytochrome $\underline{a}_3$, with the splitting of the high-field

resonance being due to interaction with another paramagnetic center of the enzyme.

The low values of E ($E \lesssim 0.1$ cm^{-1}) required for consistency in the assignments of the "g12" and "g5" EPR signals indicate that the environment of cytochrome $\underline{a}_3$ is fairly axial. This is in line with the observed high-spin cytochrome $\underline{a}_3$ EPR signals in partially oxidized cytochrome $\underline{c}$ oxidase (7). The biochemical significance of the variation in the magnitude of the exchange coupling among the various states of the oxidized enzyme mentioned above is harder to assess, as is the significance of the posited quantum mechanically mixed spin state giving rise to the "g5" EPR signal. The reason for this is simply that too little is known about either of these phenomena to allow quantitative deductions to be made about structures in which they are present. However, it is interesting to note that cyanide bound to oxidized cytochrome $\underline{a}_3$ facilitates an antiferromagnetic coupling of about 40 cm^{-1} (3), as opposed to the hypothesized coupling in the fluoride-bound species of less than 1 cm^{-1}. A reasonable explanation for this difference is that fluoride, being much smaller than cyanide, allows a much smaller orbital overlap between the two ions, causing a reduction in the antiferromagnetic coupling. Similarly, if fluoride ion displaces hydroxide ion as the bridging ligand in the "oxygenated" enzyme to give rise to the fluorocytochrome $\underline{a}_3$ species, as suggested by Brudvig *et al.* (5), a smaller orbital overlap would again result and the antiferromagnetic coupling would be correspondingly diminished. The source of the large (>200 cm^{-1}) coupling in the oxidized, "resting" enzyme, however, remains a mystery.

References

1. Van Gelder, B. F. & Beinert, H. (1969) Biochim. Biophys. Acta 189, 1-24.
2. Griffith, J. S. (1971) Mol. Phys. 21, 141-143.
3. Tweedle, M. F., Wilson, L. J., García-Iñiguez, L., Babcock, G. T., & Palmer, G. (1978) J. Biol. Chem. 253, 8065-8071.
4. Moss, T. H., Shapiro, E., King, T. E., Beinert, H., & Hartzell, C. (1978) J. Biol. Chem. 253, 8072-8073.
5. Brudvig, G. W., Stevens, T. H., Morse, R. H., & Chan, S. I. (1981) Biochemistry 20, 000-000.
6. Greenaway, F. T., Chan, S. H. P., & Vincow, G. (1977) Biochim. Biophys. Acta 490, 62-78.
7. Beinert, H. & Shaw, R. W. (1977) Biochim. Biophys. Acta 462, 121-130.
8. Boelens, R. & Wever, R. (1979) Biochim. Biophys. Acta 547, 296-310.
9. Shaw, R. W., Hansen, R. E., & Beinert, H. (1978) J. Biol. Chem. 253, 6637-6640.
10. Condon, E. U. & Shortley, G. H. (1963) "The Theory of Atomic Spectra", Cambridge University Press.
11. Reinhammar, B., Malkin, R., Jensen, P., Karlsson, B., Andréasson, L.-E., Aasa, R., Vänngård, T., & Malmström, B. (1980) J. Biol. Chem. 255, 5000-5003.
12. Smith, T. D. & Pilbrow, J. R. (1974) Coord. Chem. Rev. 13, 173-278.

13. Palmer, G. (1979) Adv. Inorg. Chem. 2, 153-182.

14. Tinkham, M. (1964) "Group Theory and Quantum Mechanics", McGraw-Hill.

15. Brudvig, G. W., Stevens, T. H., & Chan, S. I. (1980) Biochemistry 19, 5275-5285.

16. Scholes, C. P., Isacson, R. A., & Feher, G. (1971) Biochim. Biophys. Acta 244, 206-210.

17. Hartzell, C. R. & Beinert, H. (1974) Biochim. Biophys. Acta 368, 318-338.

18. Stevens, T. H., Brudvig, G. W., Bocian, D. F., & Chan, S. I. (1979) Proc. Natl. Acad. Sci. U.S.A. 76, 3320-3324.

19. Maltempo. M. M. & Moss, T. H. (1976) Q. Rev. Biophys. 9, 181-215.

Chapter V. Conclusion.

The studies described in this thesis have been aimed at gaining new insight into structure and function, and the relationship between them, in the oxygen-utilizing proteins. EPR spectroscopy has proven a particularly apt tool in the study of the metal centers in metalloenzymes, as it is highly sensitive to the immediate ligand environment around a paramagnetic center (or centers), whereas the bulk of the protein is transparent. At the same time, nitric oxide, being analogous in many respects to O_2, is an excellent paramagnetic probe of the metal centers. Hence, I have given emphasis in my studies to the interaction of nitric oxide with the oxygen-binding sites of several oxygen-utilizing proteins. In particular, I have investigated (with some help) the interactions of NO with the metal centers of the oxygen-carrying protein myoglobin and some inorganic heme complexes, and with tree and fungal laccase and cytochrome c oxidase.

The variable temperature EPR spectroscopic studies of Chapter II led to the discovery that two conformations of the nitrosyl ferrous heme moiety exist in equilibrium for the nitric oxide adducts of reduced myoglobin, cytochrome c, and protoheme. These investigations were designed to address a single question, namely, what was the origin of the previously unassigned resonance in the EPR spectra of nitrosyl ferrous heme complexes. As is so often the case, though, the results have successfully resolved the original problem, only to raise a number of new questions in its stead. Does a similar equilibrium (also involving movement of the heme iron to opposite sides of the porphyrin ring, if our assignment is correct) also exist for the oxygen adducts of ferrous

hemeproteins? Why have none of the theoretical studies on the structure of nitrosyl ferrous heme complexes predicted the existence of two conformers with only slightly different ground state energies? Might a similar kind of equilibrium be involved in the R→T state transition of hemoglobin? In this latter regard, a number of studies (for example, 1 - 4) report work on hemoglobin and hemoglobin mutants in which the EPR spectra of nitrosyl derivatives of the proteins were used to gauge the effect of substituted amino acid residues at or near at least one of the oxygen-binding sites, adding detergent, or varying other conditions, on the R→T state transition induced by the protein's binding NO. However, in none of these studies were temperature effects considered, and in many of them all three types of signals reported in Chapter II are present in the published EPR spectra. Many of these studies are consequently in need of revised interpretation.

A final question raised by the results of Chapter II is why only the Type II EPR signal is exhibited by the nitrosyl adducts of reduced cytochrome c oxidase and cytochrome c peroxidase, and probably cytochrome P-450 and horseradish peroxidase as well. (One might also wonder whether the existence of a single stable conformer of the NO adduct is a property of all heme-containing enzymes which catalyze reactions using oxygen.) The most reasonable explanation is that the extra stabilization of species II in these enzymes is simply a consequence of the protein structure. For example, it is quite likely that the close proximity of the Cu_{a_3} center in cytochrome c oxidase would foster an interaction with the oxygen atom of the NO molecule when it was bound to reduced cytochrome

$\underline{a}_3$. Such an interaction could easily stabilize one conformer over the other by a few kcal/mole, which is all that would be required to account for the observed temperature-independent EPR spectra.

The investigations on the reactions of NO with tree and fungal laccase were instigated by Professor Bo Malmström's temporary sojourn at Caltech, which made the enzymes available to our group, and by the results obtained shortly before Professor Malmström's arrival by Gary Brudvig and Tom Stevens of the Chan group on the reactions of nitric oxide with cytochrome $\underline{c}$ oxidase (5). We found that tree laccase, like cytochrome $\underline{c}$ oxidase, catalyzes both the reduction and oxidation of NO. The metal centers of fungal laccase have much higher reduction potentials than those of tree laccase or cytochrome $\underline{c}$ oxidase (see Table I of Chapter I), and it is almost certainly as a consequence of this difference that fungal laccase can be reduced, but not reoxidized, by NO.

The metal centers of tree laccase have reduction potentials close to the reduction potentials of the cytochrome $\underline{a}_3$ and Cu_{a_3} sites of cytochrome $\underline{c}$ oxidase, and tree laccase behaved somewhat analogously to cytochrome $\underline{c}$ oxidase with regard to its reactions with NO. However, some interesting dissimilarities between these two oxidases also emerged during these studies. The most obvious difference is in the metal centers which react with NO. In cytochrome $\underline{c}$ oxidase, only cytochrome $\underline{a}_3$ and Cu_{a_3} participate in the reactions with NO, while the Cu_a and cytochrome $\underline{a}$ sites remain oxidized or, in the reduced enzyme, function only to transfer electrons from the reductant to the cytochrome $\underline{a}_3$ and

Cu_{a_3} sites. In tree laccase, on the other hand, all four metal centers are implicated in the reactions of the enzyme with NO. This contrasting behavior may be in part a manifestation of the differing reduction potentials between the two enzymes; whereas the reduction potentials of cytochrome a and Cu_a are lower than those of cytochrome a_3 and Cu_{a_3} by about 150 mV (see Table I of Chapter I), the reduction potentials of all four metal centers of tree laccase are within 80 mV of each other. This may result in electron transfer among the various metal sites in tree laccase being relatively reversible, whereas in cytochrome c oxidase electron transfer, under most conditions, is unidirectional from cytochrome a and Cu_a to cytochrome a and Cu_a. The difference in reduction potentials between the cytochrome a and Cu_a and the cytochrome a_3 and Cu_{a_3} sites is probably tied into the function of cytochrome c oxidase as an energy-conserving enzyme. The energy gained in transferring electrons from cytochrome a and Cu_a to cytochrome a_3 and Cu_{a_3} (which will be much more than 150 mV when oxygen is present) could be exploited to effect a conformational change in the enzyme, which could then be utilized to create the proton gradient which the enzyme is known to build up during turnover *in vivo* (6). This proton gradient is presumably used by F1-ATPase to catalyze the phosphorylation of ADP to ATP. From our perspective as beneficiaries, the evolution of the Rube Goldberg-like sequence of events occurring in the electron transfer chain is a remarkable achievement of Nature.

Aside from the difference in reduction potentials between the cytochrome a and Cu_a sites of cytochrome c oxidase and the type 1 and 2

copper sites in tree laccase, the latter metal centers also differ from the former in reacting directly with NO. The type 2 copper of both tree and fungal laccase is in fact known to bind externally added ligands, whereas neither Cu_a nor cytochrome *a* are so accessible. The type 1 copper center, in contrast, does not bind exogenous ligands, but does react with NO, presumably by an outer sphere mechanism. This dissimilarity between tree laccase and cytochrome *c* oxidase is reasonable in view of the natural specificity of cytochrome *c* oxidase for cytochrome *c* as reductant, compared to the relative nonspecificity of the laccases as oxidizing agents.

The reduction of NO to N_2O by reduced cytochrome *c* oxidase occurs by the chemical reaction of a nitric oxide molecule coordinated to cytochrome a_3 with another bound to Cu_{a_3}, the two sites involved in the binding and direct reduction of oxygen. In tree laccase, however, one of the two NO molecules which react to form N_2O in the presence of the reduced enzyme is bound to the type 3 copper, and the other to the type 2 copper. The type 2 copper is generally believed to function only in mediating electron transfer to oxygen coordinated at the type 3 site, and not to be involved directly in the binding or reduction of O_2. However, in light of the result just cited and the finding that, for tree laccase, one of the water molecules generated by the reduction of oxygen remains associated with the type 2 copper for some time (7), one might speculate that this site may be involved in the binding of oxygen or at least in stabilizing intermediate species generated during its reduction to water.

A noteworthy aspect of the reactions of NO with tree and fungal laccase is that the kinetics of reduction of the various metal centers by NO are in some cases similar to those observed in the anaerobic reduction of these enzymes. For example, whether the enzymes are reduced by ascorbate, hydroquinone, or nitric oxide, the type 2 copper site must be intact in order for the type 3 copper center to be reduced. Furthermore, the intermediate steps in the overall reduction of the enzyme (that is, the introduction of the second and third electrons to the enzyme) are rapid compared with the final reduction of the type 2 copper. Thus, these kinetic properties of the reduction of tree and fungal laccase appear to be intrinsic to the enzyme structure, and independent of the individual reductant. On the other hand, the rate-limiting step in the reduction of fungal laccase by ascorbate or hydroquinone appears to be in an intramolecular electron transfer, whereas when NO is the reducing agent, the rate-limiting steps are the initial reduction of the type 1 site and the final reduction of the type 2 site. Here, the properties of the reductant become more important than the enzyme structure in determining the kinetics of reduction of the laccases. It is just these sorts of distinctions that can enable us to get a handle on which structural elements of the oxygen-utilizing proteins are geared towards determining the unique functions of an individual protein, and which are applicable towards a broader range of functions.

The theoretical studies aimed at explaining the origin of the unusual EPR signals exhibited by three of the conformations of oxidized

cytochrome c oxidase have shed some light on the unique structural features of the oxygen-binding site of this enzyme, but some aspects remain dimly illumined at best. We have learned that the "g12" conformation of cytochrome c oxidase, which appears not to be involved in the catalytic cycle of the enzyme, exhibits an EPR signal due to a $\Delta M_s = 2$ transition between the $M_s = \pm 1$ levels of the $S = 2$ manifold. This conformation is one in which strong exchange coupling obtains between cytochrome a_3 and Cu_{a_3}, and the symmetry at the cytochrome a_3 heme is nearly axial. The fluorocytochrome a_3 EPR signal appears to arise from a weakly exchange-coupled, dipolar-coupled cytochrome a_3-Cu_{a_3} site, and the "g5" EPR signal which appears transiently during the reoxidation of the reduced enzyme by O_2 (8) is most likely due to an oxidized cytochrome a_3 site in which there is some mixing between the $S = 5/2$ and $S = 3/2$ states. If this latter assignment is correct, the two resonances exhibited at high magnetic field by the "g5" conformation must be split from each other by an interaction, probably dipolar in nature, with another paramagnetic center in the enzyme. The most likely candidate for this interaction, based on the magnitude of the splitting (about 200 G) and assuming a dipolar interaction, is the Cu_{a_3} center. However, it then remains to explain why no EPR signal has been observed from the Cu_{a_3} center concomitant with the observance of the "g5" EPR signal.

This whole question of what happens to cytochrome c oxidase upon reoxidation, of which states are involved in the catalytic cycle and in

what order, remains a murky area. Are the oxygenated or "g5" conformations intermediates in the catalytic cycle? Why is the "g5" EPR signal, which is probably due to cytochrome a_3, seen by Shaw *et al.* upon reoxidation with O_2 (8), whereas Reinhammer *et al.* (9) observe a signal from Cu_{a_3} in a similar experiment? Do either of these results, in fact, have any bearing on the actual sequence of events occurring during catalytic reduction of oxygen in the mitochondrion? How are the conformational changes which take place upon reoxidation of the enzyme tied in with energy conservation, if at all? Only recently has it become possible to ask these and other of the questions posed in this chapter; answering them is likely to help occupy research in bioenergetics for some time to come.

References

1. Trittelvitz, E., Gersonde, K., and Winterhalter, K. H. (1975) Eur. J. Biochem. 51, 33-42.

2. Chevion, M., Stern, A., Peisach, J., Blumberg, W. E., and Simon, S. (1978) Biochemistry 17, 1745-1750.

3. Hille, R., Olson, J. S., and Palmer, G. (1979) J. Biol. Chem. 254, 12110-12120.

4. John, M. E. and Waterman, M. R. (1979) FEBS Lett. 106 (1979) 219-222.

5. Brudvig, G. W., Stevens, T. H., and Chan, S. I. (1980) Biochemistry 19, 5275-5285.

6. Wikström, M., and Krab, K. (1979) Biochim. Biophys. Acta 549, 177-222.

7. Branden, R. and Deinum, J. (1977) FEBS Lett. 73, 144-146.

8. Shaw, R. W., Hansen, R. E., and Beinert, H. (1978) J. Biol. Chem. 253, 6637-6640.

9. Reinhammar, B., Malkin, R., Jensen, P., Karlsson, B. Andréasson, L.-E., Aasa, R. Vänngård, T., and Malmström, B. (1980) J. Biol. Chem. 255, 5000-5003.

APPENDIX I. Calculation of g-anisotropy for an Alternative Bonding Scheme for Nitrosyl Ferrous Heme Complexes.

If the splitting between the d_{yz}-π_y and $d_{z^2} + \pi^*_z$ orbitals in Fig. 8 of Chapter II is not much larger than λ, the spin-orbit coupling, then the orbitals will be mixed via the spin-orbit coupling. The mixing will affect the calculated g-values for the system. To see whether such a scheme could account for the observed g-values of either species of nitrosyl ferrous heme discussed in Chapter II, I have calculated the wavefunctions and g-values resulting from allowing mixing of the d_{yz} and d_{z^2} iron orbitals by the spin-orbit coupling.

The orbital scheme used is depicted in Fig. 1. Although ψ_a in Fig. 1 actually has more ligand than metal character, the spin-orbit coupling from the metal is expected to contribute much more to the anisotropy in g; hence, only the iron orbitals are considered in the figure.

If we take the initial splitting between the two orbitals of interest as Δ, as shown in Fig. 1, the energies of the two orbitals can be determined by solving the matrix of the crystal field and spin-orbit coupling Hamiltonians. This matrix is given by

	$\lvert yz\rangle$	$\lvert\overline{yz}\rangle$	$\lvert z^2\rangle$	$\lvert\overline{z^2}\rangle$
$\langle yz\rvert$	$\Delta/2$	0	0	$-i\sqrt{3/2}\lambda$
$\langle\overline{yz}\rvert$	0	$\Delta/2$	$-i\sqrt{3/2}\lambda$	0
$\langle z^2\rvert$	0	$i\sqrt{3/2}\lambda$	$-\Delta/2$	0
$\langle\overline{z^2}\rvert$	$i\sqrt{3/2}\lambda$	0	0	$-\Delta/2$

(1)

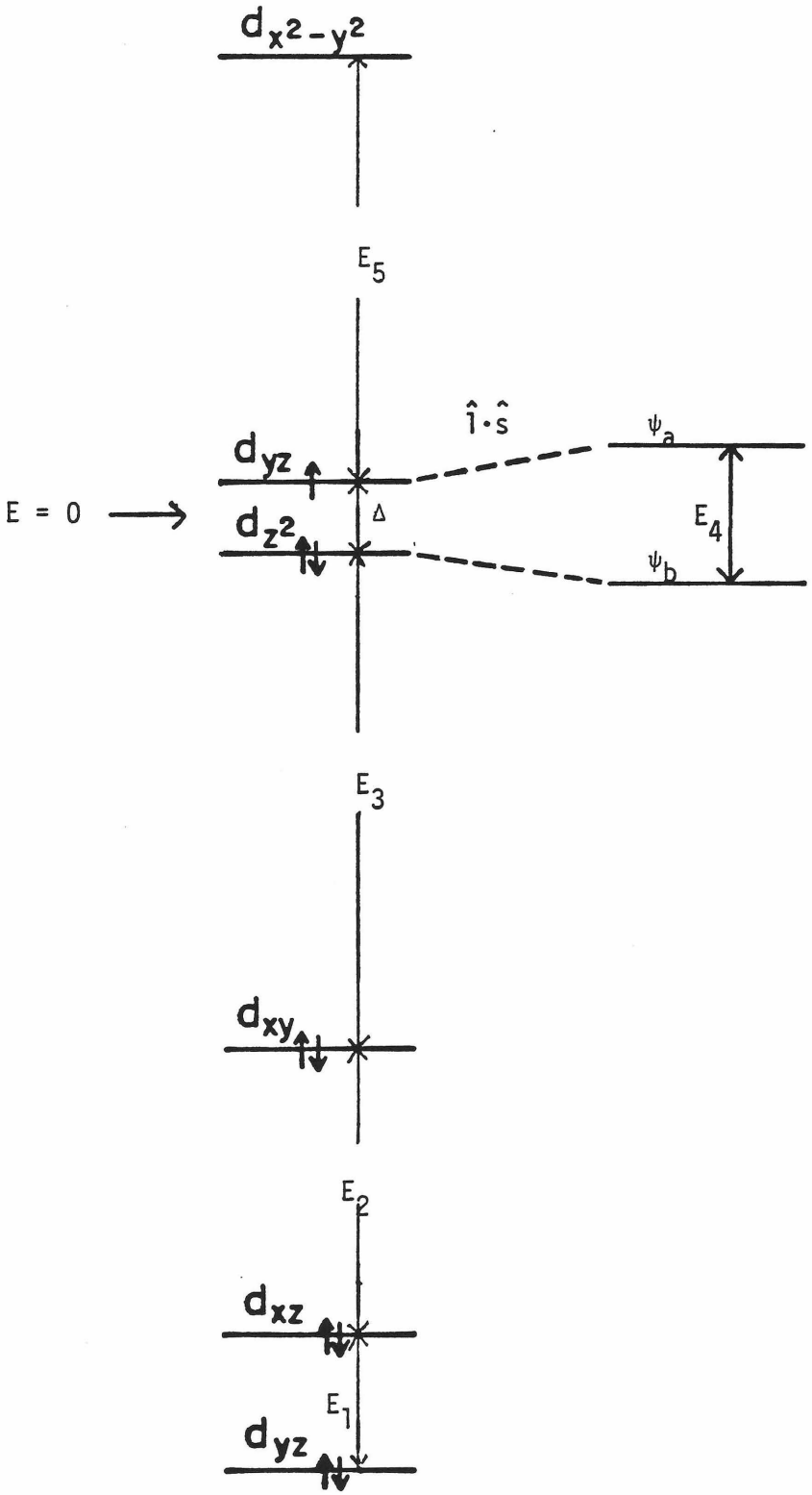
$d_{x^2-y^2}$
E_5
$\hat{l}\cdot\hat{s}$
ψ_a
d_{yz}
E = 0
d_{z^2}
Δ
E_4
ψ_b
E_3
d_{xy}
E_2
d_{xz}
E_1
d_{yz}

Figure 1.

where $|yz\rangle = d_{yz}(\alpha)$ and $|\overline{yz}\rangle = d_{yz}(\beta)$, α and β denoting up ($S = \frac{1}{2}$) and down ($S = -\frac{1}{2}$) electron spin, respectively. For convenience, the zero of energy has been chosen as lying halfway between the d_{yz} and d_{z^2} orbitals, and only the iron orbitals have been considered.

The matrix in (1) can be factored into two 2x2 matrices. Solving for the eigenvalues yields, for both matrices,

$$E_a = +\frac{1}{2}\sqrt{\Delta^2 + 3\lambda^2}$$
$$E_b = -\frac{1}{2}\sqrt{\Delta^2 + 3\lambda^2} \quad . \tag{2}$$

The corresponding wave functions are

$$\begin{aligned}
\phi_a^+ &= \cos\theta|yz\rangle + i\sin\theta|\overline{z^2}\rangle \\
\phi_a^- &= \cos\theta|\overline{yz}\rangle + i\sin\theta|z^2\rangle \\
\phi_b^+ &= i\sin\theta|\overline{yz}\rangle + \cos\theta|z^2\rangle \\
\phi_b^- &= i\sin\theta|yz\rangle + \cos\theta|\overline{z^2}\rangle
\end{aligned} \tag{3}$$

where the mixing coefficients are determined by

$$\tan\theta = \frac{1}{\sqrt{3}}\frac{\Delta}{\lambda}\left\{-1 + [1 + 3(\lambda/\Delta)^2]^{\frac{1}{2}}\right\} . \tag{4}$$

The g-values of the system can be calculated as follows (see, for example, Atherton (1)). First, excited state configurations are allowed to mix in with the ground state through the spin-orbit operator, H_{LS}, where

$$H_{LS} = \lambda \sum \hat{l}\cdot\hat{s} \tag{5}$$

The sum is over the electrons, $\hat{l}$ and $\hat{s}$ are the one-electron orbital and spin operators, and λ is the one-electron spin-orbit coupling parameter. I have assumed that λ is the same for all of the d electrons. The mixing coefficients are given by $-\langle i|\lambda\hat{l}\cdot\hat{s}|0\rangle/(E_i - E_0)$ where i refers to the excited state electronic configuration, and 0 to the ground state. Finally, using the new wavefunctions, the matrix of the Zeeman Hamiltonian,

$$H_{Zeeman} = \beta \sum (\hat{l} + g_e\hat{s})\cdot H \tag{6}$$

is solved for H aligned along each of the three principal molecular axes, yielding the anisotropy in g.

The matrix of $\hat{l}\cdot\hat{s}$ in the basis of real d-orbitals given in Table I can be used to calculate the mixing coefficients arising from H_{LS}. If the electronic configurations are written including only singly occupied orbitals, the initial ground state configurations (there are two of equal energy comprising the Kramer's doublet) are

$$\psi_a^+ = |yz\ \overline{yz}\ xz\ \overline{xz}\ xy\ \overline{xy}\ \phi_b^+\ \phi_b^-\ \phi_a^+\rangle = |\phi_a^+\rangle$$

$$\psi_a^- = |\phi_a^-\rangle \tag{7}$$

There is no inconsistency in having two orbitals (yz and ψ_a) both primarily d_{yz} in character, contributing to the electronic state of the complex, since they represent bonding and antibonding molecular orbitals which have ligand character as well.

Mixing in excited state configurations via H_{LS} now yields

Table I. Matrix of $\hat{l}\cdot\hat{s}$ in the basis of real d-orbitals (from Ref. 1)

	$\|x^2-y^2,\alpha\rangle$	$\|xy,\alpha\rangle$	$\|yz,\alpha\rangle$	$\|xz,\alpha\rangle$	$\|z^2,\alpha\rangle$	$\|x^2-y^2,\beta\rangle$	$\|xy,\beta\rangle$	$\|yz,\beta\rangle$	$\|xz,\beta\rangle$	$\|z^2,\beta\rangle$
$\langle x^2-y^2,\alpha\|$	0	$-i$	0	0	0	0	0	$+i/2$	$+1/2$	0
$\langle xy,\alpha\|$	$+i$	0	0	0	0	0	0	$+1/2$	$-i/2$	0
$\langle yz,\alpha\|$	0	0	0	$i/2$	0	$-i/2$	$-1/2$	0	0	$-i\sqrt{3}/2$
$\langle xz,\alpha\|$	0	0	$-i/2$	0	0	$-1/2$	$+i/2$	0	0	$+\sqrt{3}/2$
$\langle z^2,\alpha\|$	0	0	0	0	0	0	0	$+i\sqrt{3}/2$	$-\sqrt{3}/2$	0
$\langle x^2-y^2,\beta\|$	0	0	$+i/2$	$-1/2$	0	0	$+i$	0	0	0
$\langle xy,\beta\|$	0	0	$-1/2$	$-i/2$	0	$-i$	0	0	0	0
$\langle yz,\beta\|$	$-i/2$	$+1/2$	0	0	$-i\sqrt{3}/2$	0	0	0	$-i/2$	0
$\langle xz,\beta\|$	$+1/2$	$+i/2$	0	0	$-\sqrt{3}/2$	0	0	$+i/2$	0	0
$\langle z^2,\beta\|$	0	0	$+i\sqrt{3}/2$	$+\sqrt{3}/2$	0	0	0	0	0	0

$$\psi_a^{+'} = \psi_a^+ - \frac{\lambda\cos\theta}{2E_{34}} |\phi_a^- \overline{xy}\ \phi_a^+> - \frac{i\lambda\cos\theta}{2E_5} |\overline{x^2 - y^2}>$$

$$+ \frac{i}{2}\lambda \frac{(\cos\theta - \sqrt{3}\sin\theta)}{E_{234}} |xz\ \phi_a^-\ \ \phi_a^+> \qquad (8)$$

$$\psi_a^{-'} = \psi_a^- + \frac{\lambda\cos\theta}{2E_{34}} |xy\ \phi_a^+\ \phi_a^-> - \frac{i\lambda\cos\theta}{2E_5} |x^2 - y^2>$$

$$- \frac{i}{2}\lambda \frac{(\cos\theta - \sqrt{3}\sin\theta)}{E_{234}} |\phi_a^+ \overline{xz}\ \phi_a^->$$

where $E_{234} = E_2 + E_3 + E_4$ (see Fig. 1), and so forth.

Using equation (8) and Table I, the matrix elements of H_{Zeeman} can be calculated. First, for $H \| H_{zz}$,

$$<\psi_a^{+'}|\hat{l}_z|\psi_a^{+'}> = <+|\hat{l}_z|+> = \lambda(\cos^2\theta - \sqrt{3}\sin\theta\cos\theta)/E_{234}$$

$$<-|\hat{l}_z|-> = -\lambda|\cos^2\theta - \sqrt{3}\sin\theta\cos\theta)/E_{234}$$

$$<+|\hat{S}_z|+> = (\cos^2\theta - \sin^2\theta)/2 \qquad (9)$$

$$<-|\hat{S}_z|-> = -(\cos^2\theta - \sin^2\theta)/2$$

$$<-|\hat{l}_z|+> = <-|\hat{S}_z|+> = 0\ .$$

Solving the 2x2 energy matrix defined by the elements in (9) gives

$$E_z = \pm \frac{1}{2} \beta H_z [g_e(\cos^2\theta - \sin^2\theta) + 2\lambda(\cos^2\theta - \sqrt{3}\ \sin\theta\cos\theta)/E_{234}]$$

and

$$g_{zz} = g_e\ \cos 2\theta + 2\lambda(\cos^2\theta - \sqrt{3}\ \sin\theta\cos\theta)/E_{234}\ . \qquad (10c)$$

Solving similarly for g_{xx} and g_{yy} results in

$$g_{xx} = g_e + 4\sqrt{3}\ \sin\theta\cos\theta - 2\lambda\cos^2\theta/E_5 \qquad (10a)$$

$$g_{yy} = g_e\ \cos 2\theta + 2\lambda\cos^2\theta/E_{34} + 2\sqrt{3}\ \lambda\ \cos\theta\sin\theta/E_{234}\ . \qquad (10b)$$

If (10a) is rewritten to solve for E_5, and the orbital reduction factors included (see Chapter II), the result is

$$E_5 = 2\lambda\ k^2\ \cos^2\theta/(g_e - g_{xx} + 4\sqrt{3}\ \beta^2\delta^2\ \sin\theta\cos\theta) \qquad (11)$$

where k, β and δ are the orbital reduction factors for the ϕ_a orbital, the (upper) d_{yz} and d_{z^2} orbitals, respectively. Solving equation (11) for the reasonable values of θ (assuming $\Delta < 4000\ cm^{-1}$, see equation (4)); where g_{xx} is assigned to <u>any</u> of the g-values of either Species I or II in Chapter II, the values obtained for E_5 are unreasonably small (less than $2000\ cm^{-1}$). We estimate β^2 and δ^2 to be about 0.2 and 0.8, respectively, in these calculations, but the exact value is unimportant if they are not too close to zero. A precisely analogous difficulty arises when the energiesof ϕ_a and ϕ_b are reversed (that is, when the $d_{yz} - \pi^*$ orbital is assumed to be lower in energy than the $d_{z^2} + \pi$ orbital).

The problem, then, with the orbital scheme depicted in Fig. 1 is that the predicted anisotropy in $\underset{\approx}{g}$ is larger than that observed for the Type I and II EPR signals, when reasonable values for the d-orbital splittings are used. It may be, then, that the unpaired spin in nitrosyl ferrous heme complexes actually resides primarily on the nitric oxide moiety, and that the slight anisotropy in $\underset{\approx}{g}$ observed is due to spin-orbit coupling from NO. It would seem in any case that the details of the bonding cannot be deduced from the EPR data alone.

Reference

1. Atherton, N. M. (1973) "Electron Spin Resonance", Wiley and Sons, Inc.

APPENDIX II. Inclusion of the Dipolar Interaction in the Calculation of the Energy Levels and Wavefunctions of the Coupled Spin System of Cytochrome c Oxidase.

The form of H_{dip} is

$$H_{dip} = \hat{\underset{\sim}{S}}_1 \cdot \underset{\approx}{J} \cdot \hat{\underset{\sim}{S}}_2 \tag{1}$$

where $S_1 = \frac{5}{2}$, $S_2 = \frac{1}{2}$, and J is the dipolar coupling tensor. The elements of $\underset{\approx}{J}$ are give by

$$J_{\alpha\beta} = g_{1\alpha}\left[\sum_{i=x_2,y_2,z_2} g_{2i} d_{\beta i}\left(d_{\alpha i} - 3\sigma_\alpha \sum_{j=x_1,y_1,z_1} d_{ji}\sigma_j\right)\right]\frac{\beta^2}{r^3} \tag{2}$$

where the d_{ij}'s are direction cosines connecting the two ions, and the σ_i's are direction cosines of r with respect to x_1, y_1 and z_1. Obtaining the various $J_{\alpha\beta}$'s, given the relative coordinates of the two ions and their principal axes, is straightforward. To include H_{dip} in the coupled, or S_1S_2SM representation, the elements of H_{dip} (there are nine) can be written out, and the $\hat{S}_x$'s and $\hat{S}_y$'s rewritten in terms of $\hat{S}_+$ and $\hat{S}_-$. The elements of H_{dip} can then be calculated easily in the $S_1S_2M_1M_2$ representation. Finally, by using equation (2) in Chapter IV, these elements can be transformed into corresponding matrix elements in the coupled representation, and then used in the calculation of the energies and wavefunctions of the S=2 system.

The calculations are done with the coordinate frame of the iron atom (Fe_{a_3}) as reference, taking the z-axis as perpendicular to the

heme plane. This assumes that the matrix of D is diagonal in this same coordinate frame, which is not unreasonable.

The elements of H_{dip}, then, are:

$$\begin{aligned} H_{dip} = {} & J_{xx}\hat{S}_{1x}\hat{S}_{2x} + J_{xy}\hat{S}_{1x}\hat{S}_{2y} + J_{xz}\hat{S}_{1x}\hat{S}_{2z} \\ & + J_{yx}\hat{S}_{1y}\hat{S}_{2x} + J_{yy}\hat{S}_{1y}\hat{S}_{2y} + J_{yz}\hat{S}_{1y}\hat{S}_{2z} \\ & + J_{zx}\hat{S}_{1z}\hat{S}_{2x} + J_{zy}\hat{S}_{1z}\hat{S}_{2y} + J_{zz}\hat{S}_{1z}\hat{S}_{2z} \end{aligned} \tag{3}$$

The elements can be rewritten in terms of $\hat{S}_{1z}$, $\hat{S}_{2z}$ and the raising and lowering spin operators:

$$\begin{aligned} \hat{S}_{1x}\hat{S}_{2x} &= \tfrac{1}{4}(\hat{S}_1^+ + \hat{S}_1^-)(\hat{S}_2^+ + \hat{S}_2^-) = \tfrac{1}{4}(\hat{S}_1^+\hat{S}_2^+ + \hat{S}_1^+\hat{S}_2^- + \hat{S}_1^-\hat{S}_2^+ + \hat{S}_1^-\hat{S}_2^-) \\ \hat{S}_{1x}\hat{S}_{2y} &= -\tfrac{i}{4}(\hat{S}_1^+ + \hat{S}_1^-)(\hat{S}_2^+ - \hat{S}_2^-) = -\tfrac{i}{4}(\hat{S}_1^+\hat{S}_2^+ - \hat{S}_1^+\hat{S}_2^- + \hat{S}_1^-\hat{S}_2^+ - \hat{S}_1^-\hat{S}_2^-) \\ \hat{S}_{1x}\hat{S}_{2z} &= \tfrac{1}{2}(\hat{S}_1^+\hat{S}_{2z} + \hat{S}_1^-\hat{S}_{2z}) \\ \hat{S}_{1y}\hat{S}_{2x} &= -\tfrac{i}{4}(\hat{S}_1^+\hat{S}_2^+ + \hat{S}_1^+\hat{S}_2^- - \hat{S}_1^-\hat{S}_2^+ - \hat{S}_1^-\hat{S}_2^-) \\ \hat{S}_{1y}\hat{S}_{2y} &= -\tfrac{1}{4}(\hat{S}_1^+\hat{S}_2^+ - \hat{S}_1^+\hat{S}_2^- - \hat{S}_1^-\hat{S}_2^+ + \hat{S}_1^-\hat{S}_2^-) \\ \hat{S}_{1y}\hat{S}_{2z} &= -\tfrac{i}{2}(\hat{S}_1^+\hat{S}_{2z} - \hat{S}_1^-\hat{S}_{2z}) \\ \hat{S}_{1z}\hat{S}_{2x} &= \tfrac{1}{2}(\hat{S}_{1z}\hat{S}_2^+ + \hat{S}_{1z}\hat{S}_2^-) \\ \hat{S}_{1z}\hat{S}_{2y} &= -\tfrac{i}{2}(\hat{S}_{1z}\hat{S}_2^+ - \hat{S}_{1z}\hat{S}_2^-) \\ \hat{S}_{1z}\hat{S}_{2z} &= \hat{S}_{1z}\hat{S}_{2z} \end{aligned} \tag{4}$$

The equations in (4) may be used to rewrite H_{dip} by combining like terms as follows:

$$\begin{aligned} H_{dip} &= \tfrac{1}{4}(J_{xx} - iJ_{xy} - iJ_{yx} - J_{yy})\hat{S}_1^+\hat{S}_2^+ \\ &+ \tfrac{1}{4}(J_{xx} + iJ_{xy} - iJ_{yx} + J_{yy})\hat{S}_1^+\hat{S}_2^- \\ &+ \tfrac{1}{4}(J_{xx} - iJ_{xy} + iJ_{yx} + J_{yy})\hat{S}_1^-\hat{S}_2^+ \\ &+ \tfrac{1}{4}(J_{xx} + iJ_{xy} + iJ_{yx} - J_{yy})\hat{S}_1^-\hat{S}_2^- \\ &+ \tfrac{1}{2}(J_{xz} - iJ_{yz})\hat{S}_1^+\hat{S}_{2z} + \tfrac{1}{2}(J_{xz} + iJ_{yz})\hat{S}_1^-\hat{S}_{2z} \\ &+ \tfrac{1}{2}(J_{zx} - iJ_{zy})\hat{S}_{1z}\hat{S}_2^+ + \tfrac{1}{2}(J_{zx} + iJ_{zy})\hat{S}_{1z}\hat{S}_2^- \\ &+ J_{zz}\hat{S}_{1z}\hat{S}_{2z} \end{aligned} \tag{5}$$

or

$$\begin{aligned} H_{dip} &= A_1\hat{S}_1^+\hat{S}_2^+ + \bar{A}_1\hat{S}_1^-\hat{S}_2^- + A_2\hat{S}_1^+\hat{S}_2^- \quad \bar{A}_2\hat{S}_1^-\hat{S}_2^+ \\ &+ A_3\hat{S}_1^+\hat{S}_{2z} + \bar{A}_3\hat{S}_1^-\hat{S}_{2z} + A_4\hat{S}_{1z}\hat{S}_2^+ + \bar{A}_4\hat{S}_{1z}\hat{S}_2^- \\ &+ J_{zz}\hat{S}_{1z}\hat{S}_{2z} \end{aligned} \tag{6}$$

where $\bar{A}$ denotes the complex conjugate of A. Equation (6) makes clear that the matrix of H_{dip} is properly Hermitian.

The elements of H_{dip} may now be calculated in the $S_1S_2M_1M_2$ representation, using the operators of equation (6):

$$\begin{aligned} \langle M_1 + 1, M_2 + 1 | \hat{S}_1^+\hat{S}_1^- | M_1M_2 &= \left[S_1(S_1 + 1) - M_1(M_1 + 1)\right]^{\frac{1}{2}}\left[S_2(S_2 + 1)\right. \\ \left. - M_2(M_2 + 1)\right]^{\frac{1}{2}} &= \left[\tfrac{35}{4} - M_1(M_1 + 1)\right]^{\frac{1}{2}}\left[\tfrac{3}{4} - M_2(M_2 + 1)\right]^{\frac{1}{2}} \end{aligned} \tag{7a}$$

$$\langle M_1 - 1, M_2 - 1 | \hat{S}_1^- \hat{S}_2^- | M_1 M_2 \rangle = \left[\frac{35}{4} - M_1(M_1 - 1)\right]^{\frac{1}{2}} \left[\frac{3}{4} - M_2(M_2 - 1)\right]^{\frac{1}{2}} \quad (7b)$$

$$\langle M_1 + 1, M_2 - 1 | \hat{S}_1^+ \hat{S}_2^- | M_1 M_2 \rangle = \left[\frac{35}{4} - M_1(M_1 + 1)\right]^{\frac{1}{2}} \left[\frac{3}{4} - M_2(M_2 - 1)\right]^{\frac{1}{2}} \quad (7c)$$

$$\langle M_1 - 1, M_2 + 1 | \hat{S}_1^- \hat{S}_2^+ | M_1 M_2 \rangle = \left[\frac{35}{4} - M_1(M_1 - 1)\right]^{\frac{1}{2}} \left[\frac{3}{4} - M_2(M_2 + 1)\right]^{\frac{1}{2}} \quad (7d)$$

$$\langle M_1 + 1, M_2 | \hat{S}_1^+ \hat{S}_{2z} | M_1 M_2 \rangle = M_2 \left[\frac{35}{4} - M_1(M_1 + 1)\right]^{\frac{1}{2}} \quad (7e)$$

$$\langle M_1 - 1, M_2 | \hat{S}_1^- \hat{S}_{2z} | M_1 M_2 \rangle = M_2 \left[\frac{35}{4} - M_1(M_1 + 1)\right]^{\frac{1}{2}} \quad (7f)$$

$$\langle M_1, M_2 + 1 | \hat{S}_{1z} \hat{S}_2^+ | M_1 M_2 \rangle = M_1 \left[\frac{3}{4} - M_2(M_2 + 1)\right]^{\frac{1}{2}} \quad (7g)$$

$$\langle M_1, M_2 - 1 | \hat{S}_{1z} \hat{S}_2^- | M_1 M_2 \rangle = M_1 \left[\frac{3}{4} - M_2(M_2 - 1)\right]^{\frac{1}{2}} \quad (7h)$$

$$\langle M_1 M_2 | \hat{S}_{1z} \hat{S}_{2z} | M_1 M_2 \rangle = M_1 M_2$$

The next step is to use the relations in equation (7) to calculate the matrix elements of H_{dip} in the $S_1 S_2 SM$ representation. The equations needed to accomplish this are given by Griffith as

$$|S_1 S_2 3M\rangle = \left(\frac{3 + M}{6}\right)^{\frac{1}{2}} |S_1 S_2 M - \tfrac{1}{2}, \tfrac{1}{2}\rangle + \left(\frac{3 - M}{6}\right)^{\frac{1}{2}} |S_1 S_2 M + \tfrac{1}{2}, -\tfrac{1}{2}\rangle$$

$$|S_1 S_2 2M\rangle = -\left(\frac{3 - M}{6}\right)^{\frac{1}{2}} |S_1 S_2 M - \tfrac{1}{2}, \tfrac{1}{2}\rangle + \left(\frac{3 + M}{6}\right)^{\frac{1}{2}} |S_1 S_2 M + \tfrac{1}{2}, -\tfrac{1}{2}\rangle. \quad (8)$$

Combining (7) and (8), we can calculate:

$$\langle 3M + 2 | \hat{S}_1^+ \hat{S}_2^+ | 3M\rangle = \frac{1}{6}[(4 + M)(2 - M)(5 + M)(3 - M)]^{\frac{1}{2}}$$

$$\langle 3M + 2 | \hat{S}_1^+ \hat{S}_2^+ | 2M\rangle = \frac{1}{6}[(4 + M)(2 - M)(5 + M)(3 + M)]^{\frac{1}{2}}$$

$$\langle 2M + 2 | \hat{S}_1^+ \hat{S}_2^+ | 3M\rangle = -\frac{1}{6}[(4 + M)(2 - M)(M - 1)(M - 3)]^{\frac{1}{2}}$$

$$\langle 2M+2|\hat{S}_1^+\hat{S}_2^+|2M\rangle = \frac{1}{6}\left[(4+M)(2-M)(M+3)(1-M)\right]^{\frac{1}{2}}$$

$$\langle 3M|\hat{S}_1^+\hat{S}_2^-|3M\rangle = \frac{1}{6}(3-M)(3+M) = \frac{1}{6}(9-M^2)$$

$$\langle 3M|\hat{S}_1^+\hat{S}_2^-|2M\rangle = -\frac{1}{6}(9-M^2)^{\frac{1}{2}}(3-M)$$

$$\langle 2M|\hat{S}_1^+\hat{S}_2^-|2M\rangle = -\frac{1}{6}(9-M^2)$$

$$\langle 3M|\hat{S}_1^-\hat{S}_2^+|3M\rangle = \frac{1}{6}(9-M^2)$$

$$\langle 3M|\hat{S}_1^-\hat{S}_2^+|2M\rangle = \frac{1}{6}(9-M^2)^{\frac{1}{2}}(3+M)$$

$$\langle 2M|\hat{S}_1^-\hat{S}_2^+|2M\rangle = -\frac{1}{6}(9-M^2)$$

$$\langle 3M+1|\hat{S}_1^+\hat{S}_{2z}|3M\rangle = \frac{1}{6}(M+\tfrac{1}{2})(3-M)^{\frac{1}{2}}(4+M)^{\frac{1}{2}} \qquad (9)$$

$$\langle 3M+1|\hat{S}_1^+\hat{S}_{2z}|2M\rangle = \frac{1}{6}(M-\tfrac{5}{2})(3+M)^{\frac{1}{2}}(4+M)^{\frac{1}{2}}$$

$$\langle 2M+1|\hat{S}_1^+\hat{S}_{2z}|3M\rangle = -\frac{1}{6}(M+\tfrac{7}{2})(3-M)^{\frac{1}{2}}(2-M)^{\frac{1}{2}}$$

$$\langle 2M+1|\hat{S}_1^+\hat{S}_{2z}|2M\rangle = -\frac{1}{6}(M+\tfrac{1}{2})(3+M)^{\frac{1}{2}}(2-M)^{\frac{1}{2}}$$

$$\langle 3M+1|\hat{S}_{1z}\hat{S}_2^+|3M\rangle = \frac{1}{6}(M+\tfrac{1}{2})(3-M)^{\frac{1}{2}}(4+M)^{\frac{1}{2}}$$

$$\langle 3M+1|\hat{S}_{1z}\hat{S}_2^+|2M\rangle = \frac{1}{6}(M+\tfrac{1}{2})(3+M)^{\frac{1}{2}}(4+M)^{\frac{1}{2}}$$

$$\langle 2M+1|\hat{S}_{1z}\hat{S}_2^+|3M\rangle = -\frac{1}{6}(M+\tfrac{1}{2})(3-M)^{\frac{1}{2}}(2-M)^{\frac{1}{2}}$$

$$\langle 2M+1|\hat{S}_{1z}\hat{S}_2^+|2M\rangle = -\frac{1}{6}(M+\tfrac{1}{2})(3+M)^{\frac{1}{2}}(2-M)^{\frac{1}{2}}$$

$$\langle 3M|\hat{S}_{1z}\hat{S}_{2z}|3M\rangle = \frac{1}{6}(M^2-\tfrac{3}{2})$$

$$\langle 3M|\hat{S}_{1z}\hat{S}_{2z}|2M\rangle = -\frac{M}{6}(9 - M^2)^{\frac{1}{2}}$$

$$\langle 2M|\hat{S}_{1z}\hat{S}_{2z}|2M\rangle = -\frac{1}{6}(M^2 + \frac{3}{2})$$

Note that the elements of $\hat{S}_1^-\hat{S}_2^-$, $\hat{S}_1^-\hat{S}_{2z}$ and $\hat{S}_{1z}\hat{S}_2^-$ are not given in equation (9). These elements are given by the complex conjugates of the elements of $\hat{S}_1^+\hat{S}_2^+$, $\hat{S}_1^+\hat{S}_{2z}$ and $\hat{S}_{1z}\hat{S}_2^+$, respectively. Calculated values of the elements not shown check, as they should, with this property of the Hermitian matrix.

The last step is simply to regroup the elements given in (9):

$$\langle 3M|H_{dip}|3M\rangle = \frac{1}{6}J_{zz}(M^2 - \frac{3}{2}) + \frac{A_2}{6}(9 - M^2) + \frac{\overline{A_2}}{6}(9 - M^2)$$

$$\langle 3M + 1|H_{dip}|3M\rangle = \frac{1}{6}(A_3 + A_4)(M + \frac{1}{2})(3 - M)^{\frac{1}{2}}(4 + M)^{\frac{1}{2}}$$

$$\langle 3M + 2|H_{dip}|3M\rangle = \frac{A_1}{6}[(4 + M)(2 - M)(5 + M)(3 - M)]^{\frac{1}{2}}$$

$$\langle 2M + 1|H_{dip}|3M\rangle = -\left[\frac{A_3}{6}(M + \frac{7}{2}) + \frac{A_4}{6}(M + \frac{1}{2})\right](3 - M)^{\frac{1}{2}}(2 - M)^{\frac{1}{2}}$$

$$\langle 2M + 2|H_{dip}|3M\rangle = -\frac{A_1}{6}(4 + M)^{\frac{1}{2}}(2 - M)^{\frac{1}{2}}(M - 1)^{\frac{1}{2}}(M - 2)^{\frac{1}{2}}$$

$$\langle 3M|H_{dip}|2M\rangle = -\frac{1}{6}[J_{zz}M + A_2(3 - M) - \overline{A_2}(3 + M)](9 - M^2)^{\frac{1}{2}}$$

$$\langle 3M + 1|H_{dip}|2M\rangle = \frac{1}{6}\left[A_3(M - \frac{5}{2}) + A_4(M + \frac{1}{2})\right](3 + M)^{\frac{1}{2}}(4 + M)^{\frac{1}{2}}$$

$$\langle 3M + 2|H_{dip}|2M\rangle = \frac{A_1}{6}(4 + M)^{\frac{1}{2}}(2 - M)^{\frac{1}{2}}(5 + M)^{\frac{1}{2}}(3 + M)^{\frac{1}{2}}$$

$$\langle 2M|H_{dip}|2M\rangle = -\frac{J_{zz}}{6}(M^2 + \frac{3}{2}) - \frac{1}{6}(A_2 + \overline{A_2})(9 - M^2)$$

$$\langle 2M+1|H_{dip}|2M\rangle = -\frac{1}{6}(A_3 + A_4)(M+\tfrac{1}{2})(3+M)^{\frac{1}{2}}(2-M)^{\frac{1}{2}}$$

$$\langle 2M+2|H_{dip}|2M\rangle = \frac{A_1}{6}[(4+M)(2-M)(M+3)(1-M)]^{\frac{1}{2}}$$

The A_i's (and J_{zz}) have been incorporated using equation (6). The elements in equation (10) may be combined with the other parts of H, where

$$H = -J_{ex}\hat{S}_1\cdot\hat{S}_2 + D(\hat{S}^2_{1z} - \frac{35}{12}) + E(\hat{S}^2_{1x} - \hat{S}^2_{1y}) + \beta\underset{\sim}{H}\cdot\underset{\approx}{g}\cdot\hat{\underset{\sim}{S}} + H_{dip} \qquad (11)$$

The resulting matrix is diagonalized as usual to yield the energies and wavefunctions of the coupled system. Note that setting $J_{ex} = 0$ will give energies for the two centers in the presence of dipolar coupling only. When the calculation is performed with $J_{ex} = 0$ and the resulting wavefunctions transformed back into the $|S_1S_2M_1M_2\rangle$ representation, it is found that to first approximation, the wavefunctions are split into three energy levels with $W = -\frac{8}{3}D$, $-\frac{2}{3}D$ and $\frac{10}{3}D$, as expected. The wavefunctions in a given level are then further split even at zero magnetic field by E, the rhombic splitting, and the dipolar interaction between the two ions.

Proposition 1

Low-Temperature Studies on the Mechanism of Reduction of NO_2^- and NO by Cytochrome *cd*$_1$ from *Pseudomonas aeruginosa*

Cytochrome *cd*$_1$ from *Pseudomonas aeruginosa* is a terminal electron carrier which can accept electrons from cytochrome *c*-551 or from *Pseudomonas* azurin. There is some debate over whether the enzyme, which is sometimes referred to as *Pseudomonas* cytochrome oxidase or, less misleadingly, as nitrite reductase, reduces NO_2^- to NO or to N_2O *in vivo* (1,2). To aid in resolving this matter, and to help establish the nature of the mechanism of catalysis, I propose doing low-temperature studies on the intermediates produced when the isolated enzyme reacts with NO_2^-.

Investigations of the low-temperature intermediates in the catalytic cycle of cytochrome *c* oxidase by optical and EPR spectroscopy have been instrumental in characterizing the mechanism by which this enzyme reduces oxygen to water (3,4). The approach used has been to prepare, in a medium containing 30% ethylene glycol, the reduced or partially reduced enzyme with CO bound to cytochrome a_3^{+2}, mix this sample with O_2-saturated buffered solution rapidly (<5 s) at about 250 K in an EPR tube, and freeze in a solid CO_2/ethanol bath (195 K). The CO molecules may then be photolyzed from cytochrome a_3^{+2} by white light at 77 K, and slow warming allows the reduction of oxygen by the enzyme to proceed. The reaction may be stopped by reimmersing the sample in liquid nitrogen.

A similar approach could be used with cytochrome *cd*$_1$ since, as the name implies, this enzyme contains a heme *c* and a heme d_1. The heme d_1,

which is probably the site of nitrite reduction, can bind CO in the reduced enzyme (5), so the low-temperature photolysis could be done much as described above, substituting NO_2^--containing buffer for O_2 saturated buffer. By monitoring the EPR and optical spectra as the enzyme is slowly warmed following photolysis of the CO molecule, it might be possible to determine how NO_2^- is reduced by the enzyme, and whether it can be completely reduced to N_2O without being released into solution. A number of other techniques could also potentially be brought to bear upon this problem. Magnetic circular dichroism and resonance Raman spectroscopy could be helpful in determining the magnetic and vibrational properties of the hemes in the intermediate states of the enzyme. Since heme $\underline{d}_1$ is actually a chlorin (a heme with one of the pyrrole bonds saturated), the resonance Raman studies would best be done concurrently with studies on isolated heme $\underline{d}_1$ or model studies on chlorins. MCD studies have already proved helpful in determining the properties of the oxidized enzyme as isolated (6), and would be especially informative as to the spin states of the two hemes.

In summary, a wealth of information regarding the mechanism of nitrite reduction by cytochrome $\underline{cd}_1$ from Pseudomonas aeruginosa could be extracted by applying optical, EPR, MCD and resonance Raman spectroscopy to the study of the intermediates isolated at low temperatures.

References

1. Wharton, D. C. and Weintraub, S. T. (1980) Biochem. Biophys. Res. Comm. 97, 236-242.

2. Zumft, W. G. and Vega, J. M. (1979) Biochim. Biophys. Acta 548, 484-499.

3. Chance, B., Saronio, C., Waring, A. and Leigh, J. S., Jr. (1978) Biochim. Biophys. Acta 503, 37-55.

4. Clore, G. M., Andréasson, L-E., Karlsson, B., Aasa, R. and Malmström, B. G. (1980) Biochem. J. 185, 139-154, 155-167.

5. Parr, S. R., Wilson, M. T. and Greenwood, C. (1975) Biochem. J. 151, 51-59.

6. Walsh, T. A., Johnson, M. K., Greenwood, C., Barber, D., Springall, J. P. and Thomson, A. J. (1979) Biochem. J. 177, 29-39.

Proposition 2

Studies of Nucleosomal Structure by the Spin-Probe Spin-Label Technique

Measuring solvent accessibility to a particular residue, the cysteine of histone H3, in chemically modified and unmodified nucleosomes, could provide specific structural information that would constitute a beginning towards understanding the detailed nature of changes induced by chemical modifications of nucleosomes occurring in vivo. The nucleosome consists of an association of about 200 base pairs of DNA and an octamer of two copies each of the histone proteins H2A, H2B, H3, and H4, and is the recurring unit of chromatin. While the precise function of the nucleosome is unknown, it is likely that conformational changes occur in it during transcription and replication of the associated DNA, and that it participates in the regulation of gene expression (1). Additionally, some chemical changes are known to accompany increases in transcriptional or translational activity; for example, acetylation increases template activity in vivo (2), and histone H1 is phosphorylated just prior to mitosis in *Physarum* (3).

The in vivo chemical modifications of nucleosomes may well be accompanied by conformational changes, which could serve as the basis for changes in transcriptional or translational activity. This possibility could be explored through use of the spin-probe spin-label technique, which takes advantage of the effect a fast-relaxing, paramagnetic spin probe ion, such as Mn^{+2} or Cu^{+2}, has upon the magnetic properties of a

more slowly relaxing spin label (4). By measuring the intensity of the EPR signal due to the spin label as a function of microwave power in the presence of the spin probe, specific distances as large as 50 Å between spin label and spin probe can be measured (5).

To investigate the effect of chemical modification of nucleosomes on their conformation, using the spin-probe spin-label technique, we require a chemically modified nucleosome with a covalently attached spin label, and we need a spin probe. Wallace et al. (6) have developed a procedure for the mild acetylation of histones in vitro, which could be used in these experiments, or attempts could be made to isolate homogeneous preparations of nucleosomes chemically altered in vivo (a much more arduous procedure!). Histone H3 from chicken erythrocytes contains a single cysteine residue, which is suitable for the attachment of a nitroxide spin label. This may be done on the isolated histone, and the nucleosome then reconstituted, as has been achieved by Hyde and Walker, who observed an EPR signal from the spin-labeled nucleosome (7). Finally, Mn^{+2} in solution as the spin probe would allow solvent accessibilities to be measured for chemically modified and unmodified nucleosomes. The Mn^{+2} could be complexed with EDTA to prevent conformational changes due to free manganese ion in solution.

Necessary controls would include measuring the physical properties of both the modified and unmodified nucleosomes — electrophoretic mobility, circular dichroism, sedimentation properties, and nuclease digestion patterns — before and after attachment of the spin label, to ensure that the presence of the spin label was not altering the structural

properties of the nucleosomes. Experiments in which Mn^{+2} was replaced by diamagnetic Mg^{+2} could be done to determine whether observed effects on the magnetic properties of the spin label were solely due to the magnetic properties of the spin probe.

References

1. Woodcock, C. L. F. (1978) in "The Cell Nucleus" V. 5, H. Busch, ed., Academic Press, 185-211.

2. Marushige, K. (1976) Proc. Natl. Acad. Sci. U.S.A. 73, 3937-3941.

3. Fischer, S. G. and Laemmli, U. K. (1980) Biochemistry 19, 2240-2246.

4. Hyde, J. S., Swartz, H. M., and Antholine. W. E. (1979) in "Spin Labelling II: Theory and Applications", L. J. Berliner, ed., Academic Press, 71-113.

5. Kulikov, A. V. and Likhtenstein, G. I. (1977) Adv. Mol. Relaxation Processes 10, 47-79.

6. Wallace, R. B., Sargent, T. D., Murphy, R. F., and Bonner, J. (1977) Proc. Natl. Acad. Sci. U.S.A. 74, 3244-3248.

7. Hyde, J. E. and Walker, I. O. (1977) Biochim. Biophys. Acta 490, 261-271.

Proposition 3

Computer-Assisted Synthesis of Isotopically Labeled Organic Molecules

A number of approaches have been taken towards computer-assisted organic synthesis (1). The most promising and successful to date is the LHASA (logic and heuristics applied to synthetic analysis) program, pioneered by E. J. Corey and co-workers (2 - 5).

LHASA is an interactive, computer graphics program. The program accepts as input a molecule drawn on the graphics screen by the chemist and then builds synthetic routes to that molecule, working backwards from the target molecule and using various strategies at the user's behest. LHASA consists of five modules: (1) graphical communication, (2) strategy and control, (3) perception, (4) symbolic structural manipulation, and (5) evaluation of precursors. The strategy and control module contains the executive which calls the other modules into core for use, so this module is always in core. Only one other module need be in core at any one time.

The program at present is capable of deriving syntheses for a wide variety of organic molecules, including complicated bridged structures and particular stereoisomers. I suggest that it would be useful to modify the program so that it would allow the user the option of including isotopically labeled compounds as targets for synthesis.

Because of the expense of isotopically labeled starting materials, strategy should center on minimizing loss of label in the synthesis. Normally, the overriding consideration in retrograde synthesis, as done

by the organic chemist or by LHASA, is simplification. One seeks to simplify the target molecule by removing functional groups (corresponding to, for example, nitration in the synthetic direction) or by breaking off large chunks of the molecule (corresponding to, for example, a Diels-Alder reaction), or else one seeks to perform functional group interchanges that will lead to simplifying steps (for instance, transforming an amino group to a nitro group in the anti-synthetic direction). In the retrograde synthesis of labeled compounds, this strategy would have to be modified to minimize loss of isotopic label. This could be accomplished by giving high priority to breaking off small pieces of the target molecule containing the label, and by eliminating those transformations involving the label which are likely to proceed in low yield.

This means that in the evaluation of transformations (steps in the anti-synthetic direction) performed by LHASA, steps in which the labeled atom is split off from the target molecule should receive high ratings. (The ratings are derived by the program, for any transformation, from various empirical formulae for determining the likelihood of success of the synthetic step corresponding to that transformation.) The minimal rating, that is, the minimal criterion for storing in memory a particular transformation, should be increased for steps in which the label is contained in both target and precursor. A factor should be included in the rating which estimates the yield of the transformation. The reason yield should be included in evaluating a step only as one factor in the rating, rather than as an independent criterion, is the difficulty in evaluating yields for general transformations.

The perception and graphical communication modules would have to be slightly modified to allow the input and recognition of isotopic labels. Because availability of starting materials must be an important criterion in the retrograde synthesis of a given target molecule, different isotopes of the same atom, such as ^{3}H and ^{2}H, obviously must be differentiated.

A list of commercially available isotopically labeled compounds should be included as a part of the program for comparison with precursors generated from each target molecule (that is, comparison with each molecule along each synthetic route to the original input target molecule). Because the synthesis of isotopically labeled compounds would be optional and probably infrequently used relative to other syntheses, this list ought to be stored separately from the five modules mentioned above, and called up either when the user thinks he/she has generated a commercially available compound or else routinely called after generation of each precursor. The lists for each label could be divided into aromatic and nonaromatic compounds.

These proposed changes in strategy and evaluation for synthesizing isotopically labeled compounds would, of course, have to be experimented with for a while before it could be determined which changes were optimal. LHASA is designed to produce a large number of synthetic paths to a given target molecule, which it is up to the chemist to trim. Therefore, one would first modify the existing program in mild ways to see what syntheses were generated for various labeled compounds, and develop rules to eliminate the really bad syntheses created by the program. A thorough

study would be necessary to decide at what stage to compare commercially available labeled compounds with precursors generated by the program.

LHASA is designed for flexibility; it is fairly easy to add new reactions, evaluation criteria, and strategies to the program. This flexibility would naturally hold after inclusion of the option for synthesizing labeled compounds, and among future considerations would be inclusion of a capacity for synthesizing commercially unavailable labeled heterocycles and doubly labeled compounds.

The incorporation of an option for synthesizing isotopically labeled compounds would thus be relatively straightforward, and would add significantly to the already formidable capabilities of the LHASA program for computer-assisted organic synthesis.

References

1. Bersohn, M. and Esack, A. (1976) Chem. Rev. 76, 269-282.

2. Corey, E. J. (1971) Quart. Rev. 25, 455-482.

3. Corey, E. J. and Wipke, W. T. (1969) Science 166, 178-192.

4. D. A. Pensak, PhD Thesis, Harvard Univ., 1973.

5. Corey, E. J., Howe, W. J., Orf, H. W., Pensak, D. A., Petersson, G., (1975) J. Am. Chem. Soc. 97, 6116-6124.

Proposition 4

Investigation of Borohydride Reduction in the Gas Phase by Ion Cyclotron Resonance

The hydroboration reaction, exemplified by reactions 1 - 3, has found great applicability in organic synthesis, as the resulting organoboranes can be further treated to yield a variety of new substances. This reaction has also been interesting to theoreticians, and several ab initio studies on the mechanism of reactions 1 - 3 have appeared recently in the literature (1 - 5). These studies have resulted in similar mechanisms being proposed, but there has not been complete agreement on the details. Reactions 1 and 3 appear to occur by initial formation of a pi complex between BH_3 and the double bond, which then rearranges, through a transition state having a four-center-like structure, to the observed products, as shown in Scheme 1. The pi complex I has been calculated to be formed with no energy barrier (1,2,5), and with a barrier of 7.6 kcal/mol (4). The transition state II has been calculated to lie about 4 kcal/mol in energy above I (2).

The transition state II is expected to be stabilized by interaction of the empty 2p atomic orbital on boron, which accounts for the facility of hydroboration. In borohydride reduction (reaction 2), on the other hand, there are no empty atomic orbitals on boron, and Dewar and McKee (3) have found that in the absence of solvent interactions, this reaction is expected to occur not by a concerted mechanism such as that of scheme 1, but by an initial endothermic hydride transfer followed by reaction of the alkoxide ion so generated with borane (BH_3). Thus, the ease and

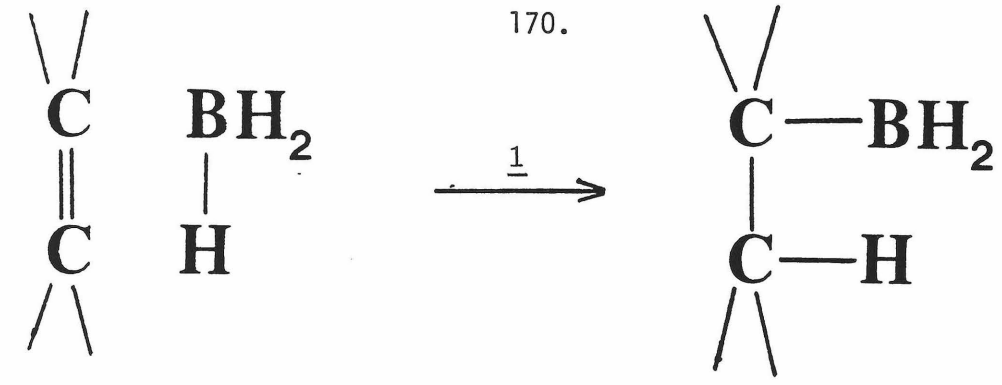
C
C
BH2
H
1
C—BH2
C—H

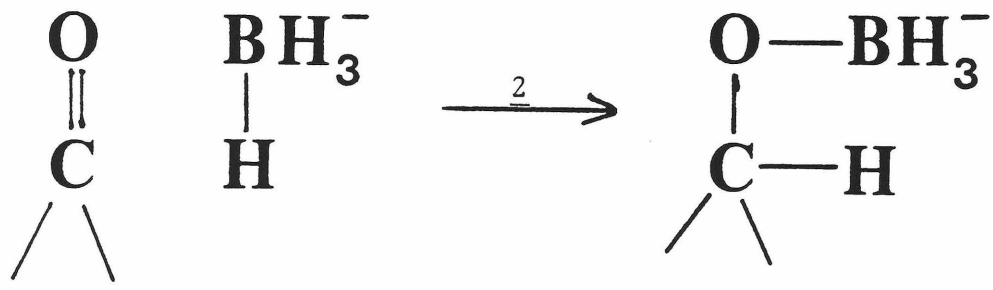
O
C
BH3−
H
2
O—BH3−
C—H

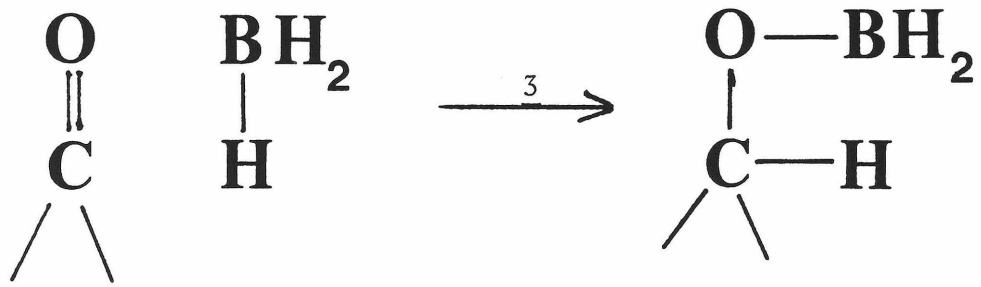
O
C
BH2
H
3
O—BH2
C—H

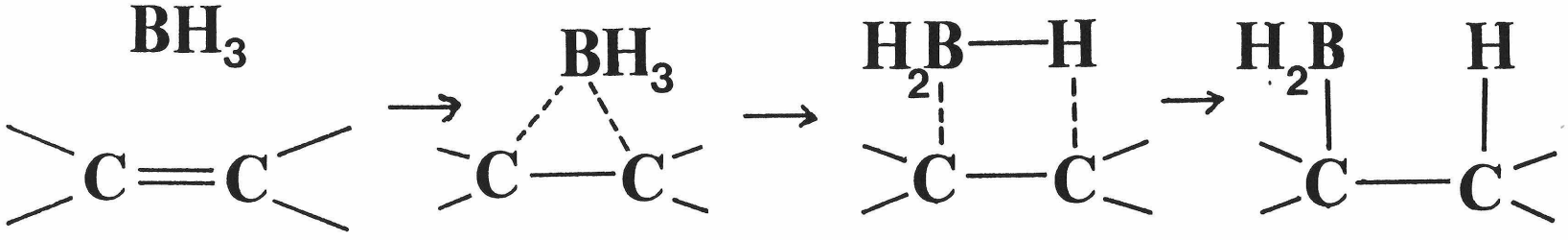

I II

SCHEME 1

rapidity of borohydride reduction in protic solvents is apparently attributable to stabilization of the intermediate alkoxide ion in solution (3).

With the exception of a study of the hydroboration of ethylene by the flow reactor technique (6), there have been, to my knowledge, no studies of the hydroboration reaction, borohydride reduction, or related reactions, in the gas phase. As solvent effects are expected to exert a large influence on these reactions in solution, investigations of the gas-phase reactions should yield mechanistic information not obtainable by solution studies. I propose studying some simple reactions related to the hydroboration reaction and to borohydride reduction in the gas phase by ion cyclotron resonance (ICR).

Dewar and McKee's results (3) on borohydride reduction could be tested by ICR with relative ease. The reaction of BH_4^- with CH_2O or $(CH_3)_2CO$ is expected to have a large activation energy, on the order of 30 - 40 kcal/mol (3). Measuring rates of this reaction at different temperatures will test the accuracy of this calculated activation energy. The reaction is expected to proceed via an alkoxide intermediate which can combine with borane or transfer a hydride back to borane, both processes being exothermic. Experiments using BD_4^- could be undertaken to test this hypothesis by comparing rates of formation of isotopically mixed borohydride with that of the borohydride adduct of the carbonyl compounds. Double resonance experiments (7) could determine that observed products were due to reactions involving BH_4^- and not contaminants such as $B_2H_7^-$. The generation of BH_4^- in the ICR spectrometer is described

in Ref. 8.

Along the same lines, the reaction of BH_3 with alkoxide ions generated in the ICR spectrometer could be investigated concurrently. Reactions rates for the production of BH_4^- and R_2CHOBH_2 could be measured to confirm the results obtained using BH_4^-. BH_3 can be generated from BH_3PF_3 (6). CH_3O^- can be generated from methyl nitrite (9), and the $(CH_3)_2CO^-$ ion can presumably be generated from isopropyl nitrite in similar fashion.

Less directly applicable to solution studies, but also interesting, would be investigations on the reaction of BH_3 with alkyl cations such as $C_2H_3^+$ and $C_2H_5^+$ in the gas phase. The formation of the pi complex of BH_3 with these species should be affected by the presence of the extra proton on the alkyne or alkene, and the effect on the rate of hydroboration could be determined by ICR spectroscopy. The reverse process, the dissociation of molecules like $BH_2C_2H_5^+$, might also be amenable to investigation by ICR spectroscopy. Finally, it would be interesting to examine what effect protonation of a carbonyl compound such as acetone would have on its hydroboration reaction, and this process could also be examined by ICR spectroscopy.

In sum, the study of hydroboration and borohydride reduction of small alkenes and carbonyl compounds in the gas phase could provide new information on the kinetics and activation energies of these reactions to compare to theoretical results, and could additionally provide new insights into the mechanisms of these reactions not available from solution studies.

References

1. Sundberg, K. R., Graham, G. D., and Lipscomb, W. N. (1979) J. Am. Chem. Soc. 101, 2863-2869.

2. Nagase, S., Ray, N. K., and Morokuma, K. (1980) J. Am. Chem. Soc. 102, 4536-4537.

3. Dewar, M. J. S. and McKee, M. L. (1978) J. Am. Chem. Soc. 100, 7499-7505.

4. Dewar, M. J. S. and McKee, M. L. (1978) Inorg. Chem. 17, 1075-1082.

5. Clark, T. and Schleyer, P. V. R. (1978) J. Organomet. Chem. 156, 191-202.

6. Fehlner, T. P. (1971) J. Am. Chem. Soc. 93, 6366-6373.

7. See Beauchamp, J. L. (1971) Ann. Rev. Phys. Chem. 22, 527-561.

8. Dunbar, R. C. (1968) J. Am. Chem. Soc. 90, 5676-5682.

9. Bartmess, J. E., Hays, R. L., and Caldwell, G. (1981) J. Am. Chem. Soc. 103, 1338-1344.

Proposition 5

Variable Temperature Infrared and Resonance Raman Studies of Nitrosyl Ferrous Heme Complexes

The model we have proposed for the two stable conformers of nitrosyl ferrous heme complexes, which is shown in Fig. 7 of Chapter II, could be tested by investigating the temperature dependence of the infrared and resonance Raman spectra of these derivatives. Desbois et al. (1) have measured the low-frequency vibrations of MbNO at room temperature by resonance Raman spectroscopy with excitation at 441.6 nm, and have assigned the band at 409 cm^{-1} to the Fe-N_{ε}(histidine) stretch. If the model proposed in Chapter II for the two stable conformers of MbNO is correct, the Fe-N_{ε}(histidine) vibration should be higher in energy for species I than for species II. Since species I is favored over species II at low temperature, lowering the temperature to 77 K might be expected to cause the intensity of the 409 cm^{-1} band to decrease; a new Fe-N_{ε}(histidine) vibrational band due to species I should concomitantly grow in at higher energy.

Desbois et al. (1) found there to be no iron-NO stretch band observable by resonance Raman spectroscopy with excitation at 441.6 nm, but it is possible that this vibration might be observable by far infrared spectroscopy. For this measurement, it would be most expedient to use the Fe(II) protoporphyrin IX-NO complex with Me_2SO as solvent. If the iron-NO stretch could be observed, its intensity should vary with temperature between 77 and 200 K (see Chapter II). In this case, if the model presented in Chapter II is correct, one would expect a new

iron-NO stretch occurring at lower energy to grow in, and the iron-NO stretch due to species II to simultaneously decrease in intensity, as the temperature was lowered.

The N-O stretch itself could be monitored easily by infrared spectroscopy, as it occurs in the 1700 - 1900 cm^{-1} region for NO bound to ferrous heme (2), and Me_2SO is transparent in this part of the spectrum. Here, one would expect a band at around 1700 cm^{-1} to predominate at higher temperatures, where species II is dominant; this band should give way to a vibration occurring at higher energy as the temperature is lowered to 77 K and the more linear, less strongly coordinated NO of species I becomes predominant.

Once the vibrations characteristic of each of the two stable conformers had been determined by the variable temperature infrared and resonance Raman measurements, the equilibrium constant at a given temperature could be calculated by assuming that the only contribution to the free energy difference between the two conformers came from the vibrational part of the partition function. Comparison of the equilibribium constants calculated in this way with those actually measured would provide a way to assess the relative importance of the electronic and vibrational contributions to the free energy difference between the two conformers.

References

1. Desbois, A., Lutz, M. and Banerjee, R. (1979) Biochemistry 18, 1510-1518.

2. Wayland, B. B. and Olson, L. W. (1974) J. Am. Chem. Soc. 96, 6037-6041.